TRW No. 08710-6015-R000

NASA CR-84052

STUDY OF A NAVIGATION AND TRAFFIC CONTROL TECHNIQUE EMPLOYING SATELLITES

(Interim Report)

VOLUME IV

GROUND STATION AND SATELLITE

By David D. Otten

DECEMBER 1967

Prepared under Contract No. NAS 12-539 by

TRW SYSTEMS GROUP

One Space Park • Redondo Beach, California 90278

Electronics Research Center

NATIONAL AERONAUTICS AND SPACE ADMINISTRATION

Mr. Peter Engels
Technical Monitor
NAS 12-539
Electronics Research Center
575 Technology Square
Cambridge, Massachusetts 02139

Requests for copies of this report should be referred to:

NASA Scientific and Technical Information Facility
P. O. Box 33, College Park, Maryland 20740

TRW No. 08710-6015-R000

STUDY OF A NAVIGATION AND TRAFFIC CONTROL TECHNIQUE EMPLOYING SATELLITES

(Interim Report)

VOLUME IV

GROUND STATION AND SATELLITE

By David D. Otten

DECEMBER 1967

Prepared under Contract No. NAS 12-539 by

TRW
SYSTEMS GROUP
One Space Park • Redondo Beach, California 90278

Electronics Research Center
NATIONAL AERONAUTICS AND SPACE ADMINISTRATION

CONTENTS

CONTENTS (Continued)

CONTENTS (Continued)

ILLUSTRATIONS

ILLUSTRATIONS (Continued)

TABLES

STUDY OF A NAVIGATION AND TRAFFIC CONTROL TECHNIQUE EMPLOYING SATELLITES

Volume IV: Ground Station and Satellite

By David D. Otten

1. INTRODUCTION

This volume consists of four major sections. Sec. 2 presents a discussion of the ground network required to implement the NAVSTAR system. It can be seen that the interim Atlantic network consists of three extremely simple, low-cost ground stations. In addition, a computation center and a telemetry and command station (i.e., an existing STADAN station) are required. The commands capability includes transmission of stationkeeping and attitude control commands. Further, the ephemeris and oscillator time correction data are transmitted to each satellite approximately once every hour.

In sec. 3, the discussion covers the equipment which would go on board a satellite both to generate the navigation signal and to transmit it to the visible earth. Further, sec. 3 describes the satellite equipment required to implement voice links between low-performance terminals, e.g., aircraft.

The detailed satellite preliminary design is given in sec. 4. The overall configuration presented is followed by results of the preliminary design studies for each subsystem. The satellite design selected provides the navigation signal and ephemeris data to all users. In addition, the satellite will be used as a communication link for relay of tracking information among the network of ground stations. However, while the satellite has not yet been designed to provide traffic control links for users, this provision will be met, and the results will be documented as an addendum to this report.

Reliability considerations are documented in sec. 5.

The findings being submitted to NASA-ERC were the result of a strong team effort. While numerous technical personnel made contributions to the study results contained in the four volumes comprising this interim report, the following TRW Systems people made significant contributions to the analyses presented in this volume:

Communications Analysis for the Navigation Signal Generation Subsystem, Voice Links, Ground Station, Design of the Telemetry and Command Subsystem:	A. Garabedian
Satellite Booster Analyses (and support in study direction and the technical editing of this volume):	F. Holmes
Navigation Signal Generation Subsystem:	N. Estersohn, G. Blackman
Ground Station:	T. Nosek, L. Whitman
Appendix B, "Very Stable Oscillators — A Survey":	J. M. Andres
Satellite Structure:	A. L. Young
Satellite Mass Properties:	L. Billingsley
Satellite Attitude Control and Antenna Despin System:	J. Murrin
Satellite Dynamics:	P. Groat, D. Mitchell
Satellite Positioning/and Orientation Subsystem, and Apogee Motor:	R. C. Miller
Satellite Electric Power:	L. Leventhal
Satellite Thermal Control:	J. Verbeck
Satellite Electrical Integration Assembly:	H. Garr
Satellite Navigation Transmitter:	D. C. Obray
Study Direction, Satellite System Design (and preparation responsibility for this volume):	D. D. Otten

Satellite Reliability Analysis:	G. Pittler
Ground Station Tracking Antenna:	Gary Wong
Satellite Antenna:	L. F. Brohish
Satellite Telemetry and Command:	I. Wilkerson

2. NAVSTAR GROUND STATION NETWORK

2.1 INTRODUCTION

This section covers the preliminary study of the requirements for a ground system to support a navigation satellite system consisting of a two-orbit network with eight synchronous satellites in each orbit. Included for consideration in the ground system are:

- Tracking stations capable of receiving the satellite's transmitted ranging signal and determining range (range-difference) to visible satellites.
- Telemetry receiving and command sites to monitor satellite telemetry and transmit commands and updated information to the satellites.
- A master computation center, which would receive data from the tracking sites and compute orbital data for transmission to the satellites by the command stations.

Locations for the various stations are suggested and functional descriptions are provided. Some preliminary cost estimates are also developed.

2.2 GROUND STATION CONFIGURATION

A proposed network of supporting ground stations is shown in Figure 1. The distribution of tracking sites is designed to achieve advantageous tracking geometry resulting in higher accuracy. As discussed in vol. II, it is likely that further study will demonstrate that the total number of tracking sites can be reduced.

Figure 2 is a functional block diagram of the ground station system. All of the station systems will not be repeated at every ground station. For example, telemetry and command facilities will be restricted to one station for the interim Atlantic network. The other stations will provide tracking support for the NAVSTAR system, with the communication equipment that is required to transmit received tracking data to a computing site. This computing site can be situated at any convenient location. The functional block diagram actually represents a composite station. Widespread "geometry" of ground station coverage is desirable only for the purpose of tracking support. Centralization of the computing site requires more

Figure 1. Worldwide Ground Station Network

study with respect to the costs of communicating data from the ground stations to the central computing site versus the costs of duplicating computing facilities at remote stations.

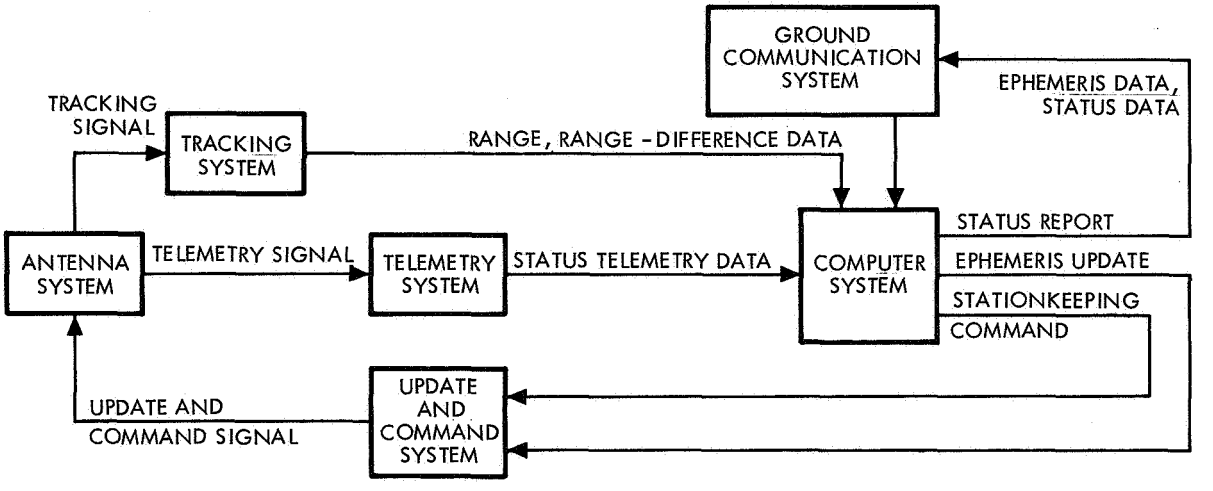

Figure 2. NAVSTAR Ground Station Functional Block Diagram

Additional ground-station functions, such as aircraft advisory, air traffic control, etc., that may influence the location and equipment for a ground station, are not considered here.

2.2.1 Tracking Stations

Navigation satellite-orbit determination may be achieved in a manner compatible with the navigation function of the satellite by utilizing the navigation-ranging signal from the satellite as the primary tracking signal. Ground stations with receivers for this signal can obtain continual ranging signals in a manner similar to a system user. Given ground station locations, these data may then be used in an orbit-determination computer program to predict the satellite's position and velocity.

Configuring the ground station to be similar to a user ensures low cost; in addition, using the navigation ranging link for tracking allows the network-computing system to evaluate biases (due to oscillator error) in the signal. This parameter is vital to accurate user position determination.

The ranging data from the ground station would be sent back to a central computing center by a communication link in the satellite, requiring a communications transmitter at the site. The equipment required for operation of the ground-station tracking (i. e., navigation signal ranging) is simple and inexpensive. Note the compact design of the antenna for receiving the ranging signal as shown in Figure 3. The ranging signal receiver would be a modified and improved version of the user receiver and, therefore, would be slightly more costly.

The ground-station building would be small and no personnel would be required except for periodic maintenance. All sites suggested for the stations are close to populated areas; hence, power should be available from commercial or public supplies.

2.2.2 Tracking Antenna

The L-band antenna, which receives the satellite ranging signal at the tracking station, must be capable of switching from satellite to satellite at 1.5-sec intervals. To meet these requirements, yet provide coverage for all satellites within view of a ground station, the array shown in Figure 3 is proposed. Being a 7-element array of dipole elements with 60° dihedral reflectors, the antenna provides a minimum of 12-db gain. It is stationary, with a beamwidth of 50° by 160°. This coverage provides $+10^{\circ}$ horizon coverage for satellites near the equator (e. g., the $\pm 18.5^{\circ}$ inclination system proposed). The axial ratio (ratio of antenna sensitivity to different polarizations of the incoming signal) is less than 2 db. The antenna is circularly polarized. Switching between elements provides capability for receiving from any of the visible satellites.

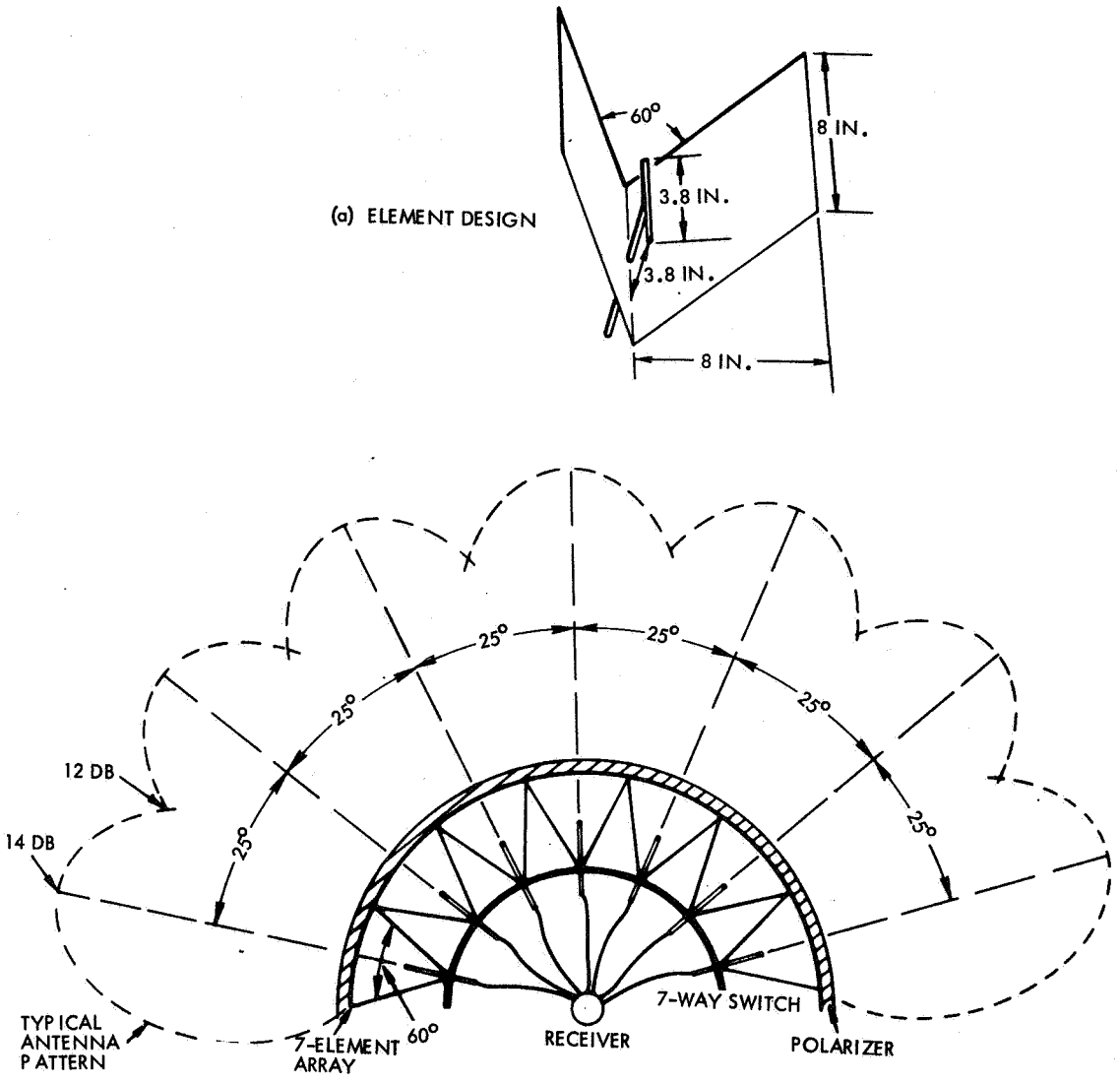

Figure 3. Ground Station Antenna

2.2.3 Telemetry and Command Stations

The telemetry/command stations are more complex, and it is suggested that the existing STADAN Network be used. The telemetry and command links require a 30-ft antenna (see par. 4.8.6).

The equipment block diagrams represent equipment requirements for telemetry and command functions (except for antenna). The probable requirement to use S-band for these functions has oriented this section primarily to that frequency.

Figure 4 shows a simplified block diagram. The data received in the telemetry would include satellite power levels and environmental data needed to detect failures. It is likely that a worldwide system, with 16 or more satellites in orbit at one time, would be designed to minimize telemetry requirements following a test phase that is sufficient to determine system MTBF. Since the primary purpose of the system is navigation data transmission, the minimum acceptable telemetry requirements should be examined in detail to make cost-effectiveness conclusions on the telemetry system which is a large cost item in the ground station. In addition to the normal telemetry represented by PAM data, satellite attitude position data are received by the telemetry channel. These data are fed to the computer for determinations of satellite attitude.

The command system is used to update the values of ephemeris and oscillator bias stored on board each satellite for retransmission to the NAVSTAR users and to transmit thruster firing pulses for repositioning the satellite attitude as determined by the attitude telemetry data. In addition, various system commands will be transmitted to control the state of satellite equipment, including oscillator frequency reset.

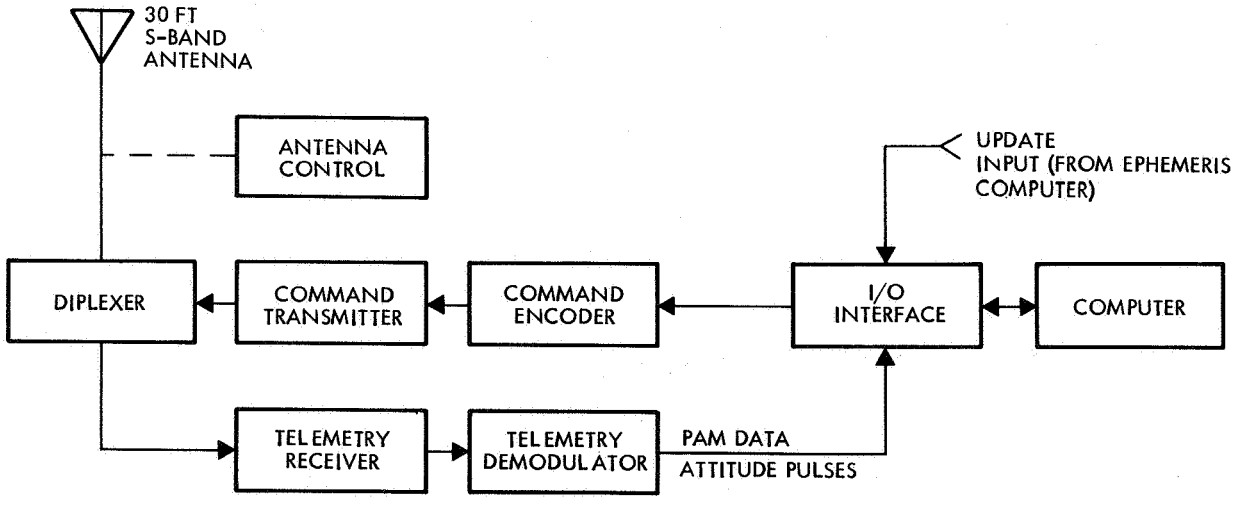

Figure 4. General NAVSTAR Ground Station for Command and Telemetry, Block Diagram

The computer is used to calculate the necessary commands, including time and duration of attitude thruster firings, and to monitor and display telemetry status. This computer may or may not be part of the ephemeris update computer depending on the location of the two functions. If two separate computers are used, ephemeris update information must be provided to the telemetry and command computer to generate the update commands.

2.2.4 Computation Center(s)

Three general functions are required of ground-station computers, as follows:

1) Satellite ephemeris (and oscillator bias) calculation

2) Maintenance of station operation in the areas of encoding, antenna switching, telemetry supervision, etc.

3) Determination of satellite attitudes.

The first function will be associated with a large "master" computer, serving a large area presumably occupied by multiple ground stations, which will transmit data on satellite measurements to the central station. The computer at the central station would be required to compute the ephemerides of a number of satellites on a continual basis.

The second function will be associated with the operation of the individual stations, such as controlling the operation of antenna, transmitting, and operating command and receiving equipment. This function may be performed by a smaller computer at each station, with the larger master system devoted primarily to ephemeris determination and to computation of system-wide operations. The sizing of computers is consistent with this possible division of tasks, with the ephemeris calculations for multiple satellites and with the subsidiary tasks separately sized.

The third function may be performed either by the master computer or by computers located at the telemetry and command stations. In either case, the computer must determine satellite attitude from received telemetry and generate, if necessary, commands for satellite reorientation.

The ephemeris-calculation for as many as 16 synchronous satellites with updates of oscillator-error values at frequent intervals will be a major computation task.

Computer requirements may be estimated by comparison with existing orbit-determination programs such as ESPOD, a large TRW orbit determination program. Processing of the data could be handled with one program sequentially by satellites if the computation cycle time were fast enough to meet data input flow for n satellites. Given a 10 to 15 min update requirement (for clock bias), it is probable that a single program similar in size to ESPOD could sequentially process data satellite by satellite. This would be equivalent to a 2-min computation cycle time per satellite for a regional system of 8 satellites. This program uses about 200,000 bytes (8 bit units) in core which, in a 32-bit word machine, occupies a 50,000-word core storage block. A system such as the IBM 360-50 computer accommodates this program. However, the program does not totally fit core since links are used which move into core sequentially for different processes in the computation. Extensive multiprogramming of such a system would be difficult in a 50,000-word core because of the complicated transfers into and out of core of the program links. Multiprogramming to handle multiple satellites simultaneously for reasonable efficiency, would require the entire orbit-determination program to exist in core at one time. Required capacity for an ESPOD class program is about 100,000 words. To this, blocks would be added to accommodate data storage for each satellite.

Current 64,000-core machines, such as the IBM 360-50, could handle an orbit determination program if satellites were processed sequentially. Simultaneous processing will require upwards of 100,000-core storage plus data storage for each satellite. Large, third-generation machines such as the GE system (128K) might accommodate a multiprogrammed system for simultaneous data reduction, although further study will be required. Such a technique would be required for a recursive computation in an efficient fashion.

A lower-level computer will be required at the master site to sort data, edit, and preprocess for the large machine. The IBM 1800 is a representative system, and is also a candidate for a telemetry/command site computer, as it is designed for data-acquisition and control system. It is available with 4,000, 8,000, 16,000 or 32,000 storage.

Figure 5 shows general data processing flow at the master computing site.

2.3 LOCATIONS

The NASA STADAN Network can provide the facilities for the telemetry and command functions. Four sites will be adequate to cover the 16-satellite system. Coverage data for the four sites are shown in Table I. Shown are the number of satellites in view at each site (elevation angle $>5^{o}$). The 30-ft antennas required for telemetry are met by the 40- or 85-ft antennas existing at these sites.

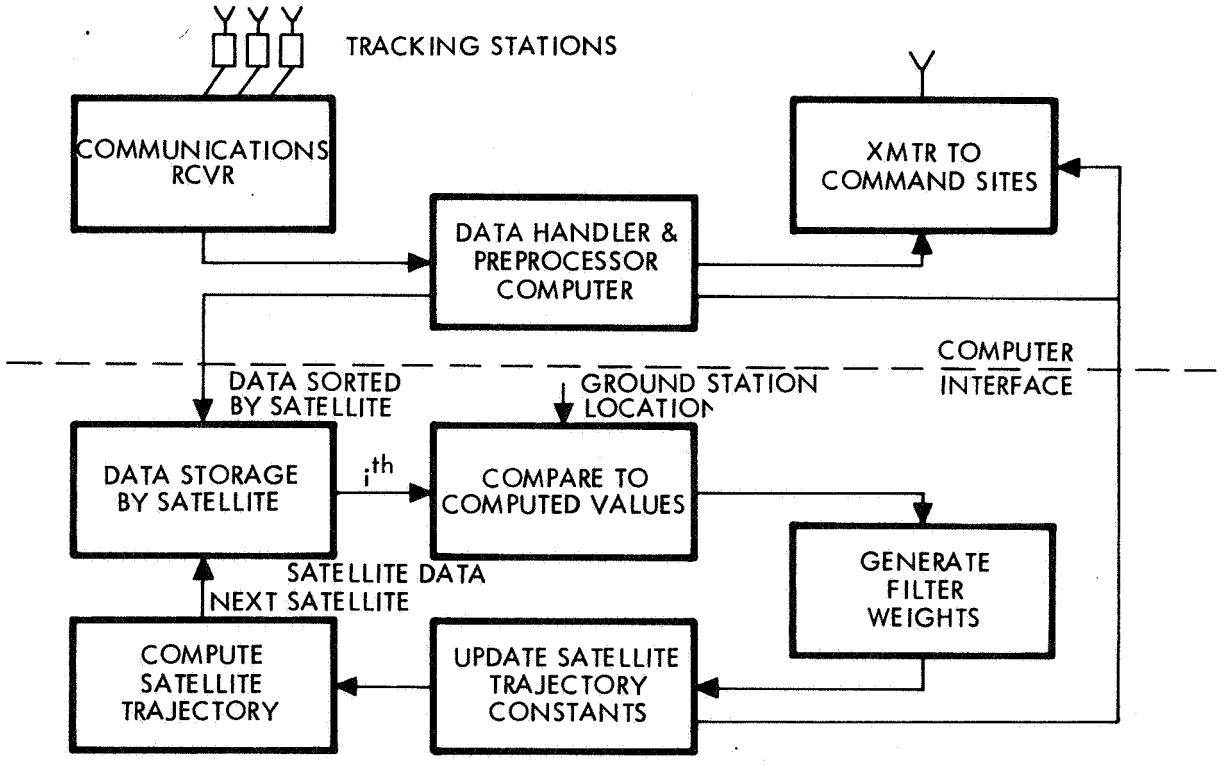

Figure 5. Computer Center Data Flow

TABLE I

STADAN TELEMETRY NETWORK/COMMAND

STADAN Station	Number of Satellites Visible
Rosman, N.C.	6
Orroral, Australia	6
Johannesburg, S.A.	6
Goldstone, Calif.	6

The NASA USB network has numerous stations providing generally good, redundant coverage on an 18.5^{o} orbit for the tracking function. (See Table II.) This network, however, has a large longitude gap of about 120^{o} between Carnarvon and Madrid so that, although all satellites are tracked, at least one will be viewed by only one ground station in this area. Hence, although USB appears to provide a reasonable network from coverage requirements, some added support in the Indian Ocean area would be required to yield redundant tracking for all satellites. The USB network contains a number of stations in the western hemisphere near the United States (Bermuda, Antigua, Grand Bahama, Cape Kennedy, Texas, Guaymas, Goldstone) so that ground stations here would give heavily redundant tracking over the United States and western portion of the Atlantic.

USB stations at Goldstone and Madrid are equipped with 85-ft dish antennas, the others with 30-ft dishes. Additional support is furnished by tracking ships. The 85-ft antennas provide data on the lunar mission primarily and the 30-ft dishes provide earth orbital data (Ref. 7). An S-band coherent doppler and pseudo-random range code system developed by the Jet Propulsion Laboratory is used; a single carrier is used for tracking and communication data.

USB requirements for Apollo support would rule out use of the system for continuous NAVSTAR support. However, again, the well-established facilities and good tracking coverage generally provided

TABLE II.

NASA USB NETWORK

USB Station	Number of Satellites Visible
Madrid	6
Grand Canary Is.	6
Ascension Is.	6
Antigua	7
Bermuda	6
Grand Bahama Is.	6
Cape Kennedy	6
Texas	8
Guaymas, Mexico	6
Goldstone	6
Hawaii	7
Guam	7
Canberra, Australia	6
Carnarvon, Australia	6

for a potential NAVSTAR system indicate further study of USB sites for a civil NAVSTAR system. Additional support in tracking would be required between Australia and Ascension or Madrid. The Seychelles Islands of the SCF network represent a possible site.

A configuration for a worldwide system, considering existing tracking sites in general and with some regard to geopolitics, was determined. These stations are listed in Table III together with the number of satellites "seen" by each.

The table illustrating the number of stations viewing each of 16 satellites is shown on Table IV for these stations. Ground station numbers in parentheses are those which track only part-time. Note that each satellite is viewed all of the time by three stations or more for two $\pm$ 18.5^{o} inclination orbits. This network then represents a reasonable one from redundant tracking considerations. Currently, about all of the above stations are sites for one or more NASA or USAF tracking/ telemetry facilities.

TABLE III.

SAMPLE WORLDWIDE NETWORK

Station	Number of Satellites Visible for $i = 18.5^{o}$
1) Samoa	6
2) Hawaii	5
3) Mojave	5
4) New Orleans	5
5) Antigua	6
6) Sao Paulo, Brazil	6
7) Ascension Islands	6
8) Johannesburg, S.A.	6
9) Seychelles Islands	6
10) Carnarvon, Australia	5
11) Guam	6

2.4 COMMUNICATIONS

The NAVSTAR satellite will provide communication from ground stations to telemetry and command sites. Although not covered in detail in this report, brief calculations were made on the required data flow.

Data to be transmitted are:

1) Time of day of ground station operation

2) Satellite ID (two required for range differences)

3) Value of range or range difference

Rate would be 1 per 2 sec for each ground station. Bit requirements are

time = 35 bits
ID = 10 bits
data = 10 bits
Total = 55 bits

TABLE IV.

ID OF GROUND STATIONS VIEWING SATELLITE

Satellite	i = 18.5°	30°	50°
1	1, 2, (3), 11, (10)	1, 2, (3), 11, (10)	1, 2, (3), 11, (10)
2	1, 2, 3, 11	1, 2, 3, 11	1, 2, (3), (11)
3	1, 2, 3, 4, (11)	1, 2, 3, 4, (11)	1, 2, (3), (4), (11)
4	1, 2, 3, 4, 5	(1), 2, 3, 4, 5	(1), (2), (3), (4), (5)
5	(2), 3, 4, 5, 6	(2), 3, 4, 5, 6	(2), (3), 4, 5, (6)
6	3, 4, 5, 6, 7	(3), 4, 5, 6(7)	(3), (4), 5, 6, (7)
7	4, 5, 6, 7	4, 5, 6, 7	(4), 5, 6, (7)
8	(4), 5, 6, 7, 8	(4), 5, 6, 7(8)	(4), 5, 6, 7(8)
9	5, 6, 7, 8, 9	(5), 6, 7, 8, 9	(5), (6), 7(8), 9
10	6, 7, 8, 9	(6), 7, 8, 9	(6), 7, 8, 9
11	7, 8, 9	7, 8, 9	(7), 8, 9
12	(7), 8, 9	(7), 8, 9	(7), (8), 9
13	8, 9, 10, 11	(8), 9, 10, 11	(8), 9, (10), 11
14	9, 10, 11	9, 10, 11	9, 10, 11
15	10, 11, 1	10, 11, 1	(10), 11, (1)
16	10, 11, 1, 2	10, 11, 1, 2	(1), 11, 1, (2)

Allowing for encoding, etc., growth to 100 bits would require 50-bps data rate. This rate is quite low and suggests that no data compaction schemes will be required.

2.5 COSTS

Specific costing for ground stations cannot be made until firm equipment specifications are drawn up. However, approximate figures for equipment costs may be estimated through comparison of the ground station's equipment with existing or proposed similar networks. The S-band unified tracking telemetry and command (SGLS) system has been chosen as a reference, since it incorporates a number of features similar to NAVSTAR ground stations, although its capability is significantly greater.

The cost estimates for internal station equipment are exclusive of such factors as building and construction, personnel support facilities, and external emergency power supply, since such factors will depend on station location and integration with existing facilities. Installation and checkout are also not included.

Cost estimates for the items of Table V (the internal equipment of the telemetry and command sites) reveal that such facilities will be significantly more expensive than the simple tracking stations; hence, the number of stations should be minimized. Based on reference to SGLS initial cost of similar units, approximate costs for the following items are presented (for one telemetry/command site):

TABLE V.
TELEMETRY AND COMMAND STATION

Item	Cost Estimate
Transmitter (1 kw class)	$50,000
Diplexer	10,000
Telemetry demodulator	35,000
Command encoder	20,000
Parametric amplifier	37,000
Receiver	55,000
Terminal assembly	50,000

These items total about $260,000. The proposed integration equipment (consoles, etc.) for an SGLS ground station material cost was about $ 280,000. Thus, without building, power supply, and installation at the telemetry/command site, a unit material cost of nearly $600,000 is reached.

To this must be added the cost (not estimated) of any communication equipment for linking these sites with the central computer or with other sites. The telemetry/command sites are thus significantly more expensive than the tracking sites, in which equipment similar to that of a user is expected to cost $20,000 to $30,000. Note also that power supply, communication equipment, and buildings must be added to these figures.

3. SATELLITE EQUIPMENT FOR NAVIGATION AND TRAFFIC CONTROL

This section presents the results of studies of the navigation and voice communication links to be used for traffic control. Details of the navigation signal generation subsystem (consisting of the oscillator and time base unit for generation of the ranging and data signals) are presented, followed by a discussion of the transmitters required.

The final subsection is devoted to a discussion of the voice links.

3.1 NAVIGATION SIGNAL GENERATION

3.1.1 Crystal Oscillator

The precision atomic clock recommended in the TRW proposal for control of "present time" generation has been replaced in the current design with a precision crystal oscillator, which will be a design similar to the one used by the Navy on Transit and other satellites.

The design will have double redundancy: two oscillators and two crystal ovens in a configuration where either oscillator may be used with either oven. The power consumption is low: 1/2 w for an oscillator and 1/2 w for an oven (at 50-percent duty cycle). The overall package is relatively large and heavy (4-lb design goal) for the low-power consumption, but this is necessary to ensure thermal stability and adequate mounting for shock and vibration. The oscillator design includes proportional control for the ovens for greater precision in temperature control and greater overall reliability.

The stability of this oscillator, when calibrated for aging, will be better than that originally anticipated for the Rubidium standard. The expected accuracy has been obtained from Reference 1. It can be seen that the error will be less than 9 ft within 1 hr elapsed time since the last calibration. If even 1 day elapses after calibration data are transmitted to the user, the error would still be less than 100 ft. Other oscillators considered are discussed in app. B.

A frequency of 5.12 MHz is recommended, but it can easily be changed if other considerations demand it when a prototype design is completed. Figure 6 presents an overall block diagram of the navigation signal system, showing how the oscillator fits into the system. Most interconnection signals are also shown.

3.1.2 Time Base and Code Generator Unit

The design for the time base and code generator unit is straightforward; a block diagram and some waveforms are shown in Figure 7. The time base unit counts down from the oscillator frequency of 5.12 MHz, in binary fashion, to 12.39 sec per cycle. A second set of counters generates time-of-day information from the 5-kHz flip-flop in the first set of counters. A group of 13 frequencies in the first set (320 kHz to 78.125 Hz) is used to generate the BINOR code for range measurement. In addition, two control signals are generated for the transmitter: (1) a signal for control of transmission to users (navigation signal control) and (2) a signal for control of transmission to ground stations tracking the satellite (tracking data control).

The majority logic block in Figure 7 is used in generating the BINOR ranging code. After examining several ways of performing this function, one was chosen because of its simplicity and reliability. This method is based on multilevel logic, using modulo 2 adders. For 13 inputs, as little as 36 gates can define the proper output, most gates having only 3 inputs. A brute-force approach to the same decision-making would take several hundred gates.

Alternate methods of mechanizing majority logic involve magnetic circuitry and analog circuitry. Analog circuits to perform this function are fairly simple: a summer, a reference voltage, and a comparator. However, it was not desirable from a reliability standpoint to use this technique. On the other hand, a highly reliable simple magnetic device can perform majority logic (a multiwinding toroidal core), but the problem here is in interfacing magnetic devices with transistor circuits. However, even though logic levels and impedances are different, the magnetic scheme becomes feasible when interfaced with magnetic counters and logic. The development of a largely magnetic digital time base and code generator unit is recommended for future study as it may offer reliability advantages.

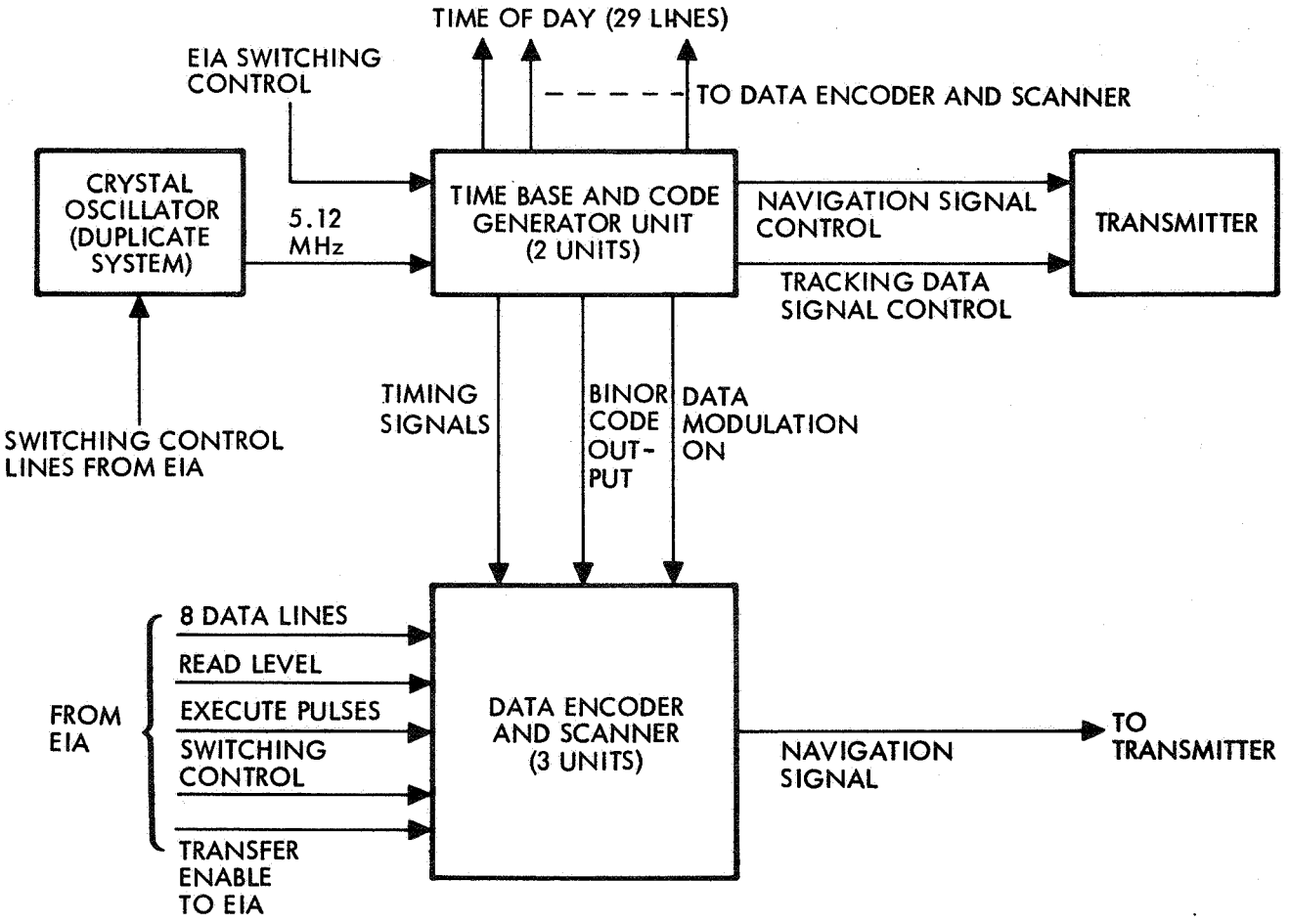

Figure 6. Navigation Signal Generator (Overall Block Diagram)

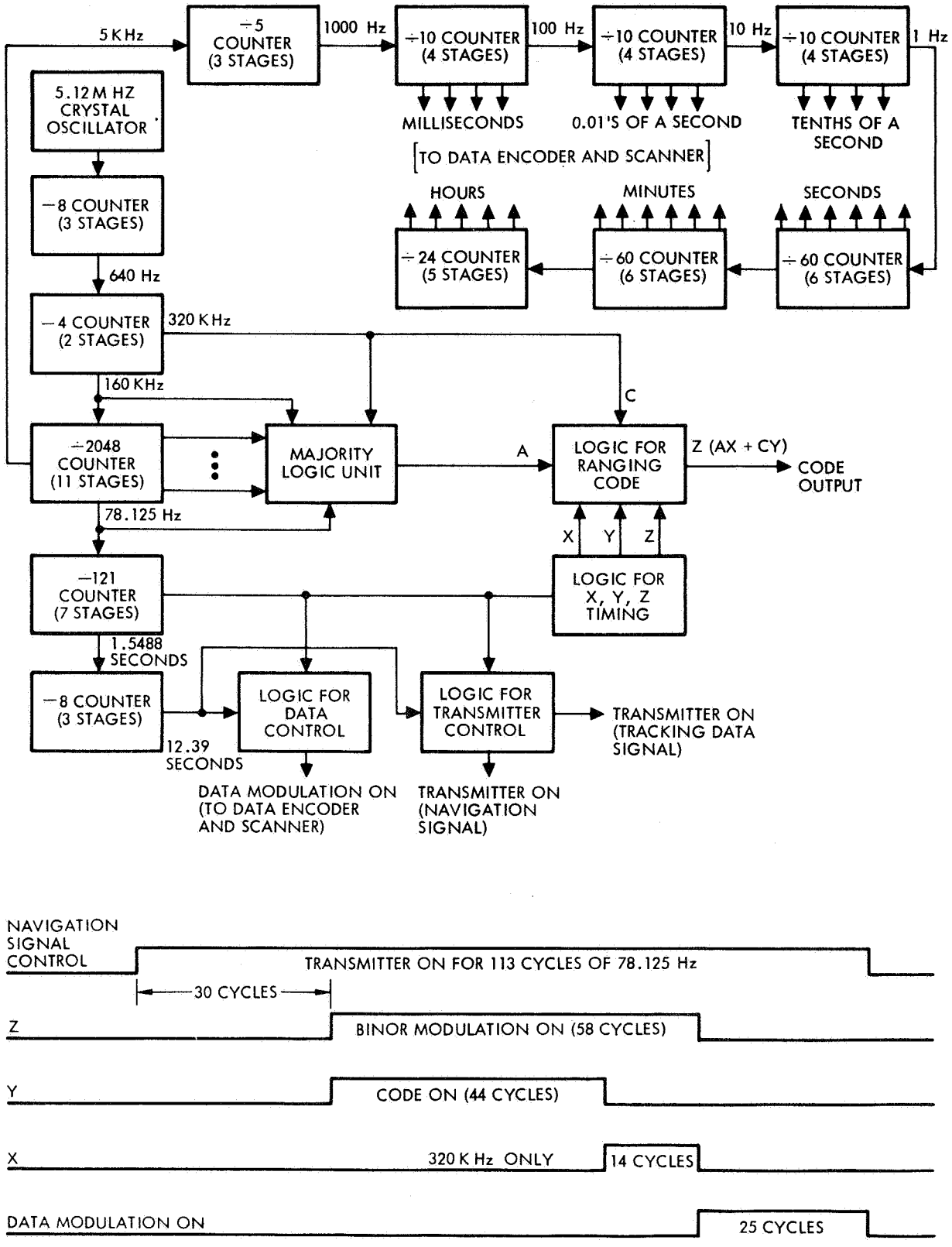

Figure 7. Time Base Unit and Code Generator

If the hardware of the time base and code generator is made up of Fairchild DTμL 9040 series flatpacks, it is estimated that the package would consist of two boards, occupying a space of 7-1/2 x 4-1/2 x 1-1/2 in. Power consumption should be about 1.0 w; weight should be about 3/4 lb. Two such units are considered necessary to meet overall reliability requirements, and the unit to be used will be selected through the telemetry command system.

3.1.3 Data Encoder and Scanner

Figure 8 gives a logic diagram for encoding data for transmission to satellite users. These data are received by the satellite from command stations at regular intervals (ephemeris and time correction information) and stored in the encoder registers. In addition, a more frequent time reference update occurs near the start of data transmission during internal timing signal DS1 (see Figure 9). At this time, the time-of-day information is transferred in parallel into the time reference register, where it is held until the next update 12.39 sec later. The only other information to be generated is fixed for each satellite (ID and frame sync codes).

The information coming out of the scanner has a format of 15 words of 11 bits each. Figure 10 gives the exact arrangement of the data. Each bit is 1/625 sec long. The first 35 bits of the data transmission allow time for the user preprocessor to achieve bit synchronization. Then, 165 bits of information are sent (the last 6, not counting parity, allow for future expansion), giving a total of 200 bits.

Timing signals DSP and DS1 through DS165 are generated from the last four flip-flops of the ÷ 2048 counter and the first five flip-flops of the ÷ 121 counter (625 Hz to 4.88 Hz). The "Data Modulation On" signal limits the scanning to the time that data are transmitted, and inhibits interference of data with the ranging code.

A ÷ 11 counter and time derivatives from it are used to control entry of ephemeris and time-correction data into the correct registers in a serial mode. A set of signals for control of information transfer from the electrical integration assembly (EIA) to the data encoder registers is shown in Figures 6 and 8. Data bits are transferred 8 at a time via an 8-bit

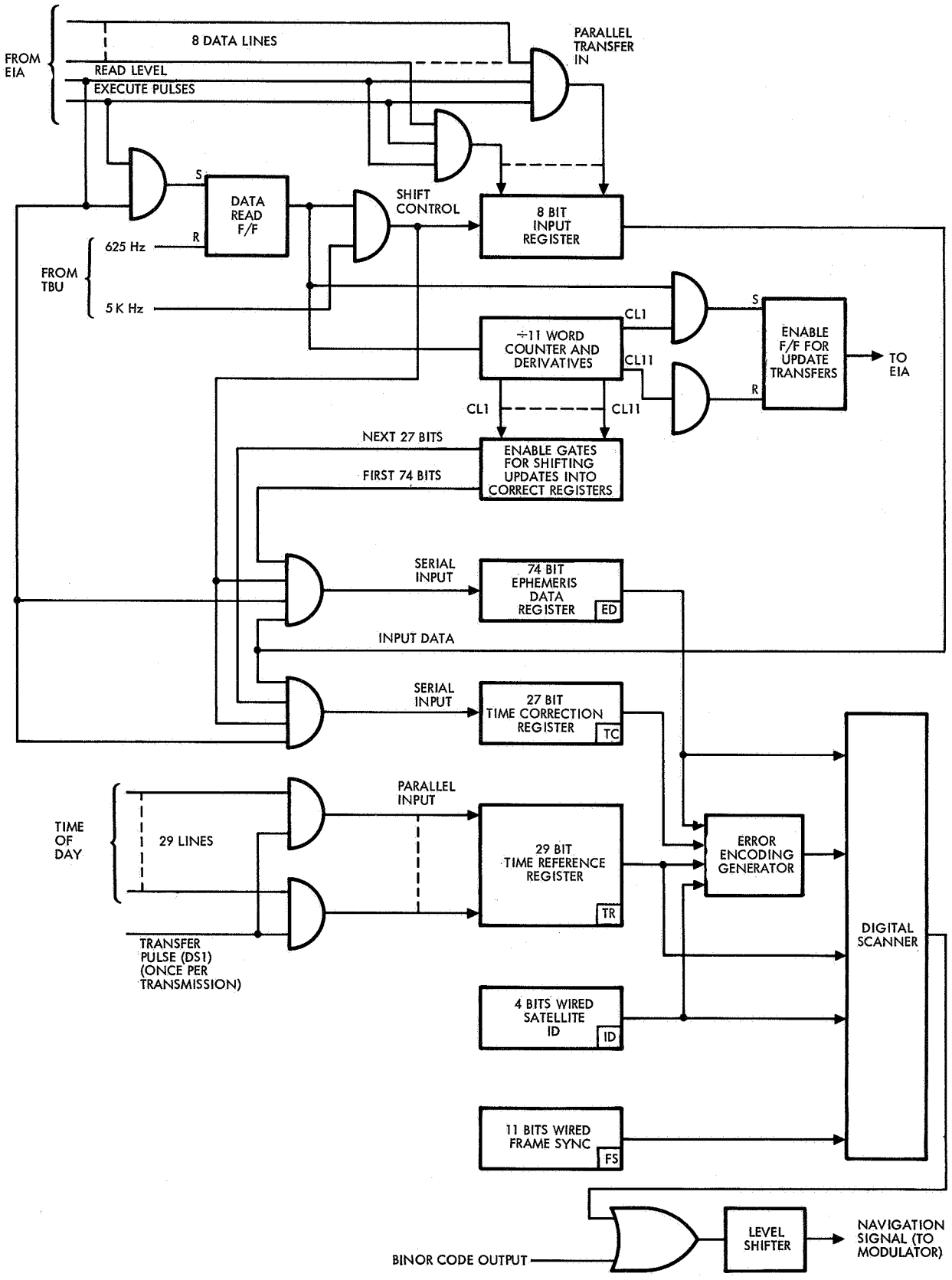

Figure 8. Data Encoder and Scanner

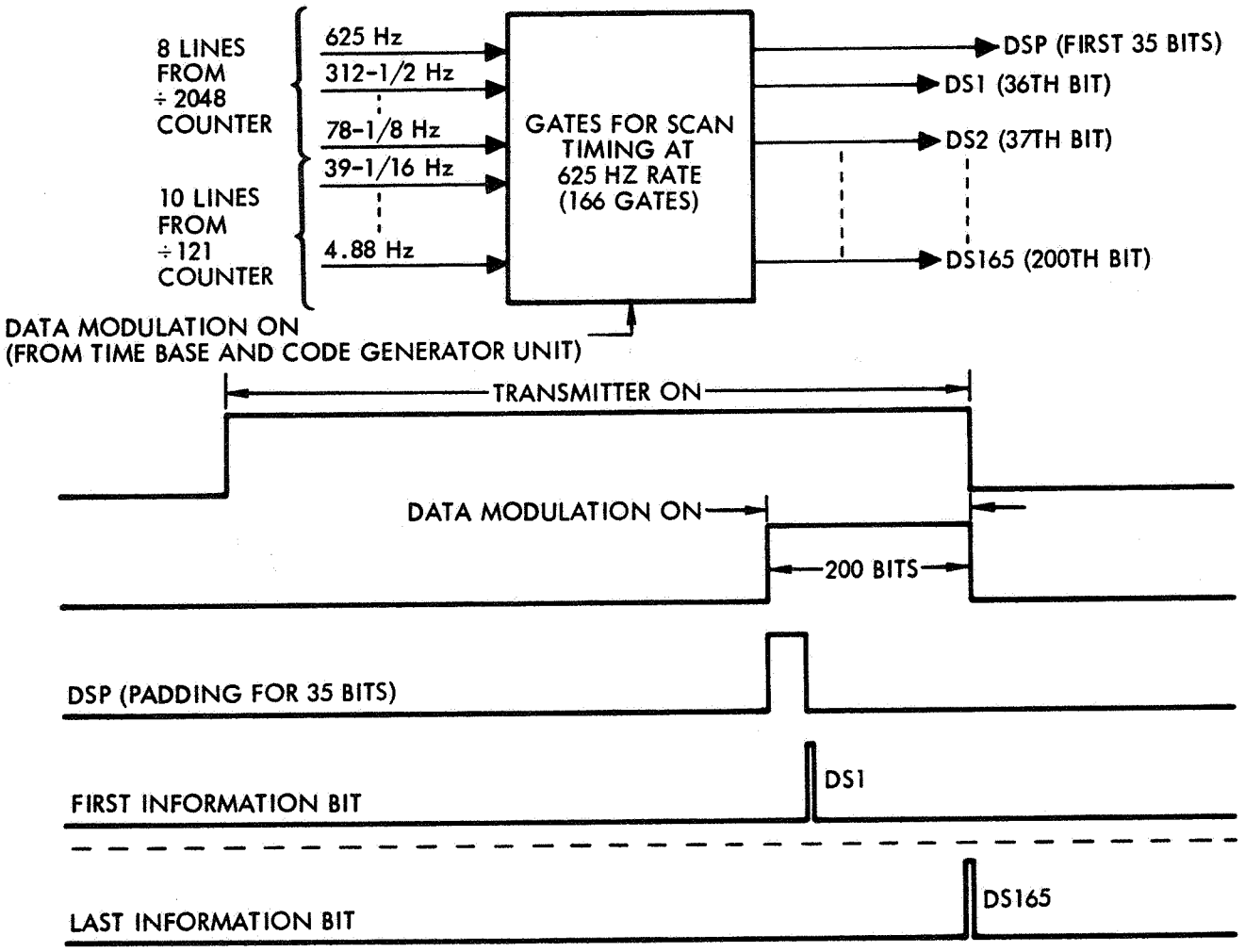

Figure 9. Timing Signals for Error Encoding and Digital Scanning

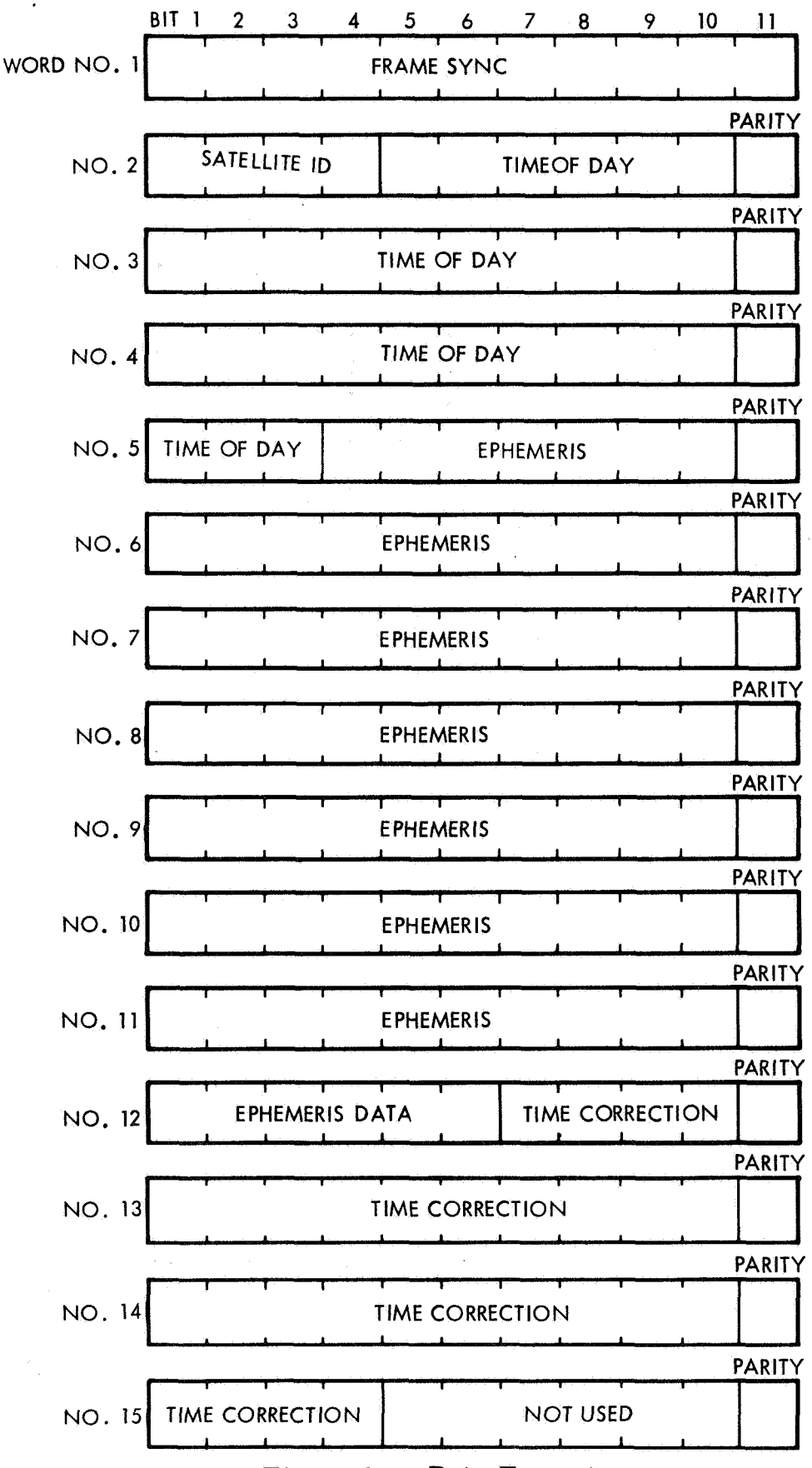

Figure 10. Data Format

input register with parallel input and serial output. A 5-kHz signal from the time base and code generator unit has been selected to control the shift rate; this rate is somewhat arbitrary and can be changed if required. A transfer enable signal is sent to the EIA to indicate when message transmission is complete; this signal is true at the start of transmission (initiated by the EIA) and for 11 words thereafter.

Figure 11 gives details of the digital scanner and error encoding generator, which are shown together since most of the input signals are the same. The DSP and DS1 through DS165 signals are gated with the proper information and then fed into a modulo 2 adder along with the output of the 625-Hz flip-flop of the time base and code generator unit. Since the data rate is also at 625 Hz, a split-phase data representation results, which is the desired form for the data. The ranging code is "or" gated with the split-phase data and level shifted to meet modulator requirements. The final signal has equal plus and minus levels, which will be adjusted in amplitude to final transmitter modulation index.

3.1.4 Error Encoding Generator

Even parity is generated with a single flip-flop. The data are fed into this flip-flop as well as to a modulo 2 adder, as described in the preceding subsection. The data are scanned in proper sequence with timing signals shown in Figure 9. The parity flip-flop will, therefore, be in the correct state at the time it is scanned for parity insertion into the data at the input of the modulo 2 adder. Meanwhile, the parity flip-flop is reset so that it can start properly in generating parity for the next word. The reset logic (DS11 through DS165) can be set up (optionally) directly from the counter outputs as the eleventh pulse of each 625-Hz count.

3.2 L-BAND TRANSMITTER—NAVIGATION SIGNAL SUBSYSTEM

3.2.1 Introduction

A 50-w output, L-band transmitter is required for transmission of the navigation signal to users. The transmitter must meet the following requirements:

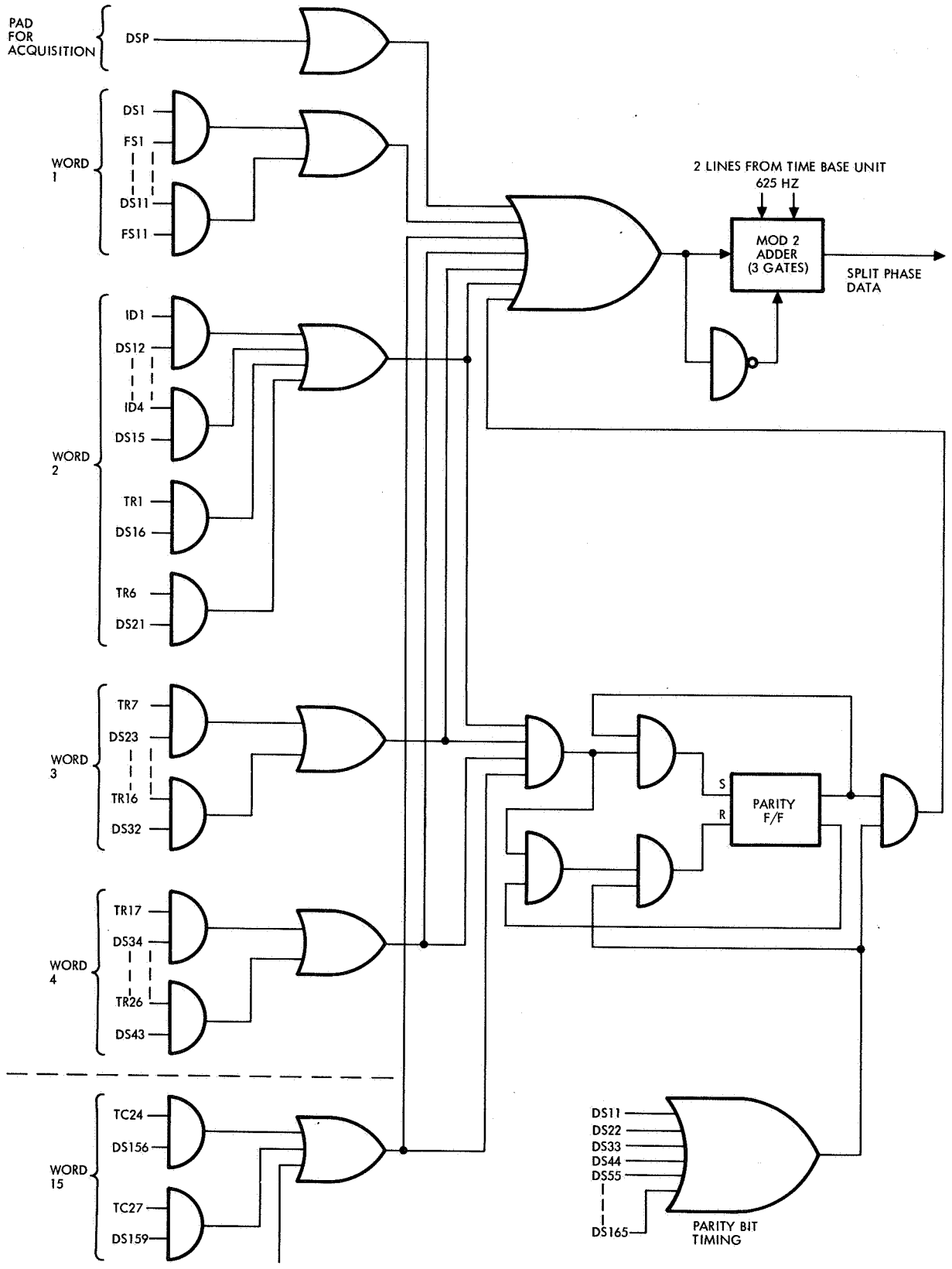

Figure 11. Details of Error Encoding Generator and Digital Scanner

Frequency band:	1540 to 1660 MHz
Bandwidth:	5 MHz*
Frequency stability:	One part in 10^8 long term
Signal modulation:	Phase shift keying (PSK)
Deviation:	1.2 rad
Output power:	50 w (min)

The frequency-stability requirement is specified to reduce the user receiver's search range for acquisition of the transmitter carrier. This stability is easily met by deriving the transmitter drive frequency from the satellite's ultra-stable oscillator (one part in 10^{10}, or better, long term). For the 50-w output, an all-solid-state design is considered here, but further study should be made to choose between solid-state and a TWT. An output of 50-w should be possible within the next year or two as varactor diodes are improved. However, a 20-w solid-state output is available today by utilizing a power amplifier followed by a varactor multiplier.

3.2.2 Transmitter Design

Figure 12 is a block diagram of a transmitter that will fulfill the requirements. The 130.36-MHz input signal is amplified and used to drive the phase modulator. After phase modulation, the signal is amplified and multiplied to 522.24 MHz. At 522 MHz, power off, 100 w is generated to drive a tripler, which provides 50 w at 1566 MHz. A bandpass filter is indicated to limit any out-of-band energy from the transmitter. Input power, gain or loss, active components and, in some cases, efficiencies are noted on each block. In the corner of Figure 12 is a breakdown of the input power anticipated and the overall efficiency of 23 percent that can be expected from such a design. The only part of the design that is limited is

*This bandwidth is adequate to meet the navigation signal requirements. However, since the transmitter will be time-shared with another signal (see Tracking Data Subsystem, subsec. 4.9) the transmitter should be designed for a bandwidth of 20 MHz.

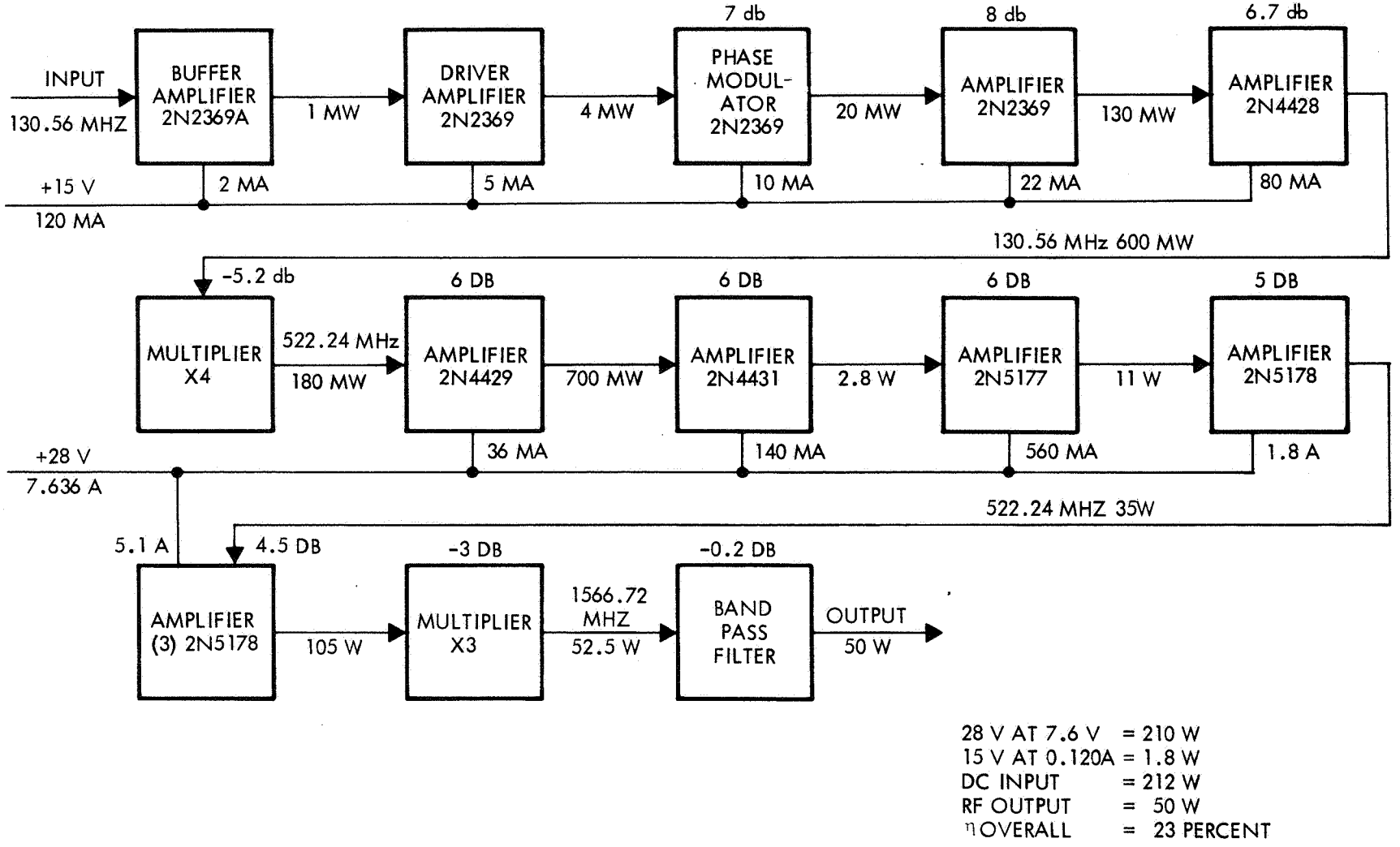

Figure 12. 50-W Transmitter

the final tripler, and available diodes for this application fall short of the capability required. A diode for this application would have the following requirements:

Maximum diode loss:	1.5 db
Diode efficiency, n:	70 percent
W_o/W_c:	0.025 (min)
$f_c = \frac{1.5 \text{ gHz}}{0.025}$:	60 gHz (min)
Dissipation:	50 w
Temperature gradient, θ_{jc} for 100°C temperature rise	
2 diodes :	4°C/w
4 diodes:	8°C/w

A block diagram of the tripler stage is shown in Figure 13. A total of 3 db is allowed for dissipation in the tripler stage, and one-half of that loss is in the diode. Diodes that are now available for this application are the VAB-811, made by Varian-Bomac, and the MV1807-1, made by Motorola. Both have 60 gHz cut-off frequency. The VAB-811 has a θ_{jc} of 7°C/w, and the MV1807-1 has a θ_{jc} of 6°C/w. As can be seen from these figures, the capability of these diodes is very close to the requirements of the transmitter, and the multiple chip or stacked varactor developments should provide the capability needed shortly. One other possibility would be to use a power splitter, two triplers in parallel, and a power combiner in the output. These could be used with today's components at a small reduction in overall efficiency.

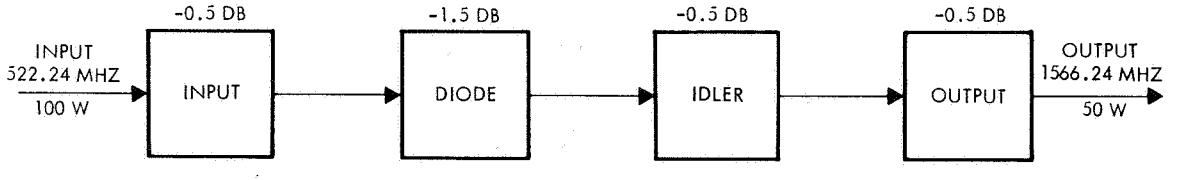

Figure 13. Tripler Stage

The 130.56-MHz input drive frequency for the transmitter is derived from the ultra-stable oscillator in the time base unit of the navigation signal subsystem. A block diagram of the frequency synthesizer is shown in Figure 14. The 5.12-MHz oscillator frequency is multiplied by 21 in a cascaded tripler and X7 multiplier to obtain 107.52 MHz. In addition, the 5.12-MHz oscillator frequency is also mixed with half the frequency obtained from the divide-down chain in the time base unit, and the 7.68-MHz frequency out of the mixer is tripled to obtain 23.04 MHz. Finally, this frequency and the 107.52-MHz frequency are mixed to obtain the 130.56-MHz drive frequency for the transmitter. Bandpass filters are shown throughout the synthesizer to remove spurs from the multipliers and mixers.

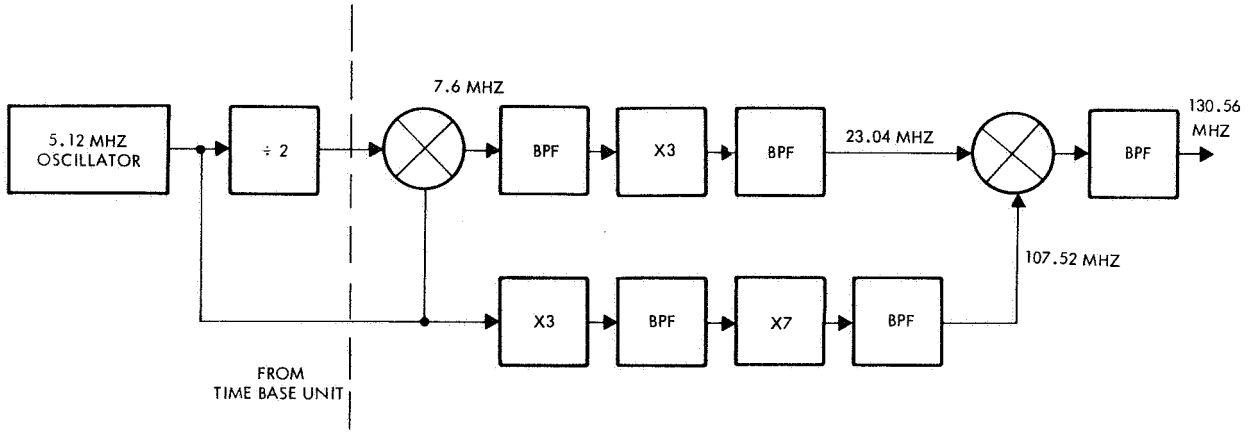

Figure 14. Frequency Synthesis for Transmitter Drive

3.3 COMMUNICATIONS (VOICE) LINKS

In this subsection, a typical voice link for air traffic control is discussed. Further study will define digital links to be used for traffic control.

The overall system block diagram and signal flow are give in Figure 15. The link from ground station to satellite is at SHF in accordance with current COMSAT corporation philosophy.

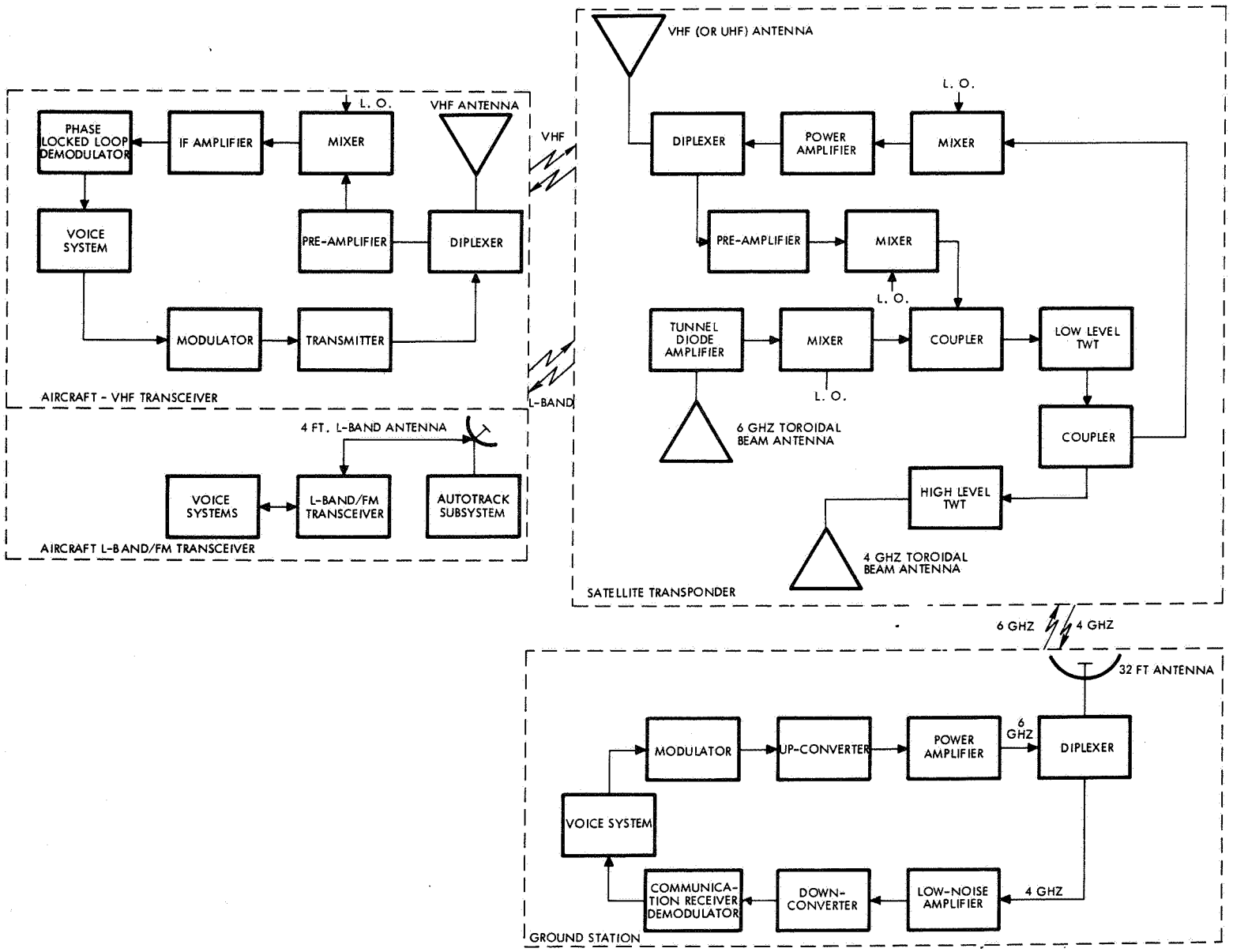

Figure 15. VHF (or UHF)/SHF Voice Link Functional Block Diagram

Although the L-band region appears as a clear choice for a high-accuracy (implying wideband width) navigation signal,* the choice of frequency band for aeronautical voice communications is not so clear cut at this time. The airlines strongly prefer the VHF region for the following reasons:

1) Assumed compatibility with existing VHF communication.

2) The ability to use a low-gain antenna.

However, spectrum limitations and international complications cloud the issue greatly, and there is pressure to use the L-band region despite the very real disadvantages from the point of view of the airlines. Since the situation is unresolved at this time, both frequency bands are considered in this analysis.

3.3.1 Link Performance

The traffic control ground station is proposed to have a 32-ft parabolic reflector, operating at 54-percent efficiency. With an uncooled paramp, the station's sensitivity parameter, G/T, is 24.0 db.

The satellite's transponder for traffic control communications consists of:

- Two toroidal beam antennas (circularly polarized, CP), a tunnel diode pre-amp, and two TWT's at SHF;
- A mechanical despun antenna (CP, diplexer, a transistor (or tunnel diode) pre-amp, and a solid-state transmitter at VHF and UHF.

The aircraft uses a VHF omnidirectional antenna (CP),** diplexer, transistor pre-amp, phase-locked loop receiver, and a power amplifier.

Table VI presents the system power budgets for the four links (i.e., ground-satellite, satellite-ground, satellite-aircraft, and aircraft-satellite) involved in creating a two-way simplex system capability. The

*See TRW Proposal No. 8710.000, "Study of Navigation and Traffic Control Employing Satellites," 24 January 1967.

**At UHF, the aircraft is required to have an electronically steerable antenna.

TABLE VI.

TWO-WAY SIMPLEX VOICE LINK-RF POWER BUDGETS PER CARRIER

Link Parameters	Ground Station to Satellite	Satellite to Ground Station	Aircraft to Satellite		Satellite to Aircraft	
			(118 to 136) VHF	(1540 to 1660) UHF	(118 to 136) VHF	(1540 to 1660) UHF
Carrier frequency, MHZ	6,000	4,000	130	1,600	130	1,600
Transmitter power output, dbw	17.0	0.0	26.9	13.0	20.0	10.0
Transmission circuit losses, db	0.5	1.0	2.0	2.0	1.0	1.0
Transmitter antenna gain, db	53.0	4.0	0.0	25.0	12.0	15.0
Effective radiated power, dbw	69.5	3.0	24.9	36.0	31.0	24.0
Path loss (R = 22,000 nmi), db	200.3	196.8	167.1	188.1	167.1	188.1
Polarization loss (CP-to-CP), db	0.2	0.2	0.2	0.2	0.2	0.2
Atmospheric effects	3.0(1)	2.0(1)	-(2)	0.5(3)	-(2)	0.5(3)
Multipath allowance			3.0(4)		3.0(4)	
Receiving antenna gain, db	3.5	49.6	12.0	15.0	0.0	25.0
Received carrier power, dbw	-130.5	-140.4	-133.4	-133.8	-139.3	-139.8
Receiver noise density,(5) dbw/Hz	-200.0	-205.6	-197.5	-199.6	-198.6	-199.6
Carrier-to-noise density ratio, db-Hz	69.5	59.2	64.1	61.8	59.3	59.8
Required carrier-to-noise density ratio, (6) db-Hz	-	53.1	-	-	53.1	53.1
Margin, db	-	6.1	-	-	6.2	6.7

Notes:
1. Rain margin (Ref. 3).
2. Value undefined; therefore, a 6-db margin should be used to account for it (Ref. 1).
3. Atmospheric and ionospheric attenuation (Ref. 2).
4. Theoretical value for elevation angles of approximately 10^{o} (Ref. 1).
5. The respective receiver system noise temperature (T_s):
   - Satellite (6 GHz) $720^{o}K$
   - Ground (4 GHz) 200
   - Satellite (VHF) 1300
   - Satellite (UHF) 800
   - Aircraft (VHF) 1000
   - Aircraft (UHF) 800
6. This required carrier-to-noise density ratio is for a simplex system using FM with a phase-locked loop demodulator (see discussion).

critical link for voice communications is the satellite-to-aircraft path, since the most severe technical limitations are in the development of the satellite transmitter and the aircraft antenna.

The proposed voice system requires a satellite transmitter power output per carrier of 100 w at VHF or 10 w at UHF. The remaining transmitters require power outputs of:

1)	Ground:	50 w
2)	Satellite (SHF):	1 w
3)	Aircraft (VHF):	500 w
4)	Aircraft (UHF):	20 w

The densities of the voice receivers, Φ_n (i.e., kT_s) are determined by their system noise temperatures (T_s referenced at pre-amp or low noise amp) where,

$$T_s = \frac{T_a}{L} + \frac{T_t(L-1)}{L} + (F-1)\,T_o + T_{sat}$$

and T_a = antenna temperature contribution (^oK)

T_t = thermal temperature of the transmission line (approximately 290^oK)

L = transmission line loss (power ratio)

F = noise figure of pre-amps or low noise amps (power ratio)

T_o = standard reference temperature (290^oK)

T_{sat} = noise contribution of satellite (applicable to ground station and aircraft, assumed 30^oK)

The following tabulation lists the elements of the T_s calculation for each of the voice system receivers:

Receiver Location	Carrier Frequency (MHz)	T_a (^oK)	L (db)	F (db)	T_s (^oK)
Satellite	6000	290	1.0	5.0	720
Ground station	4000	30	0.5	1.42/112^oK	200
Satellite	130	1000	1.0	4.0	1300
Satellite	1600	20	1.0	5.0	800
Aircraft	130	1000	2.0	2.5	1000
Aircraft	1600	20	2.0	5.0	800

3.3.2 Modulation-Demodulation Discussion

Peaks in speech power 15 db above the average speech power can be expected for about 0.1 percent of the time; however, peak clipping to reduce peaks in power to 7 or 8 db above average power still retains high speech intelligibility in voice systems. In calculating the voice output signal-to-noise ratio, $(S/N)_o$, it is convenient to use a full load tone in place of speech as the modulation signal. A sine wave has a peak factor of 3 db, i.e., the peak power is twice the average. Therefore, with a speech-peak factor (after clipping) of 7 db, a tone with the same peak power has a 4-db higher average power; or a system designed to provide a 20-db rms speech-to-rms noise ratio will have a 24-db full load tone-to-noise ratio.*

The voice system considered uses a phase-locked demodulator to take advantage of its threshold extension characteristics over a conventional FM discriminator. The design is completed by using the relationships and design curves presented in Ref. 5, where the standard FM

*P. V. Dimock and J. O. Repogle, "Technical Characteristics of Voice Communications Systems for Earth-Space Links" prepared for CCIR Study Group IV Subgroup I, 1 September 1961.

improvement (SNR) formula is rewritten as

$$\left(\frac{S}{N}\right)_o = \frac{3}{2} \frac{k^2 \Delta f^2}{(4.25\, f_o)^3} \left(\frac{C}{\Phi}\right)$$

where

k = peak speech-to-rms speech (7 db)

Δf^2 = mean square frequency deviation (Hz^2)

f_o = the break frequency of an average speech spectra, (800 Hz)

$\frac{C}{\Phi}$ = carrier-to-noise density ratio in the IF predetection bandwidth of the receiver.

For a demodulator specified to have an upper bound of 2 percent out-of-lock condition, combined with a peak factor of 7 db for voice, yields an rms frequency deviation of 1.92 kHz and a 20-kHz predetection bandwidth for the receiver.* For a full load tone signal-to-noise ratio of 24 db, the required IF carrier-to-noise ratio is 10 db. This gives a C/Φ of 53 db or 53.1 db, as is presented in Ref. 3, and this value is used as the required C/Φ in the power budget table.

Because the tropospheric and ionospheric effects are still undefined, the design allows a power margin of 6 db. Each additional carrier would require a 3-db increase in the effective radiated power of the satellite in each link tested.

---

*The voice channel bandwidth is equal to $4.25\, f_o$ or 3.4 kHz, and the equation for Δf (rms frequency deviation) is given by the relationship

$$\left(\frac{S}{N}\right)_o = 0.023\, k^2 \left(\frac{\Delta f^2}{p}\right)^{5/4}$$

where p = the percentage of out-of-lock time (2 percent)

3.3.3 Satellite Weight and Power Requirements for a Voice Channel

An estimate of the weight contribution and power requirements of the voice communications for a satellite VHF transponder are itemized in Table VII. The estimates are based on recent configuration studies completed at TRW (see TRW Report No. 8800.5.2-061 "Satellite Configuration Study for VHF Aeronautical Communications," by G. McDaniel, 10 April 1967). The dc-to-RF power efficiency criteria is 50 percent at VHF and 27 percent at SHF. Similar estimates for an L-band link are given in Table VIII.

TABLE VII

WEIGHT AND POWER REQUIREMENTS FOR THE VHF VOICE SYSTEM OF THE SATELLITE

Item	Weight (lb)	Regulated Power (w)	Unregulated Power (w)
Tunnel diode amplifier (SHF)	1.5	1.7	
Mixer	0.6		
Local oscillator (LO)	1.3	0.8	
Two couplers	0.4		
Low-level TWT	3.5		4.6
High-level TWT	8.5		3.7
Bandpass filter	1.2		
VHF lo-modulator (mixer)	0.7	0.5	
VHF power amp (with converter)	23.0		200.0
VHF pre-amp	1.5	1.0	
VHF mixer	0.5		
VHF lo	0.7	1.0	
VHF diplexer	2.5		
Cables and connectors	1.5		
Totals	47.4	5.0	208.3

TABLE VIII.

SATELLITE L-BAND WEIGHT AND POWER REQUIREMENTS
(SUPPLEMENT TO TABLE VII)

Item	Weight (lb)	Regulated Power (w)	Unregulated Power (w)
LO - modulator	3.0	1.0	
Power amplifier*	6.0		61.2
Pre-amplifier	1.0		6.0
Mixer	2.0		
Local oscillator	1.0	1.0	
Diplexer	3.3		
Cables and connectors	2.0		
Totals	18.3	2.0	67.2

*The power amplifier is comprised of a solid-state amplifier chain (i.e., 8 amps, each operating at 60 percent efficiency, with an overall 43-db gain) with a tripler and a bandpass filter.

REFERENCES

1. "Oscillator Error Statistics for NAVSAT," TRW No. 08710-6005-T00, 22 August 1967, A. J. Mallinckrodt.

2. Correspondence from E. J. Martin, Comsat Corporation, to Wm. T. Carnes, Chairman of Airlines Electronic Engineering Committee (AEEC) October 7, 1966. Contents of letter elaborate on Comsat's view of power budget values for the VHF satellite-to-aircraft link.

3 AEEC Letter No. 66-2-42 (Satcom Newsletter No. 9), Subject: Circulation of Satcom system power budget format suggested by FAA and Satcom/ATC system paper submitted by General Electric, 28 July, 1966.

4. "Navigation/Traffic Control Satellite Mission Study," proposal No. 09778.000, Part I, for NASA/ERC, 5 June 1967.

5. "Analysis of Multichannel Satellite Communications for Aeronautical Mobile Service," Hughes Aircraft Company Report SSD 60116R, March, 1966.

6. C. M. Thomas, "Optimization of Phase Lock Demodulator for Single Channel Voice," Microwave Journal, Vol. n. 7, June, 1967.

4. SATELLITE DESIGN

The satellite design presented in this section is one which provides users with complete navigation information. The ranging signal is sent with the data required to compute the satellite ephemeris. In addition, the design provides a communication link to transmit data from slave ground stations to the master computation stations. The design presented here does not provide links for traffic control data from low-performance terminals e.g., aircraft, but this capability will be considered in future studies.

The navigation-signal generation and transmitter subsystems have been discussed in detail in par. 3.2.1 and 3.2.2, and will not be repeated here.

A single-launch configuration has been considered (see Figure 16) A spacecraft weight of 516.4 lb can be boosted into the required transfer orbit using the Thor-Delta with a weight margin of 208.6 lb. A single-launch mode appears to be a desirable way to establish an interim operational capability of four satellites, as well as to replace satellites which have failed. (Further study might indicate the utility of a multiple launch using an Atlas Agena to implement the worldwide network). The proposed NAVSTAR spacecraft is spin-stabilized with a mechanically despun antenna. The rationale for the choice of spin-stabilization was documented in the original TRW proposal for this study, and need not be repeated here.

The satellite system block diagram is depicted in Figure 17. The navigation-signal generation subsystem generates the information used to modulate the transmitter whose output feeds the L-band mechanically despun antenna. The antenna is a fixed-feed design employing a despun parabolic reflector as depicted in Figure 18, the NAVSTAR satellite's inboard profile. The fixed feed is a laminated fiberglass structure. The reflector is constructed of Al honeycomb panels. This choice of material provides the required rigidity and ensures internal surface accuracies even after out panel damage (due to handling, micrometeorite, etc.) occurs. The polarizer is fabricated from Teflon-faced grid Cu sheet and honeycomb panels. The polarizer panel assembly completes the reflector's structure providing an integral, rugged, lightweight unit.

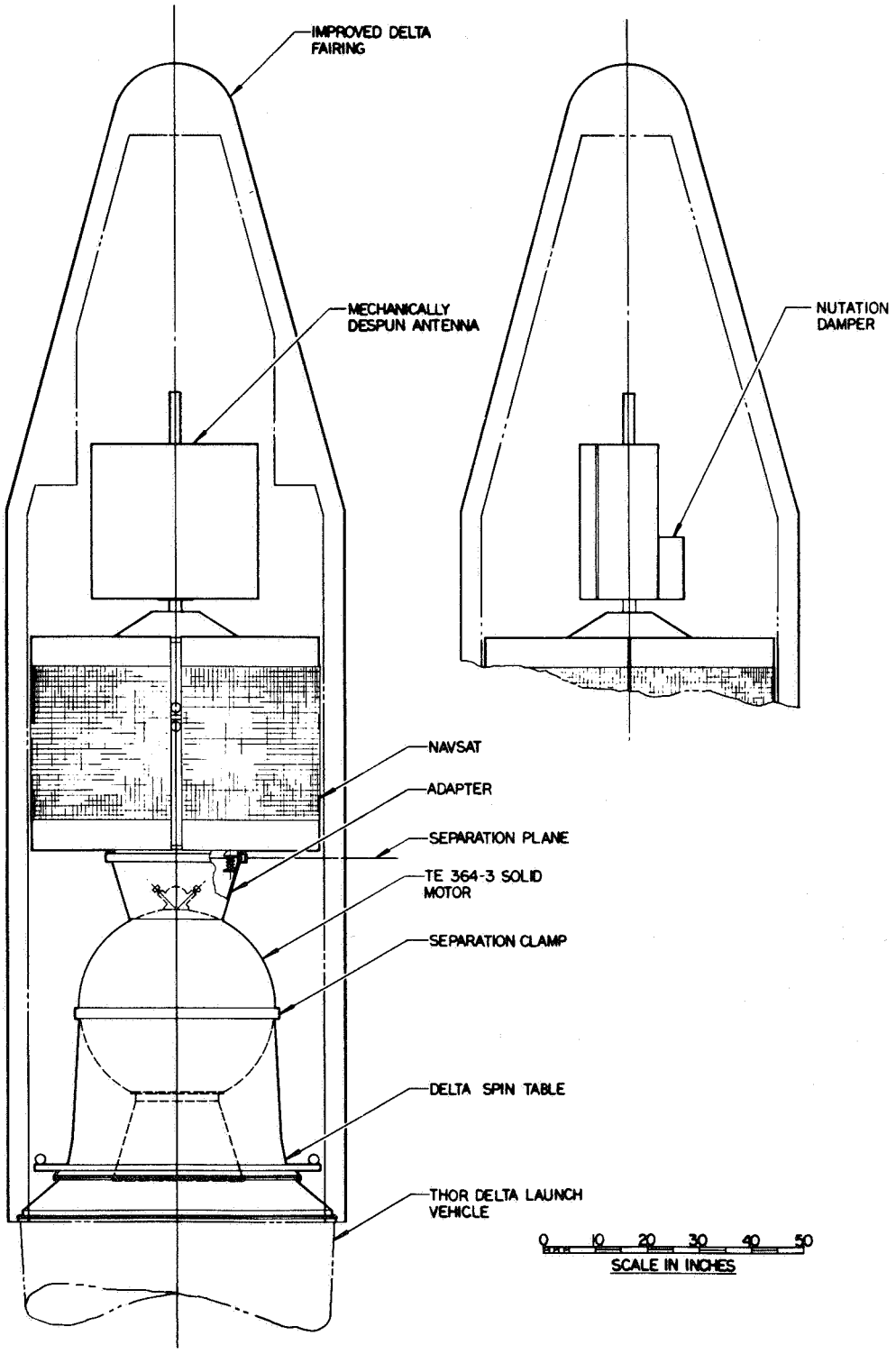

Figure 16. NAVSTAR – Single-Launch Configuration Booster Installation

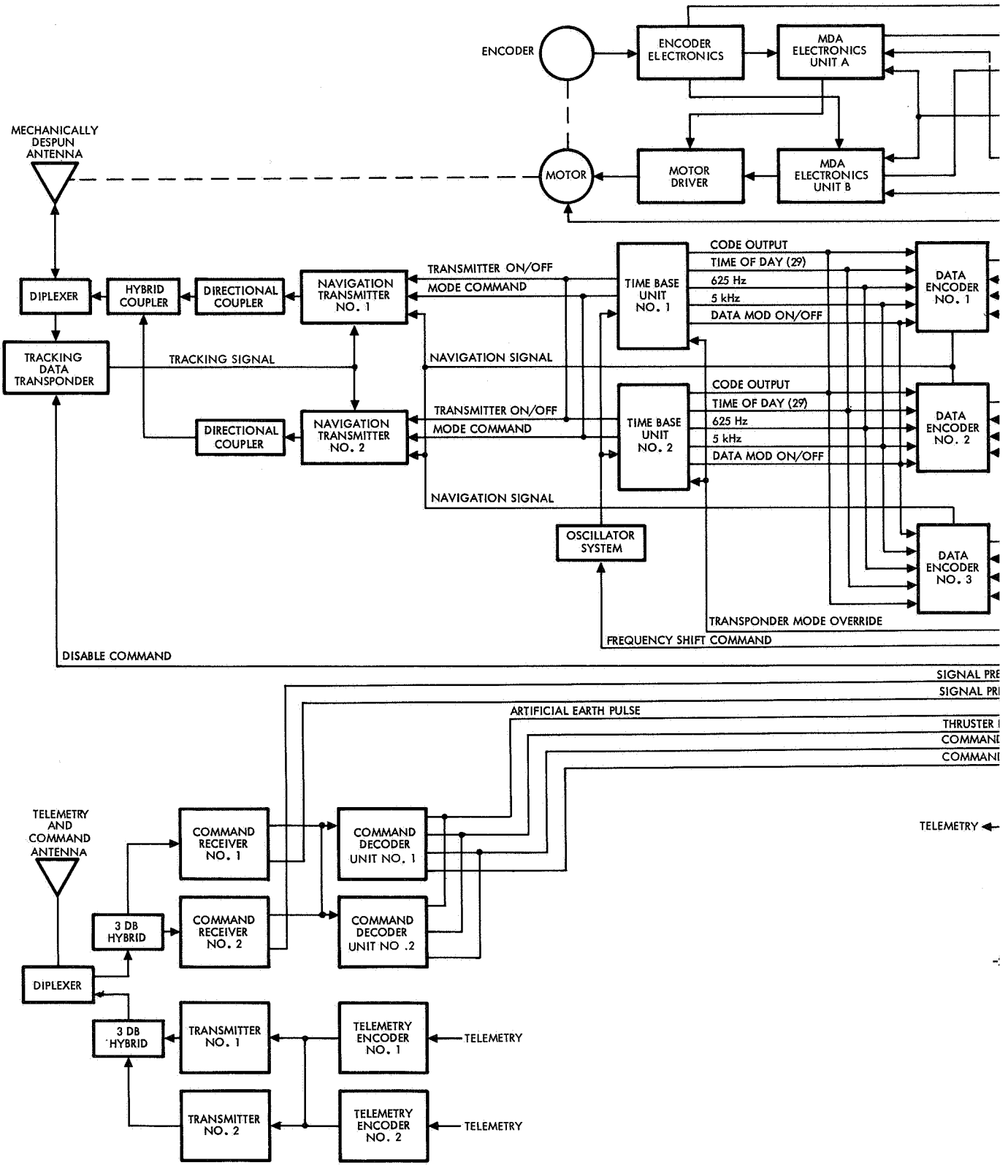

FOLDOUT FRAME 1

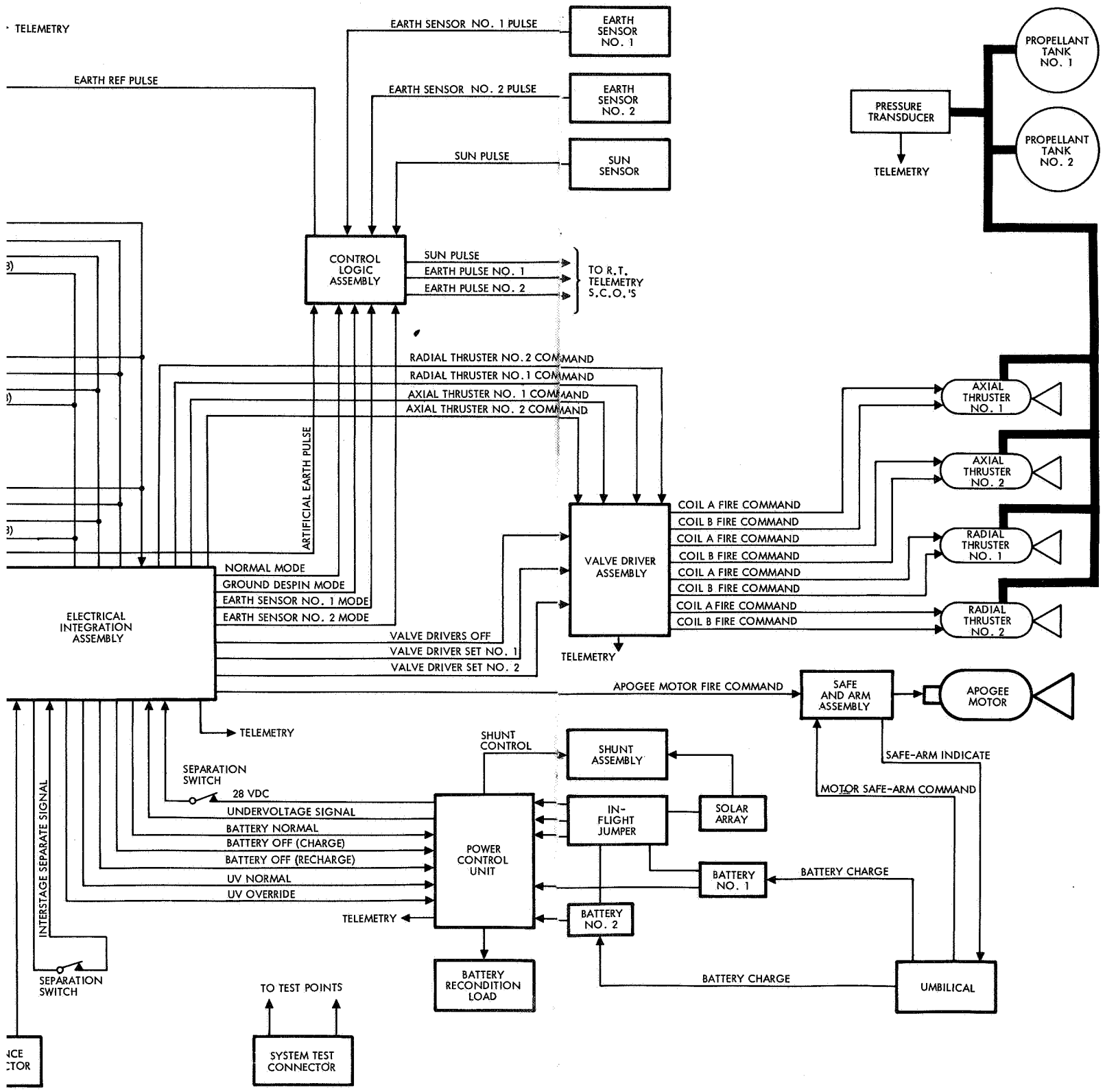

Figure 17. NAVSTAR System, Block Diagram

FOLDOUT FRAME 2

PRECEDING PAGE BLANK NOT FILMED.

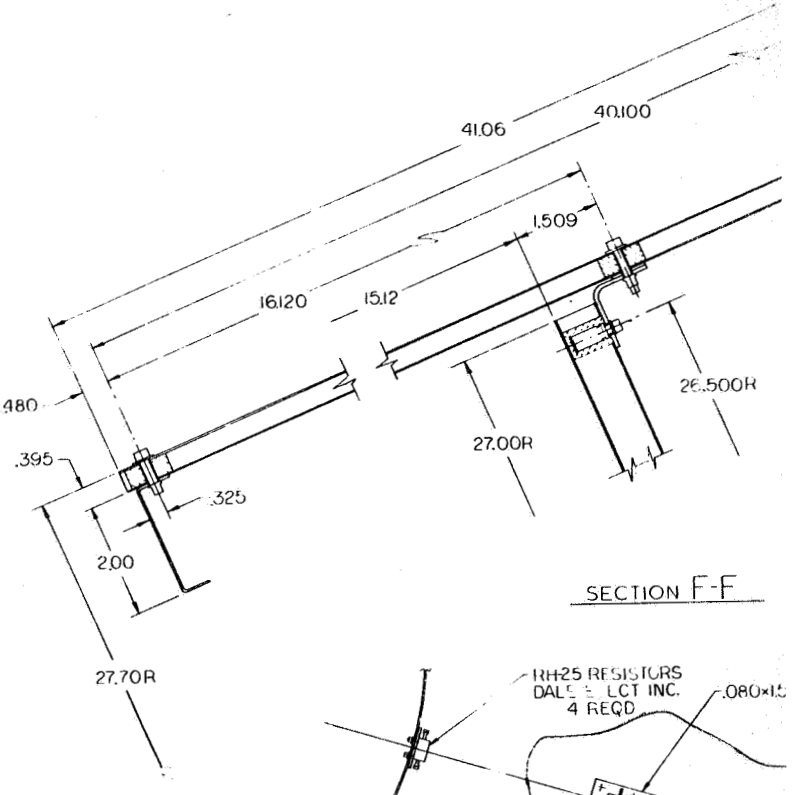

SECTION F-F

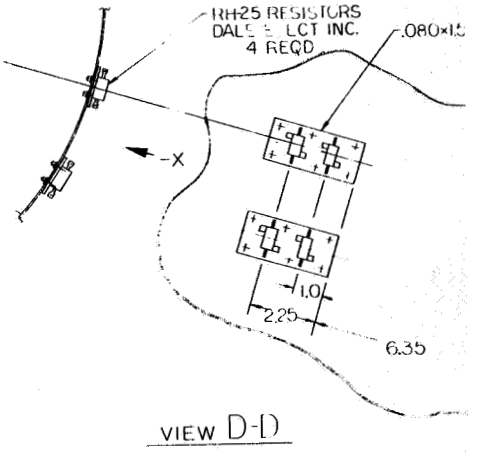

VIEW D-D

FOLDOUT FRAME 1

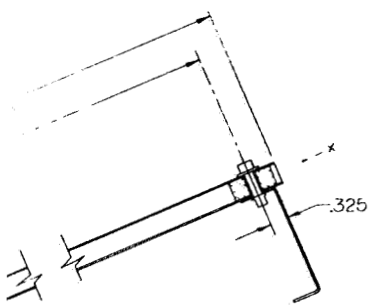

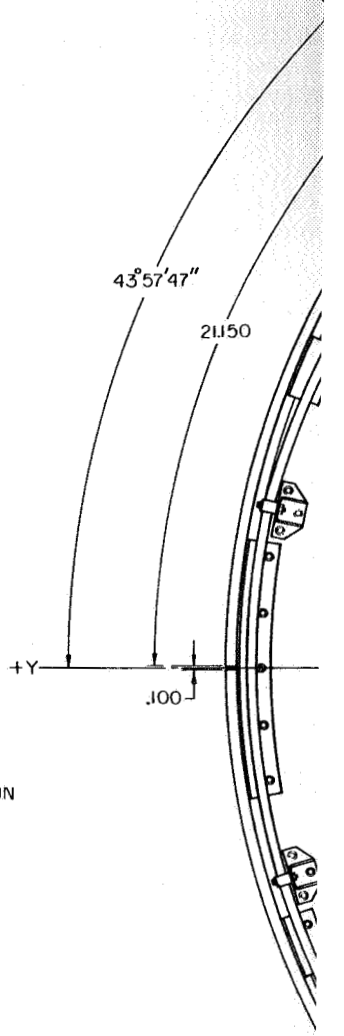

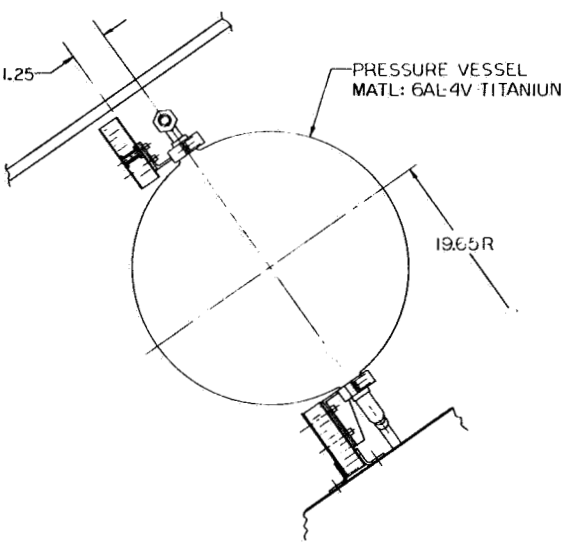

SECTION C-C

.325 AL. SHT.

FOLDOUT FRAME 2

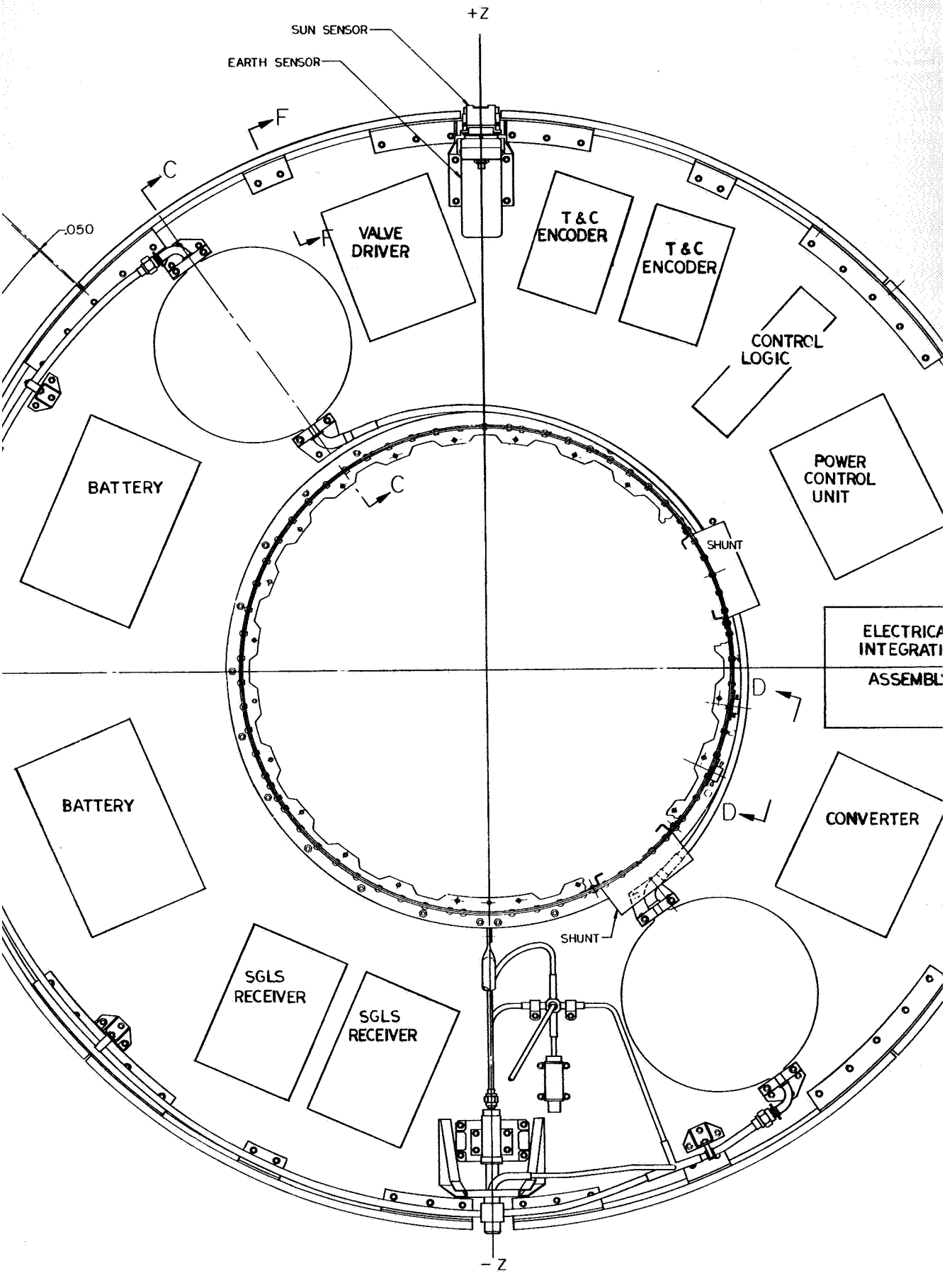

FOLDOUT FRAME

OMITTED APOGEE MOTOR
SECTION A-A

Fold

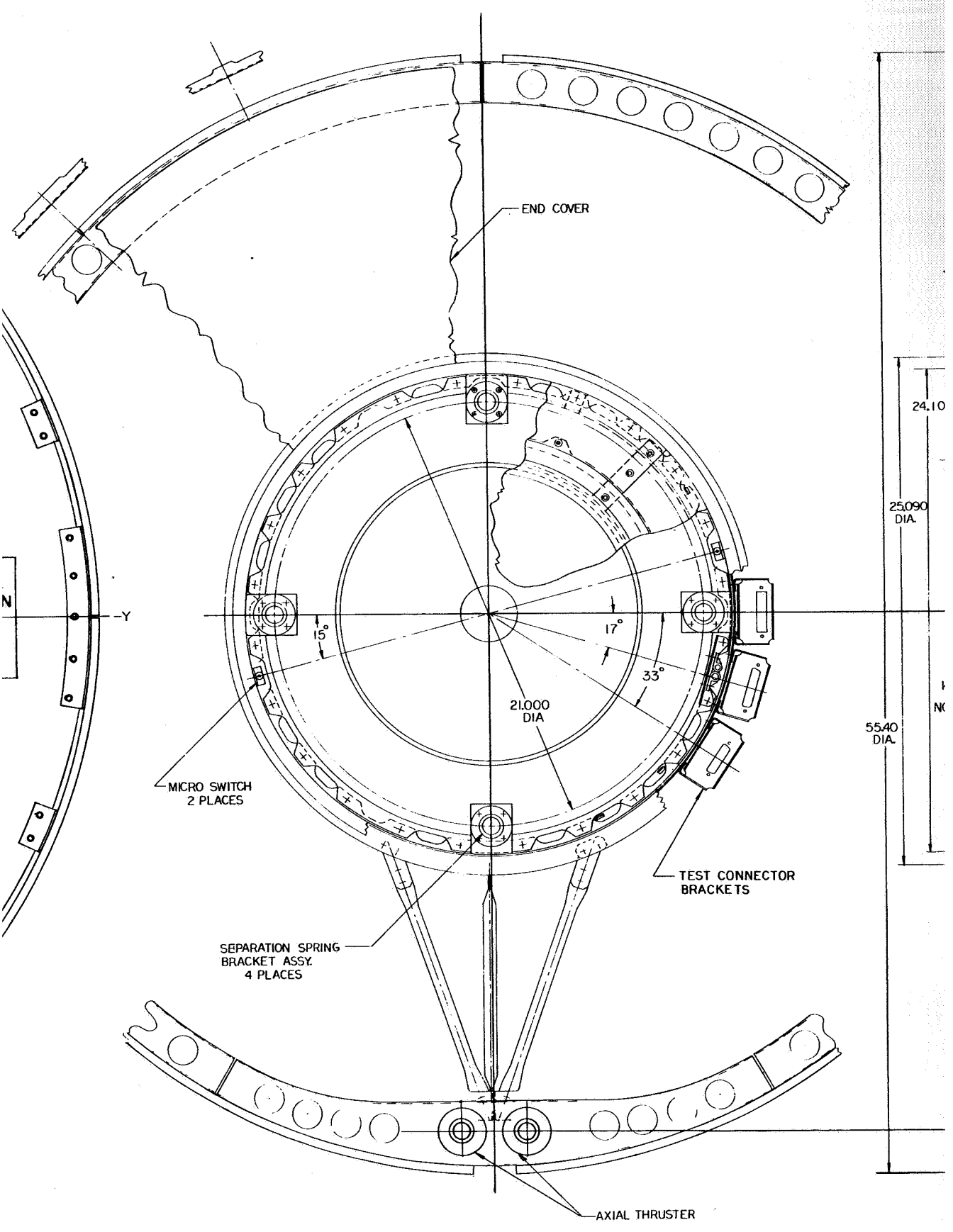

Out Frame 3

FOLDOUT FRAME

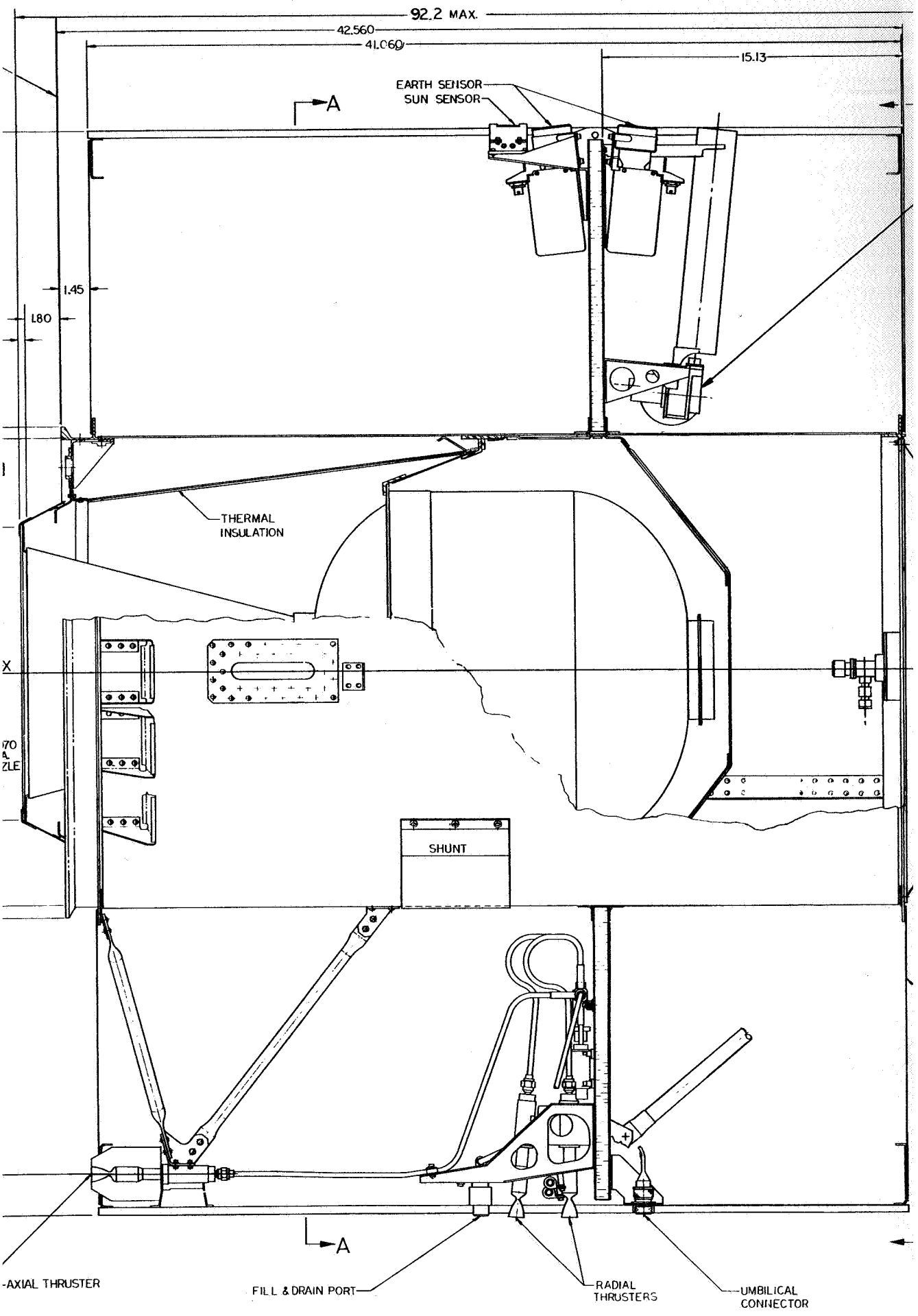

FOLDOUT FRAME 4

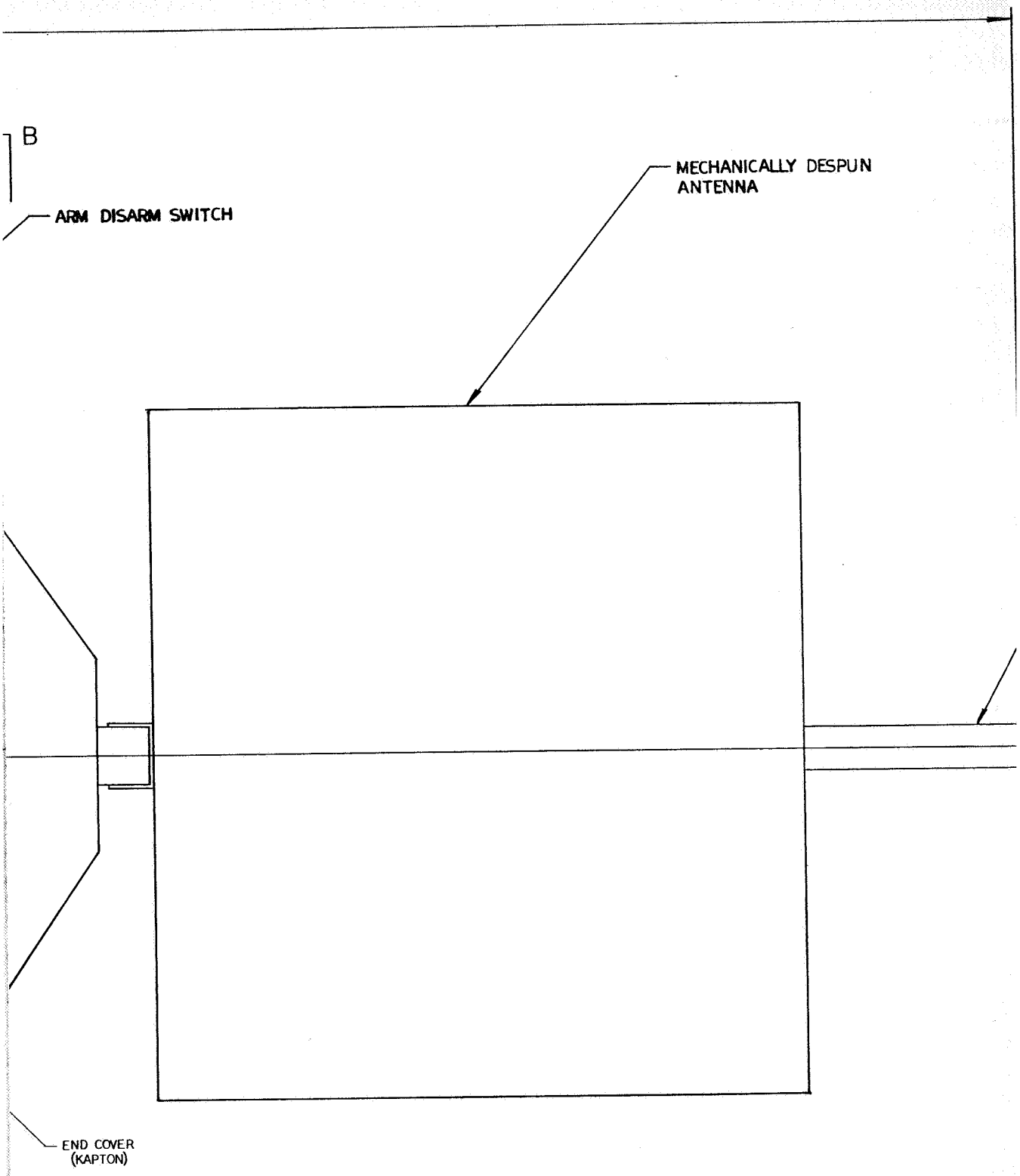

FOLDOUT FRAME 5

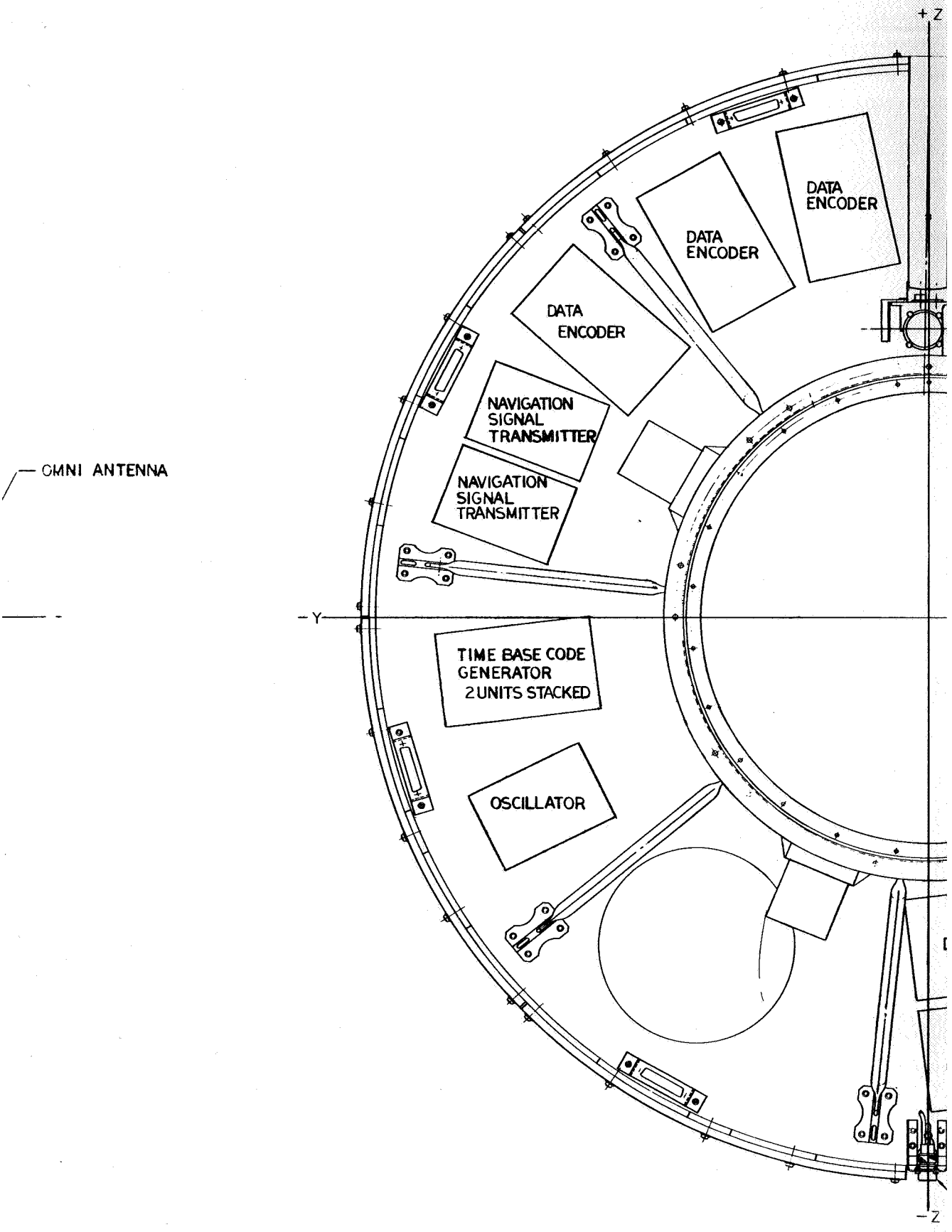

FOLDOUT FRAME 6

OMITTED ANTENNA, T
FRAME AND THRUSTERS

SECTION B-

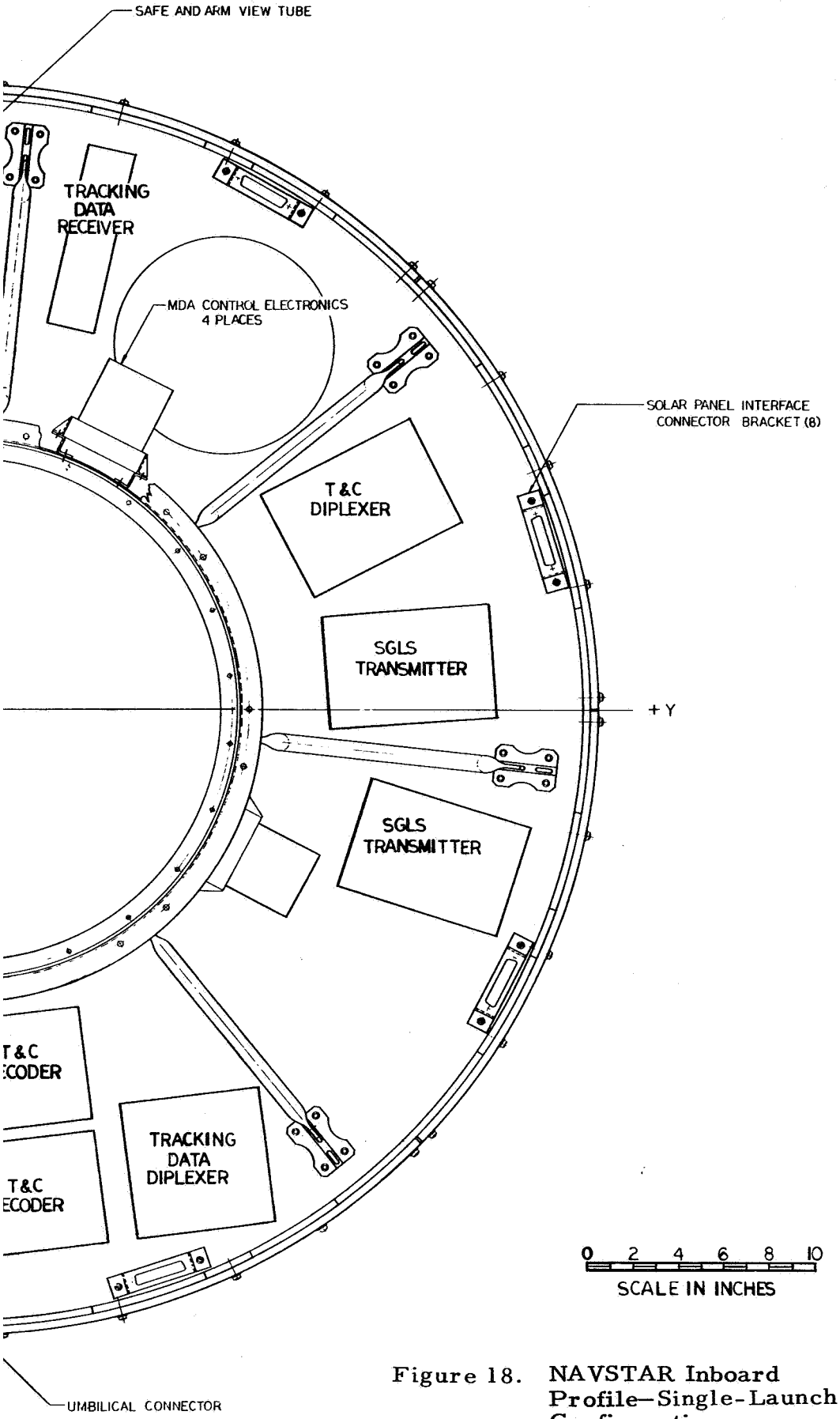

Figure 18. NAVSTAR Inboard Profile—Single-Launch Configuration

FOLDOUT FRAME 7

The omnidirectional antenna is built into an extension of the communication antenna fixed feed.

The positioning and orientation system is used to provide the impulse required for initial positioning in orbit, stationkeeping, and attitude control. It is a standard design of proven performance.

The apogee motor uses solid-propellant, providing 60,610 lb-sec of impulse in order to change from the transfer orbit to the final circular, synchronous orbit. It is a completely proven design.

The power supply is also a standard, flight-proven design consisting of solar cells, batteries, and power control units.

The telemetry subsystem relays attitude sensor data to the earth for processing control system commands along with normal housekeeping data. The command subsystem receives commands for engine firing, oscillator reset, ephemeris data, and spacecraft subsystem control.

The thermal design of the satellite is completely passive, thus providing a good thermal environment to the spacecraft with extremely high reliability.

The separation of the satellite from the interstage structure uses a system which is already in existence, and consists of a V-band clamp, redundant explosive nuts, and four match separation springs. To date, the system has been successfully flown on numerous spacecraft.

All subsystems are discussed in detail in the ensuing subsections.

4.1 NAVSTAR STRUCTURE SUBSYSTEM

The NAVSTAR structure subsystem is the basic framework of the spacecraft. Its primary function is to integrate with minimum weight the other subsystems comprising the spacecraft. It must also provide sufficient strength, rigidity, and other physical characteristics to withstand ground and mission environments and provide the required support and alignment for spacecraft components and assemblies.

4.1.1 Structural Requirements

The spacecraft structure is designed to withstand simultaneously the application of design limit loads and other environmental phenomena without experiencing excessive elastic or plastic deformation which would reduce the probability of successful completion of the mission. The design limit loads are the maximum loads that may reasonably be expected to occur in service.

The spacecraft structure is designed to withstand simultaneously the application of design ultimate loads and accompanying environments without failure. Design ultimate loads are the product of the design limit loads and a factor of safety, which is 1.50 for the general structure. The ability of the design to sustain these loads is substantiated by analysis and test during the spacecraft development.

The design limit inertia loads imposed on the structural subsystem are presented in Table IX. They are based on a 510-lb spacecraft launched by an improved Thor-Delta booster and injected into orbit by a 7700-lb thrust apogee motor. All launch and boost inertia loads are transmitted through the spacecraft central cylinder and reacted at the booster interface. Injection inertias are reacted by apogee motor thrust.

In addition to the inertia loads, the structure subsystem is designed to withstand the qualification levels of sinusoidal and random vibration shown in Table X, applied separately.

TABLE IX

LIMIT DESIGN LOAD FACTORS

	Condition	Load Factors (g) Longitudinal*	Lateral**
1)	Launch	+4	<1
2)	Transonic	+4	<1
3)	Max $q\alpha$	+6.2	<1.25
4)	Thor B.O.	+8.5	0.8
5)	TE 364-3 B.O.	+15.3	0
6)	Orbit Injection	+25.4	0

*The longitudinal direction refers to the booster thrust axis and is designated as the "X" axis on the spacecraft. The symbol + equals the load acting aft.

**The lateral direction refers to any axis normal to the X axis.

TABLE X

QUALIFICATION VIBRATION LEVELS

Sinusoidal (one sweep each axis at 2 octaves/min)

Longitudinal Axis		Lateral Axis	
Frequency (Hz)	Level (g rms)	Frequency (Hz)	Level (g rms)
10-19	2.12	5-250	1.63
19-25	3.18	250-400	2.12
25-250	2.12	400-2000	5.3
250-400	3.18		
400-2000	5.3		

Random (4 min per axis)

Longitudinal and Lateral Axes	
Frequency (Hz)	Level
20-150	0.023 g^2/Hz
150-300	3 db/octave increase
300-2000	0.045 g^2/Hz

4.1.2 Structural Description

The primary structural member of the spacecraft is the central cylinder as shown in Figure 18. It provides support for the apogee motor, antenna, equipment platform, and solar panels, and is constructed of 0.040-in. Mg sheet. Mounted to its forward end is a forged ZK-60A Mg flange, which attaches to the antenna and accommodates ground handling provisions. The flange on the aft end of the cylinder is a 7075 Al forging which transmits the spacecraft inertia loads to the booster adapter.

The annular equipment platform is an Al sandwich. The face sheets are 0.015 in. and the core is 0.75-in. thick – 1/8-0.001 honeycomb. The outer circumference is supported by eight canted Al struts while the inboard portion fastens directly to the cylinder. The rocket motor is mounted inside the cylinder and is joined to it by a support cone secured to a ring inside the cylinder.

The solar array consists of eight panels, which are bolted to the outer circumference of the equipment platform to form a cylindrical array. The upper and lower portions of the cylinder are secured together by two Al channel section rings. The rings act as redistribution members, transferring lateral loads from normally loaded panels to adjoining panels so they can be transferred as shear loads to the equipment platform. Longitudinal loads are transferred directly to the platform by the Al-fiberglass honeycomb substrates.

The panels and end rings have been designed with sufficient stiffness to minimize deflections and assure that the solar cells remain on the panel during vibration loading.

4.1.3 Wobble Damper

The spacecraft moment of inertia ratio, I_x/I_y, is less than 1. Consequently, damping in the rotor is destabilizing, and a damper must be placed on the despun portion such that its damping exceeds the damping in the rotor. For this purpose, a spherical pendulum damper will be considered (see Figure 19).

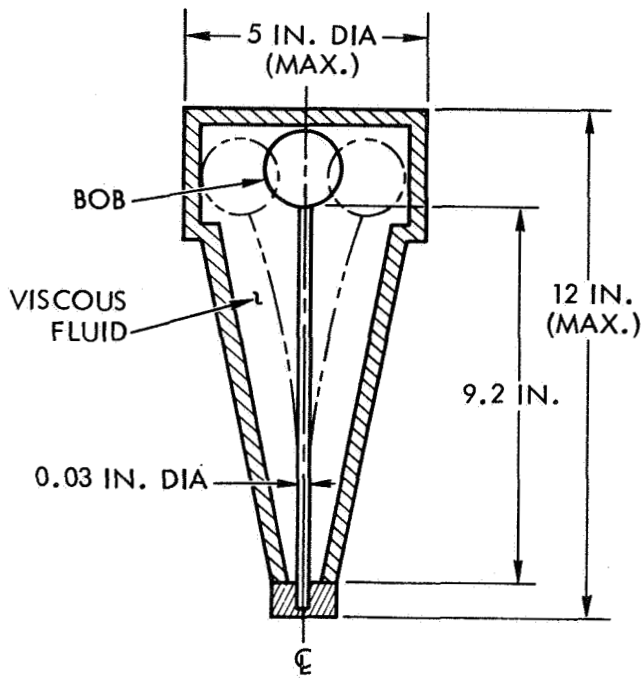

Figure 19. Conceptual Design of a Wobble Damper

A spherical damper similar to that used on OSO has been sized to exponentially decay the nutation angle with a time constant of 11.4 min. The predicted time constant is valid for nutation angles of less than 2^{o}. For larger angles, the bob will hit the case. Further analyses and tests will be required to predict the nutation decay rate for angles greater than 2^{o}.

The damper consists of a bob mass immersed in a viscous fluid and attached to the end of a cantilevered steel wire. Based on (1) a spin rate of 100 rpm, (2) the damper attached to the despun antenna, and (3) the spacecraft and damper centerlines being coincident, the basic design parameters are found to be:

Damper Design Parameters

Wire dimensions:	0.03 in. dia. by 9.2 in. long
Weight of bob:	0.5 lb
Damping coefficient:	0.092 lb/ft/sec

Using these design parameters, the following estimates are made of the maximum envelope dimensions:

Damper Envelope Parameters

Total weight:	3.0 lb
Damper envelope dimensions:	5 in. dia. by 12 in. long

4.2 MASS PROPERTIES

During the spacecraft study, a complete analysis of the mass property characteristics of the vehicle was accomplished. The objectives of the analysis were as follows:

- Assure that the payload weight does not exceed the capability of the boost vehicle, and that an adequate weight margin exists, to allow for possible growth.
- Minimize spacecraft weight, while considering spacecraft and subsystem performance, reliability, and cost.
- Position movable subsystem components within the spacecraft to assure that:
  1) The center-of-gravity of the spinning portion of the spacecraft lies on the spin axis.
  2) Lateral moments of inertia are nearly equal.
  3) Center-of-gravity travel due to expulsion of hydrazine is minimized.
  4) Products of inertia are held to a minimum to lessen the amount of balance weight required to dynamically balance the spinning portion of the spacecraft.

Spacecraft mass property characteristics are shown in Tables XI and XII. Table XI is a detailed weight breakdown showing subsystem elements, quantities, and weights. Table XII presents spacecraft weights, centers-of-gravity, and moments of inertia at launch, apogee motor burnout, and end of mission. (Figure 20 shows the spacecraft coordinate axes system used in the calculations.)

4.2.1 Mass Property Characteristics

1) Weight — As shown in Table XI, the total spacecraft weight is estimated to be 516.4 lb; the adapter between the spacecraft and the booster is estimated to weigh 25.0 lb. The Thor-Delta/TE-364-3 boost vehicle has an allowable payload weight of 750.0 lb, using a 100-nmi parking orbit; therefore, the weight margin is 208.6 lb.

TABLE XI

SPACECRAFT WEIGHT SUMMARY

Subsystem	Weight (lb)
Navigation Signal Subsystem	57.7
Oscillator (redundant)	3.6
Time base code generator (2)	1.6
Encoder (3)	4.5
Transmitter (2)	16.0
Despin assembly	8.8
Despin electronics	8.5
Cabling	1.7
Integrated antenna assembly	13.0
Telemetry and Command Subsystem	18.2
Receiver (2)	6.2
Transmitter (2)	4.8
Encoder (2)	2.2
Decoder (2)	3.6
Diplexer	1.4
Tracking Data Subsystem	4.0
Transponding receiver	3.0
Diplexer	1.0
Electrical Power Subsystem	70.1
Solar array	26.8
Battery (2)	28.6
Power control unit	8.0
Shunt (2)	3.2
Converter	3.5
Electrical Integration Subsystem	19.5
Electrical integration assembly	5.0
Cabling and connectors	14.5
Attitude Stabilization Subsystem	8.7
Control logic	1.5
Valve driver	1.5
Sensor assembly	2.7
Wobble damper	3.0

TABLE XI

SPACECRAFT WEIGHT SUMMARY (cont'd)

Subsytem	Weight (lb)
Positioning and Orientation Subsystem	7.8
Propellant valve (4)	1.5
Engine assembly (4)	0.6
Tank (2)	2.8
Fill and drain valve	0.3
Pressure transducer	0.2
Filter	0.3
Heat shield (2)	0.2
Heat sink (2)	0.3
Lines	0.8
Seals and joints	0.2
Nitrogen pressurant	0.6
Structure Subsystem	50.8
Equipment platform	11.1
Central cylinder	7.5
Motor mount	8.8
Separation ring	3.3
Antenna mount ring	1.4
Struts and fittings	2.6
Platform mount rings	0.9
Solar array ring – upper	1.1
Solar array ring – lower	1.1
Thruster support struts	0.6
Separation fittings	0.7
Hydrazine tank supports	0.5
Sensor mount	0.5
View tube	0.3
Wobble damper mount	0.5
Radial thrust mount	0.3
Aft closure	1.2
Aft end cover	1.3
Forward end cover	0.4
Miscellaneous attaching hardware	6.7
Thermal Control Subsystem	2.1
Thermal blankets	2.0
Propellant line insulation	0.1
Apogee Motor Subsystem	22.8
Apogee motor – burned out	21.5
Arm disarm switch	1.3
Balance Weights	5.0

TABLE XI

SPACECRAFT WEIGHT SUMMARY (cont'd)

Subsystem	Weight (lb)
Contingency (5%)	13.2
SPACECRAFT AT END OF MISSION	(278.1)
Attitude Control Propellant	11.8
SPACECRAFT AT APOGEE MOTOR BURNOUT	(289.9)
Apogee Motor Expendables	226.5
SPACECRAFT AT BOOSTER SEPARATION	(516.4)

TABLE XII

MISSION MASS PROPERTY CHARACTERISTICS

Spacecraft Condition	Weight, (lb)	Center-of-Gravity (in.)			Moments of Inertia, (slug-ft^2)		
		x	y	z	I_x	I_y	I_z
At booster separation	516.4	25.59	0	0	23.20	24.97	23.80
At apogee motor burnout	289.9	27.89	0	0	21.33	22.37	21.20
At end of mission	278.1	27.99	0	0	20.34	21.37	21.20

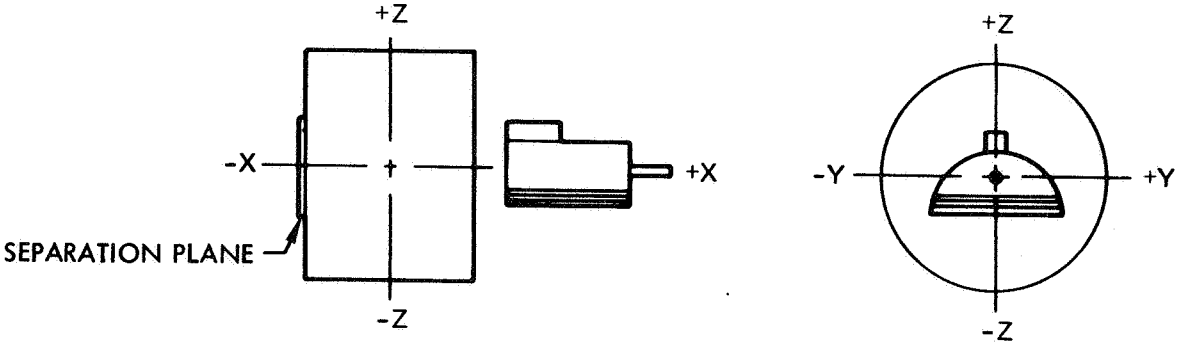

Figure 20. Spacecraft Coordinate Axes System

Many spacecraft subsystem components have been adapted for use directly from other TRW spacecraft programs. Therefore, if hardware exists for these items, actual component weights were used. All remaining subsystem weights were estimated by the designer.

2) Centers-of-Gravity — The centers-of-gravity of the spinning and despun portions of the spacecraft have been calculated to be on the spin axis and the center-of-gravity of the composite spacecraft remains on the spin axis throughout the life of the spacecraft. A longitudinal shift of 0.10 in. does, however, occur after apogee motor firing, but this is considered to be insignificant.

3) Moments-of-Inertia — As can be seen in Table XII, the ratio of the roll moment of inertia to the maximum transverse moment-of-inertia is for all conditions less than unity. The wobble damper, as a result, was placed on the despun portion of the spacecraft to maintain stability.

4) Products-of-Inertia — The spinning portion of the spacecraft will be dynamically balanced to align the principal axis with the geometric X-axis; however, no requirement exists to balance the despun antenna.

4.3 ELECTRICAL INTEGRATION ASSEMBLY

The electrical integration assembly (EIA) performs the functions of:

- Command processing and distribution
- Telemetry signal conditioning
- Power distribution
- Control of spacecraft ordnance
- Redundant command receiver control.

A functional block diagram of the EIA is shown in Figure 21. The EIA accepts a 9-bit binary coded command word from a redundant decoder interface. The command information is contained in 8 bits while the ninth bit is used as a steering pulse to determine if the information is a discrete command or data to be routed to the navigation system to update ephemeris and time information. The transmission gates interfacing with the navigation system will also accept an enable signal from the navigation system as a prerequisite for transmission of the update data. Discrete command information is accepted in redundant buffer gates and passed on to redundant decode logic, together with an execute pulse from the addressed decoder, generating one of 64 discrete commands.

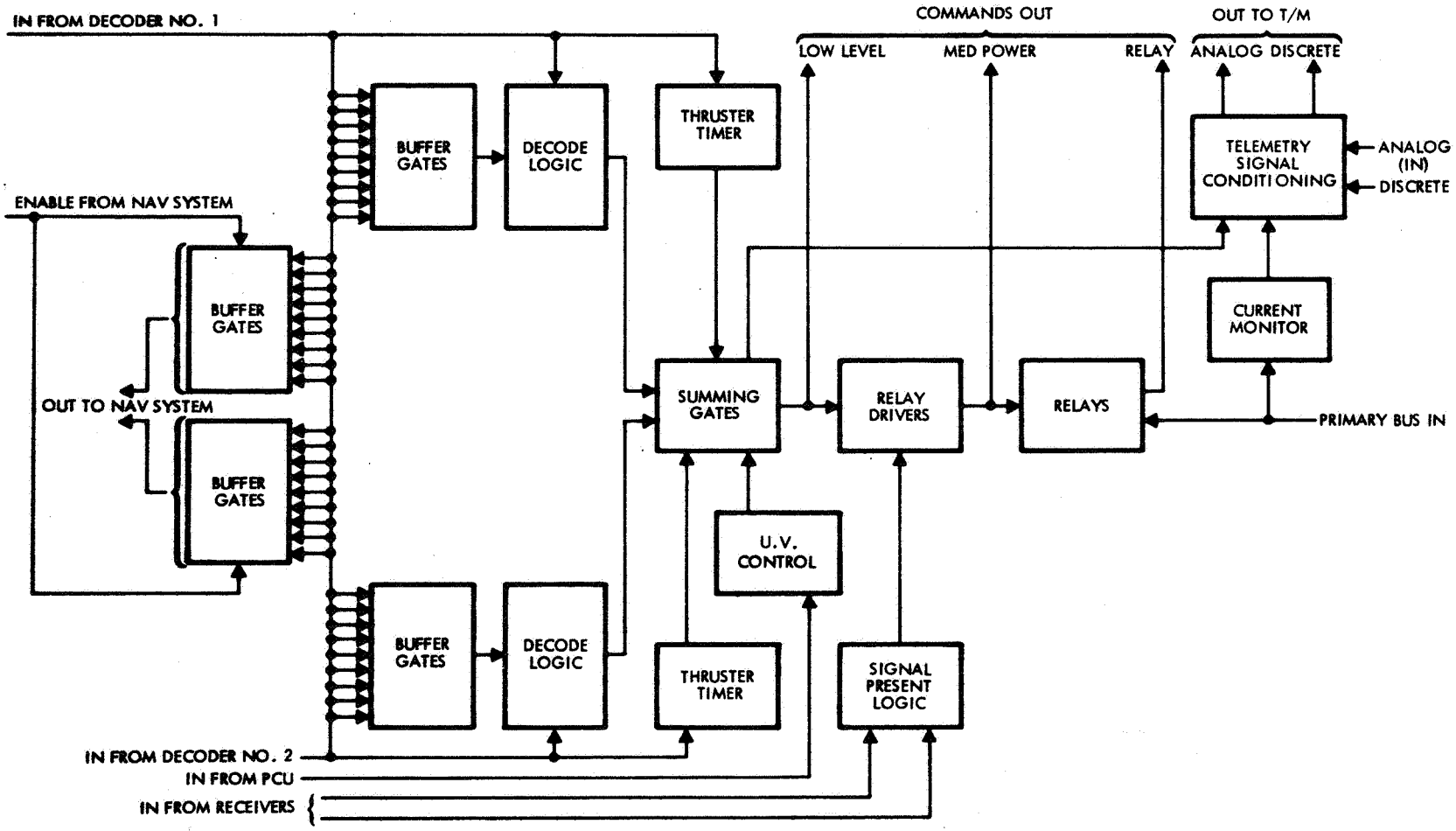

Figure 21. EIA Block Diagram

4.3.1 Command Type

The command outputs of the EIA will be of three standard types:

Type I, Low-Level Pulses

True state - 3.75 ± 1.25v
False state - 0.0 ±0.5v
Duration - 40 ±4 msec

The current amplitude cannot be defined until design is commenced and an integrated circuit family is selected; however, it is expected to be approximately 1 ma.

Type II, Medium Power Pulses

True state - 28.0 ±2.0v
False state - 0.0 ± 1.0v
Duration - 40 ±4 msec

The precise current requirements will be limited by a series resistor and will be negotiated with each using subsystem to ensure proper performance at minimum power.

Type III, Relay Closures

Momentary - 40 ±4 msec
or
Latching - Until commanded open
2A max capacity (resistive load)

In addition, any of the above commands can be provided with a pulse duration selected by ground command. The only use of this capability in the present design is for the fire periods associated with thruster firing.

App. C presents a list of the command requirements for NAVSTAR. A total of 21 spare commands exist in the present design.

The EIA will provide signal conditioning to match measured characteristics to telemetry input requirements. The EIA is currently sized (see app. D) to sum 27 discrete signals to 9 analog words (3 bits each),

supercommutation to 4 words of the main bus current monitor output, plus supercommutation to 4 words of the main bus voltage monitor, and conditioning of the 4 thruster fire periods to 1 real-time subcarrier input.

The EIA will also provide a main bus current monitor, and a main bus voltage monitor to provide sufficient load-rate information to allow a predictable state of health, and also allow vision of the effect of powering down specific equipment in a failure mode.

The EIA will accept the signal-present signal from both receivers and logically control both receivers to be "on" in the event neither receiver is in a carrier lock condition, and will turn "off" receiver No. 1 when receiver No. 2 has a carrier lock condition or turn "off" receiver No. 2 when receiver No. 1 has a carrier lock condition.

The EIA will, on receipt of an undervoltage condition signal from the power control unit, power down all equipment designated as "Nonessential Loads." This feature may be enabled or disabled at any time by means of a command override. All equipments on the nonessential bus may also be independently powered "on" or "off" by command from the ground.

The EIA will provide the electronic circuitry required to fire the apogee motor and ordnance (separation squibs, etc.) by sequenced command and will include a fail-safe provision for these command outputs.

Also, the EIA will supply thruster firing signals of a ground selected duration to the valve driver assembly (VDA). This is accomplished by the two command tones, 2.0 and 2.9 kHz, into the command decoder. The command decoder will sense the "on" or "off" conditions of these tones and provide a discrete output to the EIA, which provides the periodic pulse to the thruster. The 2.9-kHz tone is considered "on" and the 2.0-kHz tone is considered "standby." By switching, through ground command, from the 2.0 to the 2.9-kHz tone for a specific duration and then switching back, a pulse of that duration will be conveyed to the EIA. The EIA applies this pulse to one of four thruster lines to the VDA. The proper line will have been selected by a previously generated Type I command.

4.4 ANTENNA SUBSYSTEMS

4.4.1 Navigation System Antenna

The navigation system antenna will provide earth coverage to within 10° above the horizon. This cone has an earth subtended angle at synchronous orbit of about 17.4°. A margin added to either side of the earth angle to allow for antenna pointing and spacecraft orientation errors requires the spacecraft antenna to illuminate a subtended angle of about 20°. The satellite spin requires that the antenna radiate in either an omnidirectional mode about the spin axis or that the antenna be spun in the opposite direction at a rate equal to the satellite spin rate to keep the beam pointed at the earth.

In order to achieve increased gain, allowing simple user antenna systems, the mechanically despun reflector system will be used. The polarization of the spacecraft navigation antenna system is circular to permit polarization diversity to the aircraft antennas.

The proposed L-band (1540-1660 MHz) navigation system antenna consists of a mechanically despun, parabolic, cylindrical reflector illuminated by an array of four collinear dipoles. The resultant linearly polarized wave is converted to a circularly polarized wave by use of a three-sheet printed circuit polarizer in front of the antenna aperture.

The mechanically despun antenna system was selected over an electronically despun antenna system due to its superior electrical performance, lower development costs, and lighter weight.

The proposed polarizer system (Ref. 1) proved to be the most satisfactory design based on a study of various polarization techniques conducted for the Advanced Pioneer Spacecraft Program. Further investigation could possibly produce a polarizer design of one or two sheets, thus reducing weight and manufacturing costs. Figure 22 shows the design parameters for this system. The 30- by 32-in. aperture radiates a conical beam with half-power beamwidths of about 18° in both vertical and horizontal planes. The 0.4-db beamwidth of this antenna is approximately 20.5°. The 10° above-horizon, "earth-edge" gain is 16.0 db with respect to a circularly polarized isotropic source.

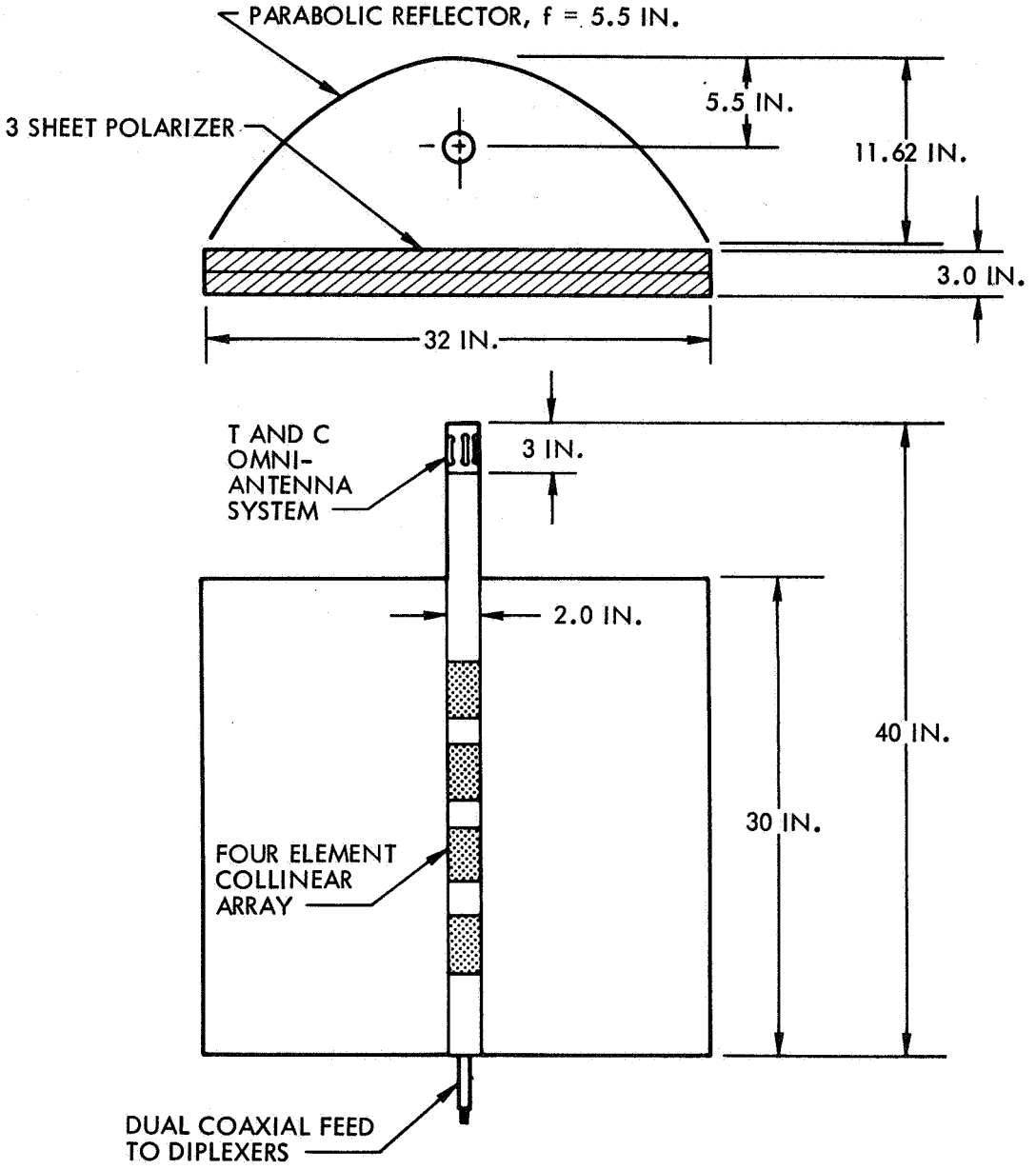

Figure 22. NAVSTAR Antenna System

4.4.2 Telemetry and Command Antenna System

The S-band telemetry and command antenna system operates at frequencies of 1800 and 2200 MHz. A diplexer system is proposed for use with the cavity-backed slot antenna to provide uplink and downlink communications. The antenna is mounted above the collinear dipole array of the navigation system antenna and fed by the center section of a dual coax system. This slot antenna has a radiation pattern similar to a half-wave dipole antenna. The cavity-backed slot antenna design is presently used on the Pioneer antenna system. Peak gain of this system is 0 db with respect to a linearly polarized isotropic source. The position of this antenna with respect to the navigation system antenna is shown in Figure 22.

4.5 ANTENNA DESPUN AND ATTITUDE CONTROL SYSTEM

4.5.1 Antenna Despun System

The mechanically despun antenna control system (MDACS) is designed to counterrotate an antenna relative to the spin-stabilized satellite so that the antenna is approximately inertially fixed, and to point the antenna at the earth. Functionally, the MDACS consists of the following six subsystems.

- Stepper motor and antenna
- Encoder
- Phase-lock loop
- Digital position circuit
- Motor damper circuit
- Motor starting circuit

The stepper motor is a rotary solenoid with 128 equally spaced positions. The motor rotates from one position to the next every time a new pulse is applied to the motor. Thus, the speed of the motor is dictated by the pulse rate applied to the motor. The antenna is part of the motor rotor and thus rotates at motor speed.

The encoder provides a measure of the angular position of the antenna relative to a null position or "fiducial mark."

The phase-lock loop is, in effect, a digital oscillator that provides the pulse train to drive the motor. The frequency or pulse rate of the oscillator is controlled by an error voltage that is determined by comparing the phase of the satellite rotation (from an earth-sensor reference pulse) with the phase of the pulse train from the oscillator.

The digital-position circuit is used to add or subtract a pulse from the pulse train that is driving the motor.

The motor-damper circuit provides rate and position feedback to ensure stable and accurate motor operation. It does this by phase shifting the pulse train being applied to the motor.

The motor-starting circuit provides a train of pulses to the motor. The pulse rate is increased from a low value to the desired rate as the motor is brought up to speed.

4.5.1.1 Operating Modes

The MDACS operates in three modes:

- Start mode
- Slew mode
- Indexing mode

A block diagram of the MDACS showing the interconnection of the six subsystems in the three operating modes is presented in Figure 23.

In the start mode, the motor is driven by a train of pulses which originate in an oscillator in the motor-starting circuit. The train of pulses is passed through the motor-damper circuit where the pulse train is modulated by the rate-plus-position feedback signals. The frequency of the oscillator is automatically increased from a low value to the desired value as the motor is brought up to speed.

When the motor reaches the desired speed, the motor-starting circuit also provides the logic to switch the pulse train from the motor-starting circuit to the pulse train from the phase-lock loop. In the slew mode the motor is driven by a train of pulses from the phase-lock loop. The pulse train from the phase-lock loop, as mentioned before, is synchronized with the satellite spin speed.

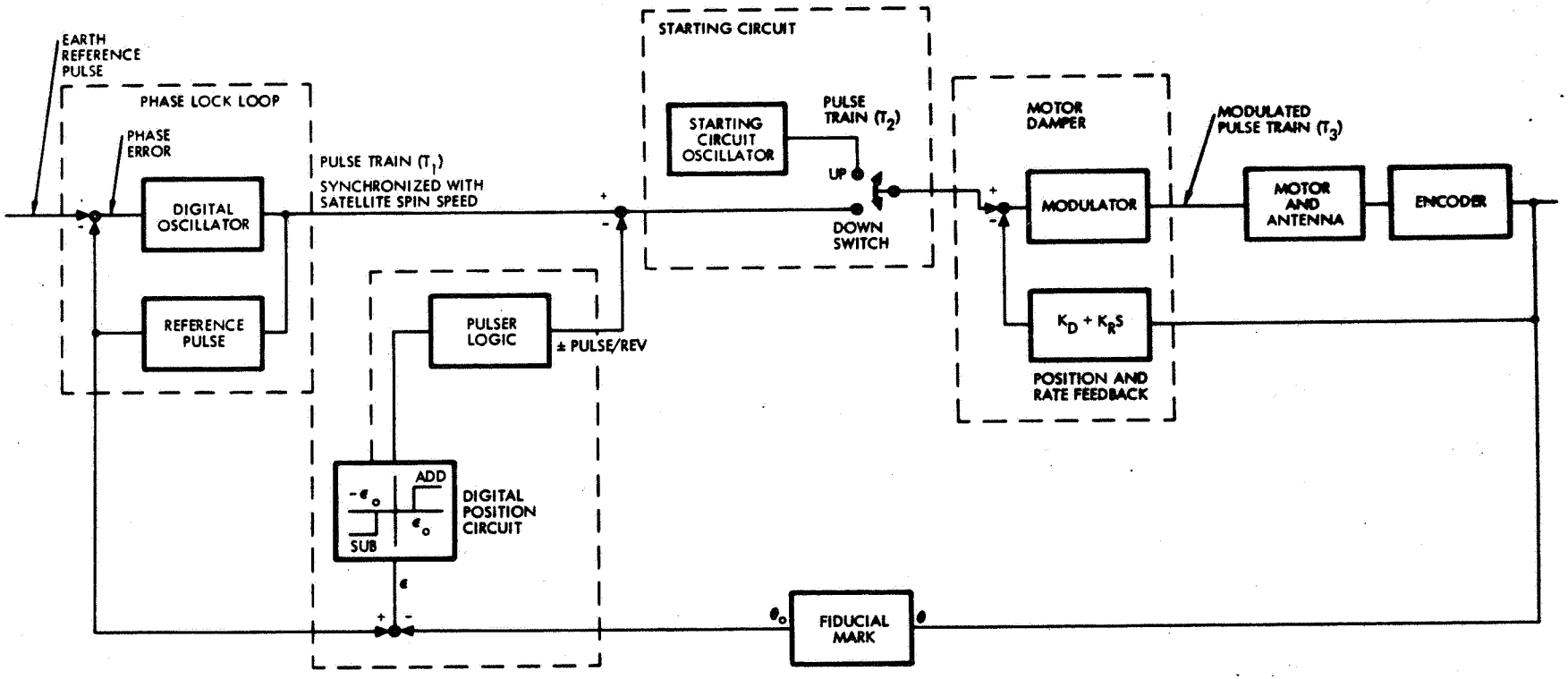

MODE	CONDITION	SWITCH POSITION
START	$\dot{t}_2 < \dot{t}_1$	UP
SLEW	$\dot{t}_2 = \dot{t}_1$	DOWN
CLOGGING	$\dot{t}_2 = \dot{t}_1$ $\lvert\epsilon\rvert > \epsilon_o$	DOWN

Figure 23. Mechanically Despun Antenna Control System

After sequencing through the previous two modes, the antenna is inertially at a standstill. However, this does not guarantee that the antenna is pointed at the earth. To accomplish this, the indexing mode is used. In this mode, the digital position circuit is used to modify the pulse train from the phase-lock loop to the motor. This modification consists of adding (or subtracting) one pulse per satellite revolution to the pulse train. This has the effect of changing the speed of the motor and results in indexing the antenna around to the desired position. This indexing maneuver is continued until the reference pulse from the phase-lock loop and the motor fiducial mark are coincident, at which time the digital-position circuit is disengaged.

4.5.1.2 Operating Characteristics

The MDACS described in par. 4.5.1 is essentially the same as that developed by Sylvania for Intelsat III. The same company has also developed the drive system for the ATS satellite. The two designs are similar in that they both are designed around the novel stepper motor described above. Taken together, these two developments provide substantial design and test experience in the area of the electromechanical equipment frequently viewed as the critical elements of a mechanically rotating drive system.

Both the Intelsat III and the ATS motor-encoder-bearing assemblies could drive the proposed antenna. They both use bearings lubricated by the Vacote process of Ball Brothers, a process which has proved its usefulness for space application in laboratory and flight tests. The ATS design uses two spring-loaded radial bearings, while the Intelsat III design uses a preloaded duplex pair and a spring-loaded radial bearing to meet its heavier-duty specifications. The running friction of the ATS bearings is approximately 0.2 oz/in., while that of the Intelsat bearings is specified to be under 3.5 oz/in. The Intelsat drive assembly has approximately a 2.5-in. ID for the antenna support and RF feed, while the ATS is appreciably smaller. The Intelsat drive provides a peak torque of over 30 oz/in., while the ATS unit provides about 5 oz/in. (higher torques could probably be obtained with different drive circuits). The Intelsat III assembly has been chosen for this application because the antenna will be larger than either the Intelsat III or the ATS designs, and

the heavier duty design of Intelsat III has shown in tests that it can start and carry appreciably larger antennas.

The control electronics have been specifically designed to operate with input pulse trains (earth-reference pulses) derived from earth sensors. The ATS uses the sharper inputs derived from a sun sensor. Performance is not materially affected if one extra earth-reference pulse should appear or if one should be dropped occasionally.

The system begins to despin as soon as power is applied. If earth reference pulses are then present, the motor-starter circuit will bring the antenna up to the satellite spin rate in about 90 sec. The antenna is then despun, but it is probably not pointing at the earth. It begins to index toward the earth at the rate of 0.7° per revolution. If the antenna were initially pointing 180° away from the earth, 256 rotations would be required before the antenna would be properly pointed. At 100 rpm, therefore, the indexing could take 154 sec (of course, the indexing time could be zero, if the antenna should initially despin at the earth).

When the satellite is at synchronous altitude, the antenna will point within 0.5° (3σ) of a direction indicated by the mean earth-reference pulse position. This assumes an earth-reference pulse jitter of about 0.7 msec (3σ).

4.5.2 Attitude Control Subsystem

The satellites are spun up to about 100 rpm prior to separation. After separation their orientation can be assessed through the use of on-board sensors (to be described). A reorientation maneuver is then performed in order that the satellite attitude is proper for the firing of the apogee motor. The satellite has sufficient angular momentum to maintain the orientation for the worst-case imbalance torques from motor firing. After motor firing, the satellite is placed in the proper attitude for on-orbit use and initial poisitioning.

The primary functions of the attitude determination and control subsystem are to provide:

- Sensor information to the ground station from which the satellite's attitude and rotational position can be determinted during transfer and final orbits.

- An earth reference pulse to the antenna for a position reference in pointing the antenna beam toward the center of the earth.

- Electronic-power amplification for energizing the propulsion solenoid valves in response to ground commands for positioning and orientation.

The configuration and characteristics of the attitude determination and control subsystem are shown in Figure 24.

A dual earth sensor and sun sensor system is proposed to fulfill the requirement for ground determination of spin-axis orientation. Two redundant earth horizon sensors and a sun aspect sensor permit satellite attitude and rotational position to be determined on the ground to an accuracy of better than 1° (3σ) with respect to the local vertical and the sun line. This accuracy will be achieved during the transfer orbit and will be exceeded during the final orbit.

The earth sensors are the primary source of spin-axis attitude information. As shown in Figure 25, each earth sensor sweeps across the earth once per satellite revolution and produces a pulse coincident with the instant of crossing the earth's horizon. Under normal conditions, spin-axis attitude with respect to the local vertical can be determined accurately and rapidly on the ground by measuring the interval between the leading edge horizon contacts of the two earth-sensor beams. When such times fail to coincide, spin-axis displacement can be computed and then corrected by ground command. In the unlikely case that one of the earth sensors should fail, the same attitude information can be obtained by measuring the interval between leading and trailing horizon pulses from the operating earth sensor. This interval, which is a measure of the earth's chord scanned by the sensor, is then compared with a nominal value based on the accurately known, fixed orbital altitude. The earth-sensor data will not be degraded during eclipses.

In the final orbit, when the spin axis is to be maintained normal to the orbit plane, attitude errors exceeding approximately $\pm 0.5^{\circ}$ are corrected to maintain antenna beam pointing accuracy. Attitude corrections are made by pulsing the axial thruster valve by means of a ground command that is properly timed with respect to the telemetered earth sensor.

PHYSICAL CHARACTERISTICS

Number Required	1 per spacecraft
Size	7.7x2.3x4.75 in.
Weight	3.0 lb
Power	1.1 watt
Output	+5v dc pulses to antenna despin control electronics. +5v dc sun pulses to Pulse Conditioner ±2.5v dc earth pulses to Pulse Conditioner

CONTROL LOGIC

PERFORMANCE CHARACTERISTICS

Optics	Infrared (14 - 16 microns)
Accuracy	±0.40°

RELIABILITY

0.956 for 5 years

PHYSICAL CHARACTERISTICS

Number Required	2 per spacecraft (redundant)
Size	5.5x2.8x2.8 in.
Weight	1.2 lb (each)
Power	1.0 watt
Output	±2.5v dc pulse to Control Logic

EARTH SENSOR

PERFORMANCE CHARACTERISTICS

Detector	Solar Cell
Angular Range	120°
Accuracy	±0.2°

RELIABILITY

0.997 for 5 years

PHYSICAL CHARACTERISTICS

Number Required	1 per spacecraft
Size	1.9x1.9x1.4 in.
Weight	0.27 lb
Power	No external power required
Output	+0.5v dc pulses to Control Logic

SUN SENSOR

SUBSYSTEM FUNCTIONS

Sun Sensor Earth Sensor	Provides satellite attitude and rotational position to telemetry for attitude determination on ground
Control Logic Electronics	Provides earth reference timing pulses to Antenna Despin Control Electronics
	Provides buffer amplifiers between the Sensors and the Pulse Conditioner Unit

FUNCTION

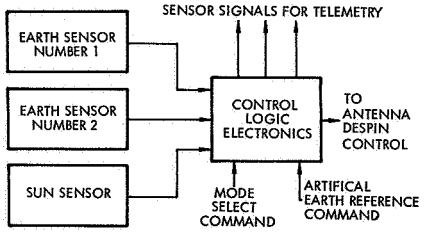

Figure 24. Attitude Determination Subsystem

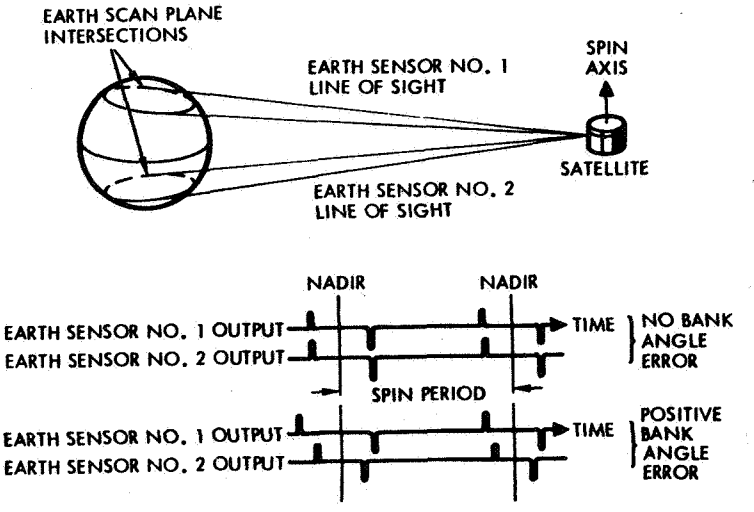

Figure 25. Earth Sensor Operation

pulses. Attitude corrections will need to occur on the order of once every 4 months or longer.

The leading edge horizon pulse is applied to the antenna control electronics. Rotational speed of the antenna with respect to the satellite is then controlled by the frequency of earth pulses. Beam position is controlled to a fixed offset angle with respect to the earth sensor optical axis in phase with the earth horizon reference pulse. This angle is mechanically preset for the earth's chord length as scanned by the sensor at orbital altitude.

4.5.2.1 Spin-Axis Corrections

To effect an attitude change, it is necessary to apply a torque about an axis perpendicular to both the desired precession and the spin axis. Because the spacecraft is rotating and the torquing system is body-fixed, it is necessary to develop a torque component fixed in inertial space. The means for generating this torque consists of pulsing one of the axially oriented hydrazine thrusters in synchronization with satellite rotation. The required number of pulses is commanded so that the total precessional angle is realized. Each actuation extends on an arc of spin $\pm 30^{\circ}$ from the direction at which a fixed thrust would provide the desired precession. Because of lags in the valve opening and in thrust buildup, the current pulse leads the desired thrust pulse.

Logic is provided for despinning the navigational signal antenna without need for command from the ground. In normal operation, logic circuits select the time of occurrence of the second of the two leading edge earth sensor pulses, and deliver it to the antenna as a despin reference. A phase displacement angle of ~6° is built into the antenna to permit the antenna beam to point directly at earth center even though the reference pulses are arriving before the antenna points down.

The second pulse is selected to prevent confusion when one of the earth sensors intercepts the moon or sun. Neither body, however, is large enough to affect both sensors simultaneously. In the event of failure of one earth sensor, the other can be used alone, but of course without automatic solar or lunar overlap protection. Using ground commands, it is possible to supply the ground reference timing pulses to the antenna and thus despin from the ground for the short time required.

To establish that the attitude stabilization system is sufficiently accurate to meet the mission requirements, an error analysis has been performed. The rss error for attitude determination, including the telemetry link and ground processing, is about 0.48° (3σ).

In despinning the antenna, the data do not pass through the telemetry link, but all the other errors affecting spin-axis alignment apply. There is an additional source of error, related to the angle between earth intercept and earth sensor. This angle can be in error due to spin axis misalignment or attitude variation. Finally, errors within the antenna itself must be included. When all these errors are combined in a root sum square manner, the result is 1.0°.

During the transfer orbit, knowledge of the elevation of the spin axis with respect to the sun and earth, in conjunction with tracking data, permits computation of the satellite attitude at the ground station. Measurement accuracies during a typical transfer orbit for a single observation close to apogee are within 0.24 to 0.28° (1σ).

4.5.2.2 Earth Sensors

The earth sensors are the same as those being used in Intelsat III. They are built by Lockheed Missiles and Space Company; a similar unit has been successfully demonstrated on the P-11 satellite program. Each

of the sensors consists of a telescope, a thermistor bolometer, and processing electronics. The sensor operates in the CO_2 infrared spectrum.

4.5.2.3 Sun Sensor

Like the earth sensors, the sun sensor is identical to that being built for Intelsat III. It consists of a photovoltaic detector mounted at the bottom of a quartz substrate that is covered by a mask at its top surface. The function of the mask is to block out all light, except that transmitted through two narrow slits which diverge symmetrically with respect to the center. As the satellite spins, the sun's image traverses each slit in sequence. The time difference between the pulses depends upon the angle between the spin axis and the sun line. A third slit creating a third pulse extends outward from the center in one direction only, to identify which end of the spin axis is closer to the sun. The quartz substrate, with its index of refraction of 1.46, aids in extending the sun sensor's field of view to $\pm 65^{\circ}$. The accuracy of the sun sensor is $\pm 0.2^{\circ}$ (3σ) when the measured data are corrected by the calibration data previously derived for that unit. The corresponding accuracy without calibration is approximately $\pm 0.4^{\circ}$.

4.5.2.4 Control Logic Assembly

The control logic assembly (Figure 26) is used to process the sensor pulses and to deliver them to the telemetry encoder. It also generates a despun antenna reference pulse from the leading edge horizon pulses. The basic logic system consists of two earth-sensor level detectors, two flip-flops, an OR-AND gate, and a pulse-generator. Another pulse generator provides an antenna reference pulse when operating in a single earth-sensor mode. The telemetry buffers are linear buffer amplifiers with unity voltage gain. The sun-sensor amplifier is also a linear buffer amplifier but has a voltage gain of 10. Magnetic latching relays are used to select the proper reference source for the generation of an antenna reference pulse for operation in any one of four modes.

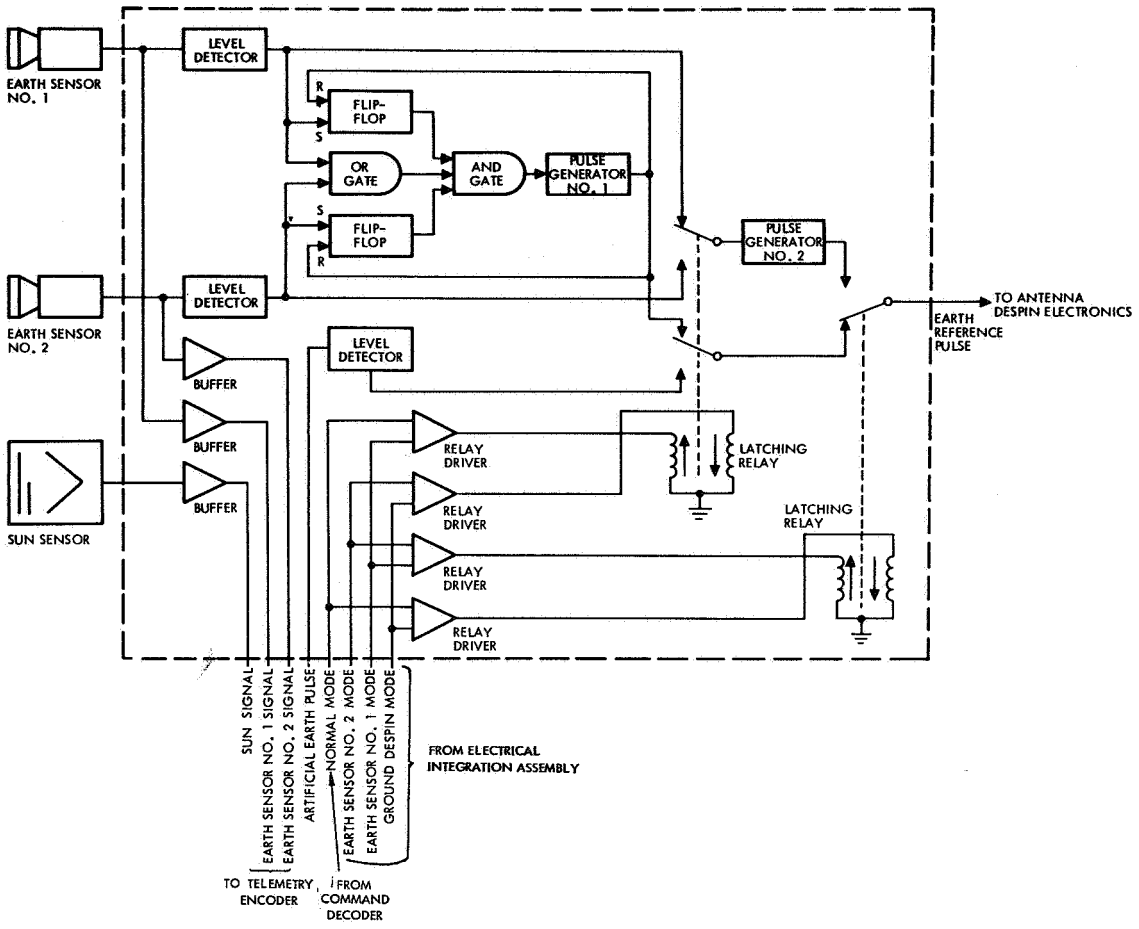

Figure 26. Control Logic Assembly Block Diagram

4.5.2.5 Valve Driver Assembly

The valve driver assembly (Figure 27) is identical to that of Intelsat III. It contains all the logic and amplification needed to operate a valve solenoid when the proper command sequence has been received.

4.6 PROPULSION

4.6.1 Apogee Motor

The solid propellant apogee motor was sized on the basis of the following criteria:

1) A transfer orbit with 100-mi perigee.

2) A velocity requirement of 5230 at apogee (synchronous altitude).

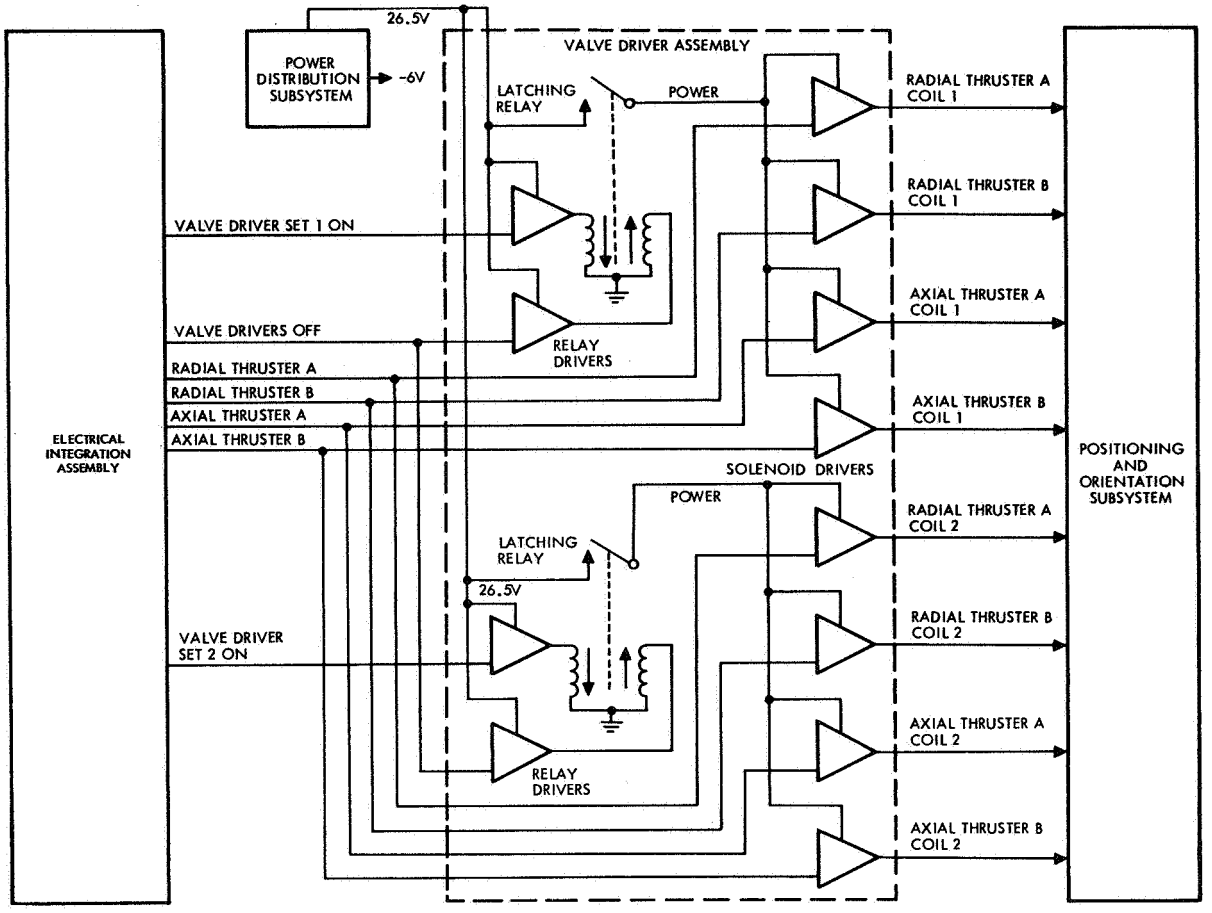

Figure 27. Valve Driver Assembly Block Diagram

3) A 10^{o} plane change.

4) A satellite weight of 516.4 lb.

Existing solid propellant motors whose performance has been substantiated were reviewed from the standpoints of performance and ease of incorporation into the NAVSTAR design.

The motor selected was the BE-3-B1 which is currently in use for orbit injection of the Vela satellite, and which is supplied in accordance with TRW specification EQ8-15, Revision A, 2/9/67. This motor has been 100 percent successful in 73 total launches on the Ranger , SPARTA, Athena, Amrad, and the advanced Vela spacecraft programs. Basic motor specifications are presented in Table XIII. Actual propellant weight may be varied (increased) by about 3 percent depending on final detailed design review of the spacecraft.

TABLE XIII
BE-3B1 ROCKET MOTOR

Physical Characteristics	
Diameter, in.	18.25
Length, in.	34.6
Weights, lb.	
Loaded	243.5
Propellant	219.6
Burnt	20.5
Ballistic Parameters (70°F, vacuum)	
Specific impulse lbf-sec/lbm	276
Total impulse, lb-sec	60,610
Average thrust, lb	7,576
Burning time, sec.	8.0
Average pressure, lb/in^2	660
Nozzle throat area, in^2	6.26
Nozzle expansion ratio, initial	18.6
Nozzle divergence angle, °	16
Firing temperature limits, °F	40-70

An approved arm-disarm switch accepted for use by the Eastern Test Range will be utilized in the motor ignition circuit since motor design does not permit the adaptation of the safe-and-arm device used in applications such as Intelsat III.

4.6.2 Positioning and Orientation Subsystem

The task of initial spacecraft positioning and later stationkeeping is closely related to that of attitude stabilization both because of the integration of the requirements and because the thruster system serves both purposes. The requirements for initial positioning and stationkeeping are discussed, and the hydrazine thruster system for these functions and attitude reorientation is described.

The ascent orbit of the spacecraft lies in a plane inclined 33° with respect to the equator. When the apogee motor fires, it not only circularizes the orbit, but changes the orbit plane to be inclined 18.5°. Out-of-plane gravitational effects of the sun and moon then cause the plane to precess about an axis which, on the average, is perpendicular to the ecliptic. This produces an orbit-inclination change, the magnitude of which will be small enough that no correction is required. Thus, latitude positioning can be accomplished entirely through the apogee motor, and no further corrections are required.

Stationkeeping for attitude corrections allows for spin-axis corrections to track the small changes in orbit plane tipping for 5-yr, variations in solar pressure, variations in radial thrusting forces not passing through the spacecraft center-of-gravity, and magnetic moment effect. (Center-of-gravity offset errors are nearly cancelled by thrusting at two equal periods, 12 hr apart.)

4.6.2.1 Thrust Requirements

All of the maneuvers requiring hydrazine thrusting are listed in Table XIV together with the thrust mode. The velocities are calculated using the vehicle weight at the time of firing. The propellant I_{sp} was selected for actual conditions of operations, i.e., taking into account I_{sp} as a function of duty cycle requirements, which accounts for the efficiency of pulse firing.

The positioning and orientation subsystem will provide an axial and a radial thrust capability for initial positioning and for attitude and longitudinal velocity control during stationkeeping.

Insertion into a near-synchronous, near-circular orbit may occur at any apogee of the ascent elipse, including the first. The exact sequencing of such operations including effects of injection errors has been handled many times by TRW Systems and the details of the procedure will not be

TABLE XIV
VELOCITY REQUIREMENTS

Satellite Maneuver	Velocity (ft/sec)	Thrust Mode
Spin axis orientation prior to apogee motor burn (90° +33.16°)	12.1	Axial, pulsed
Period correction (3 value)	200	Radial, pulsed
Spin-axis reorientation (64.08° change)	12.4	Axial, pulsed
Longitudinal stationkeeping (44° East location — worst case)	30	Radial, pulsed
Attitude corrections	2.0	Axial, pulsed

repeated here. The ±200 ft/sec velocity increment allotted for initial longitudinal positioning is sufficient to permit the satellite to be placed in orbit at the required longitude within a period of 3 weeks. After placing the satellite on station, it is necessary to maintain it there within a $\pm 5^{o}$ region. The earth's gravitational irregularities create a tendency for the satellite to drift and, therefore, limit cycle operation must be employed for longitudinal directions as discussed in vol. II. The average time between corrections can easily be several months, and the total velocity increment required for operation over 5 yr will be within the 30 ft/sec indicated in Table XIV.

4.6.2.2 Thruster Design Concept

The thrust chamber proposed by TRW Systems for satellite maneuvering and attitude control is the same unit that will be used on a current TRW flight spacecraft. This thruster is in qualification at the system level. Data from completed tests demonstrate that the thruster meets the design goals of optimum pulsing characteristics and smooth operation in the steady-state mode. The nominal operating and performance characteristics for the thruster are summarized in Table XV. Feed pressures and flow rates can be matched to the specific requirements of NAVSTAR.

TABLE XV

THRUST CHAMBER OPERATING AND PERFORMANCE CHARACTERISTICS

Thrust range, lb_f	2.9 to 1.9
Nominal chamber pressure range, psia	230 to 91
Catalyst	Shell 405
Nozzle expansion ratio	50:1
Propellant tank pressure range, psia	390 to 236
Steady-state vacuum specific impulse, sec	
2.9 lb thrust	226
1.9 lb thrust	222

The thruster is an all-welded unit and is illustrated in Figure 28. Monopropellant hydrazine is used with a blowdown type of pressurization feed. Thrust is achieved by the spontaneous decomposition of the monopropellant hydrazine (identified as optimum for this mission) upon exposure to a catalyst within a thrust chamber, with the resulting gases expanding at high velocity through a nozzle.

4.6.2.3 Subsystem Installation

A specification sheet for the positioning and orientation subsystem installation is presented in Figure 29.

The subsystem is installed in the satellite in three assemblies: the pressure vessel and gas manifold line assembly, the components line assembly, and the thrust chamber assembly. Two propellant tanks (one-half the tankage used in Intelsat III) are installed diametrically opposed near the outer circumference and, since the satellite is spin-stabilized, the resultant forces are sufficient to assure a propellant-pressure interface through its operational life. The tankage, while not optimum, offers the advantage of using existing qualified vessels, which more than offsets the fraction of a pound saved by optimizing the tankage. Two axial thrust chamber assemblies provide thrust along the direction of the spin axis in both directions and are mounted on one end of the satellite. Redundant

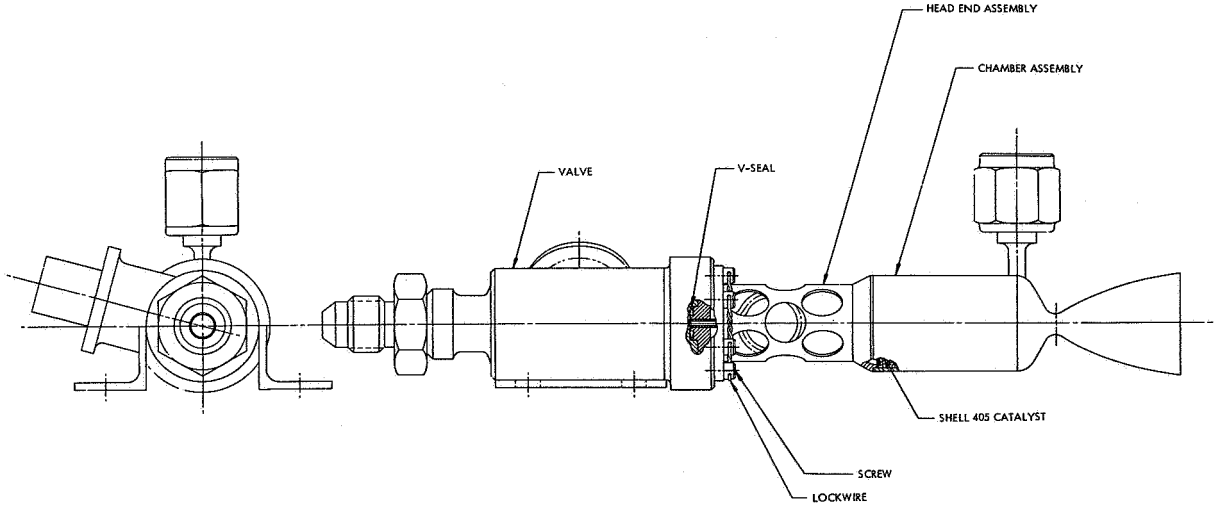

Figure 28. Engineering Drawing of Proposed TRW Thrust Chamber Assembly

SUMMARY SPECIFICATION
POSITIONING AND ORIENTATION SUBSYSTEM

CHARACTERISTICS

WORKING FLUIDS

Propellant	Hydrazine (N_2H_4)
Pressurant	Nitrogen (N_2)

THRUSTER

Thrust range	2 TO 3 lb force
Thrust chamber pressure range (initial/final)	197/143 psia
Ignition source	Spontaneous catalyst (Shell 405)
Nozzle expansion ratio	50:1
Minimum specific impulse, vacuum (continuous/pulsing)	223/218 sec
Minimum impulse bit	0.24 lb-sec
Total ΔV	266.9 ft/sec
Total impulse delivered	2100 lb-sec
Reproducibility limits	± 2 percent (in a pulse train of 10 or more)
Number thrusters per subsystem	6

PROPELLANT AND PRESSURIZATION SYSTEM

Propellant expulsion mode	Spin oriented propellant gas interface
Propellant pressurization technique	Blowdown
Initial tank pressure	390 psia
Final tank pressure	236 psia
Propellant weight	11.8 lb
Pressurant weight	0.62 lb
Tank size, diameter	9.56 in. inside diameter
Propellant tanks, number per subsystem	2 spherical
Pressure transducers, number per subsystem	1
Fill and drain valves, number per subsystem	1
Plumbing	As required
Method of construction and assembly	Welded, brazed and mechanical joints

WEIGHT

Hardware	7.5 lb
Propellant	11.0 lb
Pressurant	0.62 lb
Total	19.12 lb

PROPELLANT SOLENOID VALVE

PERFORMANCE CHARACTERISTICS

Operating pressure	600 psia (maximum)
Proof pressure	900 psia
Pressure drop (maximum thrust)	50 psi
Life	60,000 cycles (minimum)
Leakage rate	0.5 std/cm^3/GN_2 hour (maximum) at 120 to 600 psig

PHYSICAL CHARACTERISTICS

Weight	0.39 lb
Body materials	Stainless steel and 2V permendur (electroless nickel plated)
Seal material	Metal/elastomer
Operating temperature range	40 to 120°F
Maximum temperature	250°F

ELECTRICAL CHARACTERISTICS

Voltage requirements	
Peak pull-in	14 v (maximum)
Dropout	2.6 v (minimum)
Power at 31v dc, 40°F	5 w/coil (maximum)
Operating voltage	31/14vldc (maximum/minimum)
Number per subsystem	4

COMPONENT CHARACTERISTICS

PRESSURE TRANSDUCER

Type	Bonded strain gage, signal conditioning included
Electrical	
Power	Less than 0.25 watt
Output Signal	0 to +5v dc
Pressure Range	0-600 psia
Pressure Proof	900 psia
Pressure Burst	2400 psia (minimum)
Operating Temperature Range	40 to 120°F
Accuracy	±0.8 percent (static)
Resolution	0.25 percent
Weight	0.32 lb
Materials	Stainless steel and aluminum

COMPONENT CHARACTERISTICS

PROPELLANT TANKS

Inside diameter (nominal)	9.56 in.
Wall thickness (nominal)	0.020 in.
Volume	458 cu in.
Operating pressure (maximum)	390 psia
Rated proof pressure	900 psia
Rated burst pressure	1200 psia
Mounting	Trunions
Tank weight	1.38 lb
Material	6 Al 4V Titanium (heat treated)

FILL AND DRAIN VALVES

Operation	Manual loading for both gas and propellant; dual seals
Operating pressure (maximum)	600 psia
Rated proof pressure	900 psia
Rated burst pressure	2400 psia (minimum)
Rated life	100 seat and reseat cycles
Leakage	1×10^{-5} std cm^3/sec helium at 120 to 600 psia
Weight	0.30 lb
Materials	Stainless steel

Figure 29. Positioning and Orientation Preliminary Specification

radial thrust chamber assemblies are mounted to a common bracket fastened to the equipment platform. The radial thrust axis passes through the satellite center-of-gravity.

4.7 ELECTRICAL POWER

The electric power subsystem converts solar energy into electric power for use by the navigation satellite subsystems. Nickel-cadmium batteries store electrical energy when a surplus is available from the array. During periods when the array is not receiving sunlight, the batteries provide power to the subsystems. The 41.1 ft^2 body-mounted fixed solar array can delivery 121.6 w when new, and a minimum of 99.8 w after 5 yr. The array has no deploying or moving parts. Nickel-cadmium batteries were chosen because they have a longer life expectancy than any other type and because they appear to be the only type suitable for the intended mission. Because of the cycling nature of the navigation transmitter load, the battery must supply power for its operation, both during eclipse and during the sunlit portion of the orbit. Regulation of solar array and battery power within the power system is carried out by a power control unit uniquely suited to the NAVSTAR mission profile. The power subsystem delivers to the spacecraft subsystems unregulated direct current at between 22 and 29.2 v. The preliminary specification for the subsystem appears in Figure 30.

4.7.1 Requirements

The NAVSTAR is required to operate continuously for 5 yr in a synchronous orbit 26.5° inclined to the plane of the ecliptic. The average power requirements during this period of time are shown in Table XVI.

The 102.12 w required are computed on the basis that all the loads are in use. This condition is satisfied by the new solar array when the array output is 121.6 w, but this output decays with time and, after 5 yr, the output may be as low as 99.6 w. In such a condition, the telemetry transmitter can be operated on command when excess power is available. In that case, only 2.075 of the 22.39 w required for the subsystem would be on continuously. This means a saving of 20.315 w or a continuous load of only 81.805 w, safely below the minimum predicted output of 99.6 w for the solar array. However, if this load becomes a

FUNCTION

- LIMIT MAIN BUS VOLTAGE AS REQUIRED BY BATTERY TEMPERATURE REFERENCE (V_{MAX} 29.7V) BY:
  - (1) CONTROL OF BATTERY VOLTAGE AND SHUNT DISSIPATION WHEN ARRAY POWER EXCEEDS LOAD CURRENT
  - (2) LIMIT BATTERY VOLTAGE TO 29.7V DC (MAX)

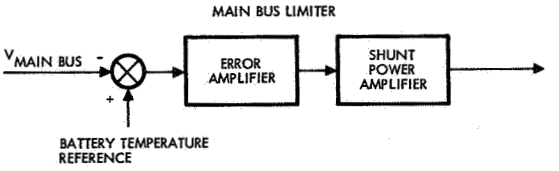

- CHARGE BATTERIES AT MAXIMUM AVAILABLE RATE WHEN ARRAY CURRENT EXCEEDS LOAD CURRENT
- PLACE BATTERIES IN A TRICKLE CHARGE RATE WHEN V_{MB} > 29.7V DC OR BY COMMAND
- PERMITS BATTERIES TO BE DISCONNECTED OR DISCHARGED IN ORDER TO RECONDITION

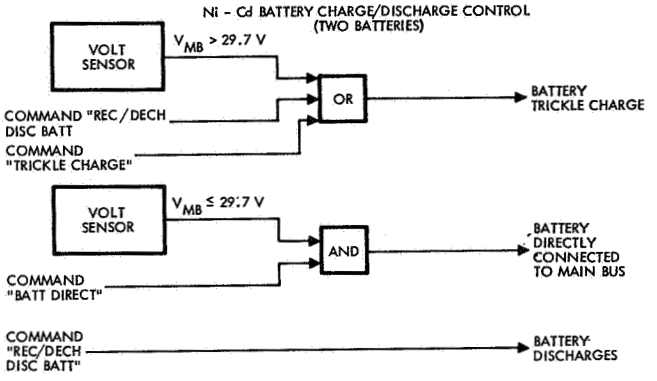

- DISCONNECT NONESSENTIAL LOADS WHEN LOAD CURRENT EXCEEDS A PRESET MAXIMUM FOR TIME EXCEEDING ≈ 10 MS
- DISCONNECT NONESSENTIAL LOADS WHEN $V_{MAIN\ BUS}$ DECREASES BELOW A PRESET MINIMUM FOR TIME EXCEEDING ≈ 100 MS

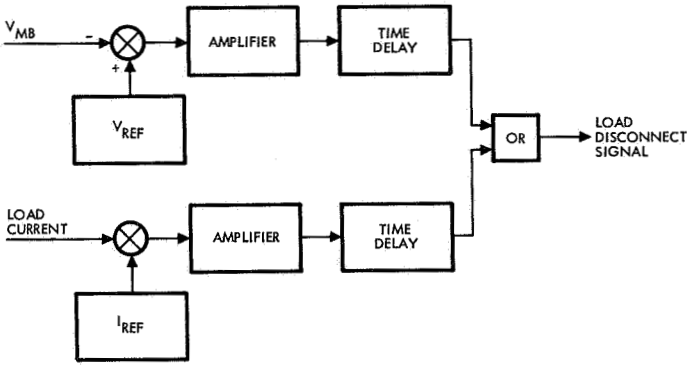

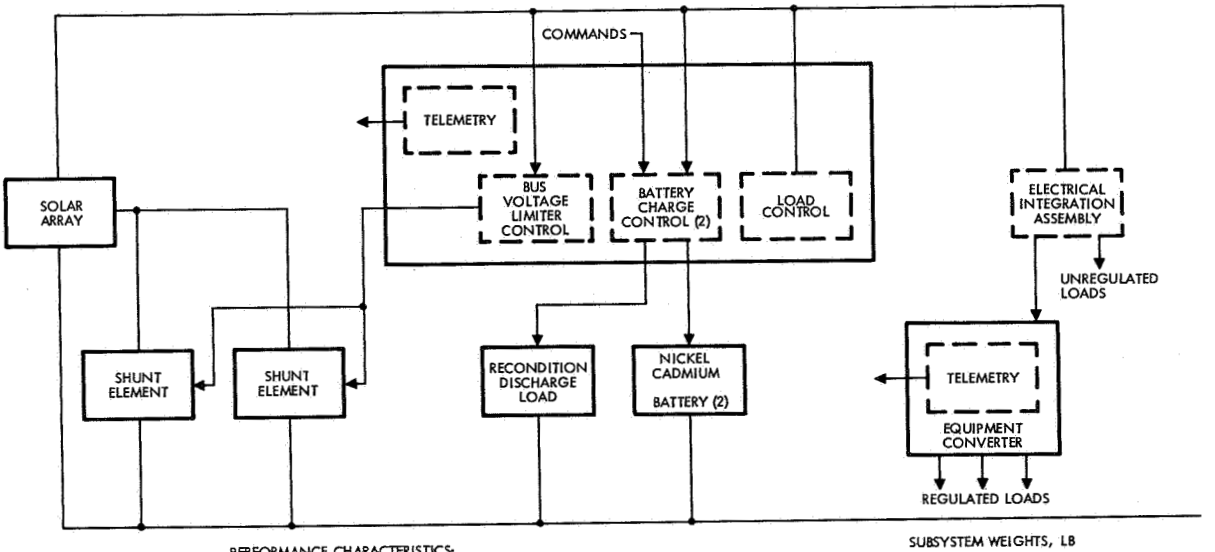

PERFORMANCE CHARACTERISTICS:

MAIN BUS VOLTAGE	22 TO 29.2V DC
SOLAR ARRAY OUTPUT	121.6 W, NEW 99.8 W, AFTER 5 YEAR (MINIMUM)
BATTERY ENERGY	300 W-hr

SUBSYSTEM WEIGHTS, LB

SOLAR ARRAY	26.8
BATTERIES	28.6
POWER CONTROL UNIT	8.0
SHUNT ASSEMBLY	3.2
DC/DC CONVERTER	3.5
TOTAL	70.1

Figure 30. Preliminary Specification for Electric Power Subsystem

TABLE XVI

NAVSTAR AVERAGE POWER REQUIREMENTS

	Watts	
Attitude control subsystem		1.70
Control logic assembly	0.29	
Earth Sensor 1	0.70	
Earth Sensor 2	0.70	
Valve driver assembly	0.01	
Navigation subsystem		47.35
Transmitter	28.10	
Data encoder	3.00	
Time base unit	1.00	
Oscillator	1.00	
Tracking data transponder	3.00	
Mechanically despun antenna	11.25	
Telemetry and command subsystem		22.39
2-w transmitter	19.3	
Receiver	1.62	
Decoder	0.455	
Encoder	1.015	
Propulsion subsystem		0.25
Electrical integration subsystem		6.20
Electrical integration assembly	5.20	
Cable losses	1.00	
Power subsystem		24.23
Power control unit	1.80	
Shunt elements	0.30	
Converter losses	13.43	
Battery charging	8.70	
Total		102.12

very desirable satellite feature, the addition of one string per panel would provide the additional power (112.3 w minimum) required to run the telemetry and command subsystem on a full-time basis without increasing the size of the other power subsystem components. This could be accomplished with a weight increase of less than 2 lb.

The navigation signal transmitter operates on a duty cycle, and the average power requirements do not give a true picture of its power needs. The 50-w RF transmitter requires 210 w for its operation. It operates on a 12.5 percent duty cycle for 1.5 sec on and 10.5 sec off. A solar array

capable of supplying all this power would have to be capable of supplying 260 w minimum. This would mean, besides the large weight and spacecraft size penalty, an excess power dissipation of over 210 w for 87.5 percent of the time. Instead of this, a battery for operation in an eclipse can be made to supply the additional power pulses for the transmitter. Satellite tracking data can be transponded using the excess power when available. When the solar array is new, after all the other loads are satisfied, 19.48 w could be made available for this purpose. This power represents an additional 1.1 sec operation during every 12-sec cycle. As the solar array decays and the power output is reduced to 99.6 w, the telemetry and command transmitter can probably be used with less frequency. This would make about 18 w available for satellite tracking data transmission or an additional second in every 12-sec cycle when the telemetry and command transmitter is not operating.

The operation of the navigation signal transmitter is of paramount importance to the success of the satellite mission. Therefore, a high reliability redundant battery system is recommended.

4.7.2 Functional Description and Performance

The main components of the electric power subsystem are a solar array, two nickel-cadmium batteries, a power control unit, a shunt element assembly, and a dc-to-dc converter. A functional description of each component is presented below.

The NAVSTAR has two main modes of operation during its entire mission. The first is a solar array/battery sharing mode, where the continuous loads are supplied by the solar array during the illuminated portion of the orbit and the battery supplies the excess power required to operate the navigation signal transmitter. The second mode occurs during eclipse when all the loads are supplied exclusively by the batteries.

The solar array is sized to meet the average power requirements for all the loads, including battery recharging at the end of 5 years' operation. This results in an array with an initial power output capacity of 121.6 w. A shunt regulator that taps a fraction of the solar array, with minimum power losses when the power requirements reach maximum,

has been found adequate for this subsystem. A maximum bus voltage of 29.2 vdc is thus obtained. The lower voltage limit of 22 vdc occurs during the end of the eclipse when all the power is obtained from the batteries.

The charge/discharge control portion of the power control unit allows the batteries to charge at a maximum rate when the power is available. The batteries are placed on a trickle charge made when the main bus voltage exceeds 29.7 vdc or by command. Batteries can be individually disconnected to recondition on command.

4.7.3 Components

The solar array is composed of N-on-P silicon solar cells (see Table XVII) interconnected in a redundant series-parallel matrix. The basic building block is a module of two cells in parallel and four or five cells in series (Figure 32); these modules are also connected in series to form a string. A string consists of 67 cells in series with two sets in parallel, for a total of 134 cells. There are eight of these strings in a panel (see Figure 31); and eight identical panels, 41.1 in. high and 21.1 in. wide, form the solar cell array. Only 33.6 in. of the panel height will be taken up by solar cells in the present design. The total number of cells in the array will be 8576. The module features a so-called overlapped cell design which provides a more effective area utilization than the flat cell layouts. The total weight of the solar array is estimated at 21.7 lb.

Two nickel-cadmium batteries, consisting of (2) six-ampere-hour cells, are used in this satellite, to provide 300-w-hr capacity at the nominal 25 vdc discharge voltage. Each battery weighs 14.3 lb and has a volume of 243 cu. in. The linear dimensions are 6 x 9 in. at the base plate and 4.5 in. in height. They can be individually reconditioned on command. In case one battery fails, the remaining battery can handle the load with a maximum depth of discharge of 50 percent for the longest eclipse.

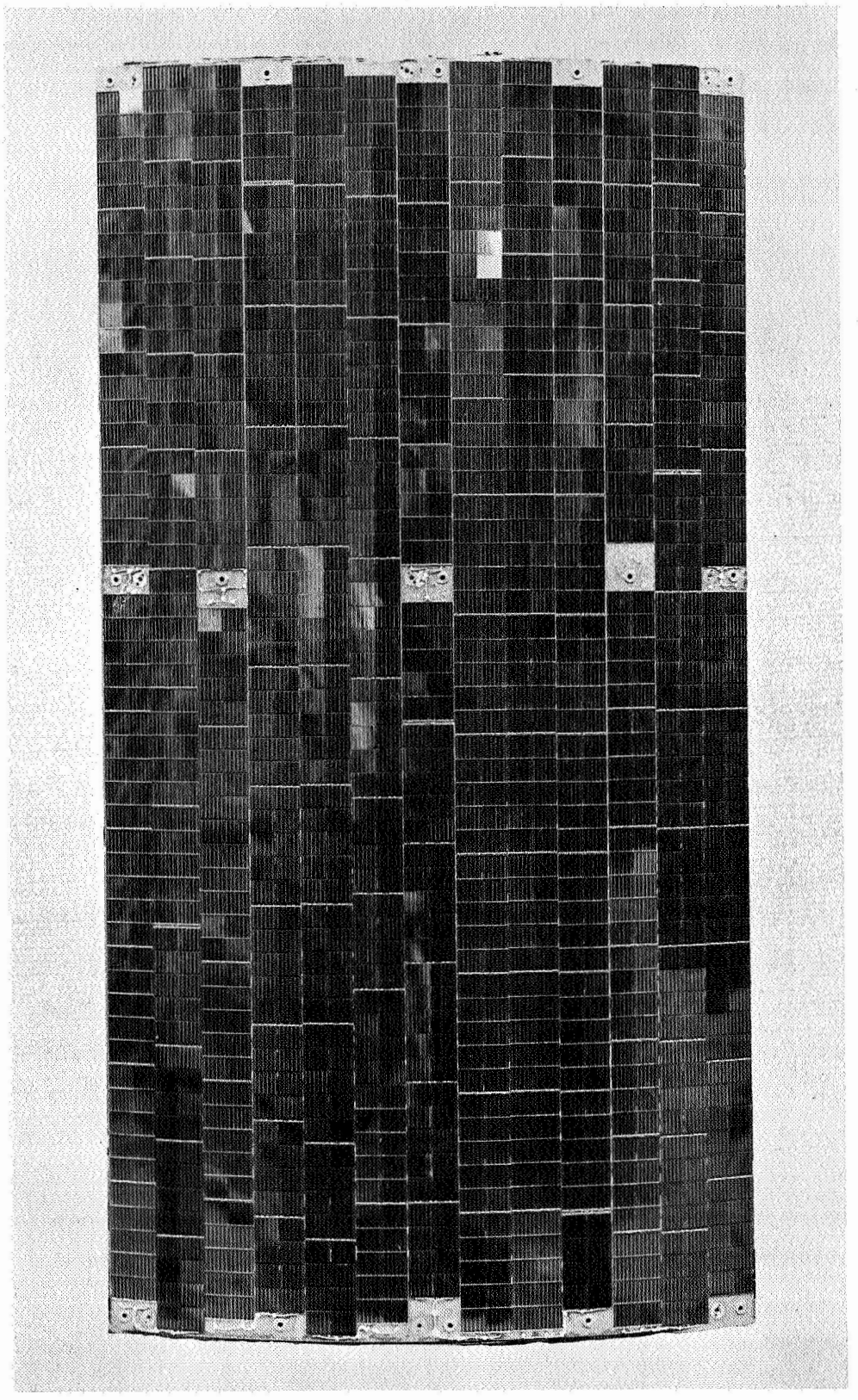

Figure 31. Solar Array Panel

TABLE XVII

SOLAR CELL AND COVER SLIDE CHARACTERISTICS

Solar cell:	Material: silicon Type: N on P (TiAg sintered contacts) Size: 2 x 2 cm Thickness: 0.010 in. Efficiency: 10.5 percent (air mass zero, 28°C) Basic resistivity: 7-14 ohm-cm Series resistance: 0.5 ohms I_{sc} = 139.0 ma V_{oc} = 0.540 v I_{op} = 126.5 ma V_{op} = 0.440 v βV_{oc} = 100°C = -2.25 mV/°C; 60°C = -2.20 mV/°C; 0°C = -2.15 mV/°C; -30°C = -2.05 mV/°C
Cover Slide:	Material: fused silica Size: 1.8 x 2 cm Thickness: 0.012 in. Cut-off frequency: 410μ
Cell-to-Cell Connectors:	Copper

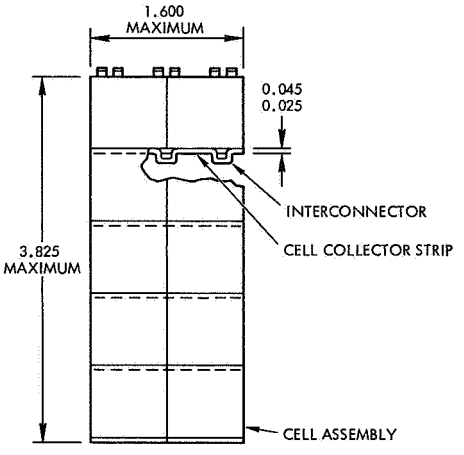

Figure 32. Solar Cell Connector Diagram
(see Table XVII)

The power control unit (PCU) (see Figure 30) consists of:

- Voltage limiter (solar array control)
- Battery charge/discharge control
- Load control
- Telemetry
- Shunt assembly (external to PCU)

The voltage limiter consists of a precision voltage reference, differential amplifier (error amplifier), complementary current amplifier, current amplifier, and power amplifier (shunt elements). The output load bus voltage is compared with the voltage reference in the differential/amplifier, and the net error is amplified. The voltage sampled is compensated by the thermistors, which monitor battery temperatures. Therefore, the bus voltage is regulated to charge the batteries at a safe voltage continuously during conditions when the load current is less than the array capacity. The temperature-compensated error signal generated is passed through the required stages of current amplification. This high-current gain signal controls the power shunt transistors that regulate the voltage produced by the bottom half of the solar array, thus regulating the bus voltage to ± 2 percent.

The method of controlling the charge of the two nickel-cadmium batteries consists of connecting the batteries directly to the main bus and charging them at a maximum rate as determined by the excess array capacity. The final voltage at the batteries is controlled by the voltage limiter and is compensated by battery temperature. The hottest battery dictates the voltage limit. By having the batteries connected directly to the bus transient, periodic loads exceeding the array capacity are supplied by the batteries.

Overload control and telemetry are other features of the PCU. Provisions are present to recondition and to control the battery by ground commands. A PCU of this type weighs approximately 8 lb, and fits within an envelope of 7.13 x 6.5 x 10 in.

The shunt assemblies are power amplifiers that combine with the PCU to limit the main bus. The quad redundant elements are divided into two assemblies, each capable of dissipating 47 w at 120°C. Each shunt of this type weighs 1.6 lb and fits within an envelope of 5.5 x 5.5 x 1.5 in.

A central dc-to-dc converter with multiple outputs supplying the different subsystems is contemplated. The output voltages required are ±28, +15, +10, +6, -6, -15 and -24 vdc. Of these, about 34 w at 28 v and 20 w at other voltages represent continuous loads. The other loads are intermittent and the largest of these is represented by the navigation signal transmitter. This transmitter requires 210 w for operation, but it operates on a duty cycle of 12.5 percent of each 12-sec period. The power for the navigation transmitter can be supplied by this same converter unit.

The supplying of power to the pulsating navigation signal transmitter load is one item deserving further study. A separate bus connected directly to the battery may prove to be superior to the mode presently recommended. Such direct connection may reduce ripple in the main bus and reduce EMC problems.

The dc-to-dc converter is expected to weigh about 3.5 lb and have as envelope dimensions 7 x 6.2 x 5.3 in.

4.8 SATELLITE TELEMETRY AND COMMAND SUBSYSTEM

The telemetry and command subsystem consists mainly of existing designs developed for and, in some cases, flight-proven on the Vela, SGLS, and Intelsat III programs. The main features of this subsystem are as follows:

- Telemetry transmitted to ground stations, which includes housekeeping data, the command status of the satellite, and high-resolution timing information pertaining to satellite attitude.
- Commands at 50 b/sec data rate from a ground station for normal satellite functions, apogee motor and attitude thruster firings, and for resetting of the satellite oscillator frequency.
- Data on satellite ephemeris and oscillator phase corrections sent via the command link for storage on board the satellite.
- Provision for command link security by additional unit and decoder modification.

The T and C subsystem block diagram, shown in Figure 33, consists of a telemetry encoder, telemetry transmitter, diplexer, S-band omnidirectional antenna, command receiver, and command decoder. The omnidirectional antenna provides hemispherical coverage from one end of the satelllite.

4.8.1 Telemetry Encoder

The telemetry encoder proposed is a design developed for the Intelsat III satellite. A simplified block diagram of the encoder is shown in Figure 34.

The analog telemetry signals are time multiplexed by a ripple counter and sample gates at such a rate that all 63 channels (a complete frame) are readout with a 1 min frame rate. Provision is made for supercommutation of critical data, such as main bus current to a rate once every 15 sec. The attitude control subsystem timing pulses are telemetered to the ground station by two IRIG subcarriers. The antenna-reference pulse and sun-sensor pulse signals are amplitude-modulated on the subcarriers while the two earth-sensor pulses frequency-modulate

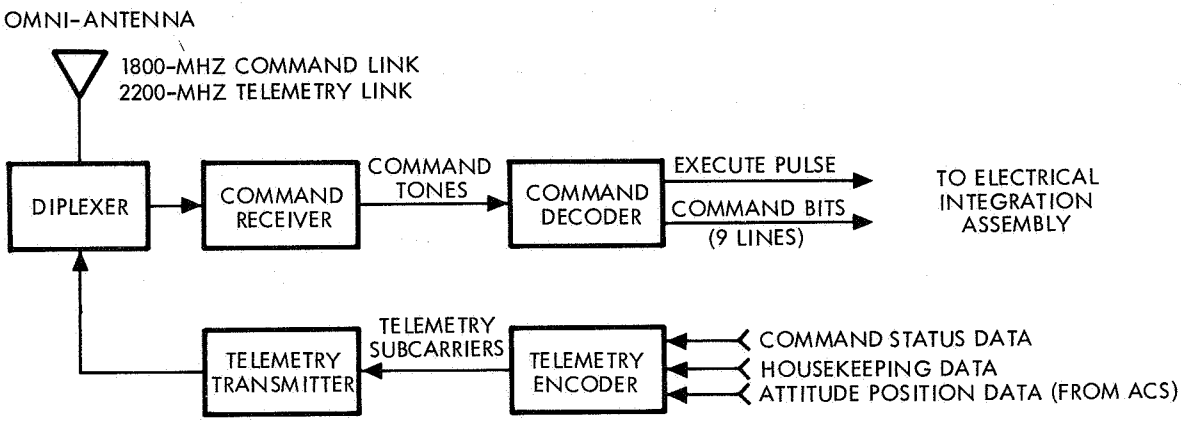

Figure 33. Telemetry and Command Subsystem Block Diagram

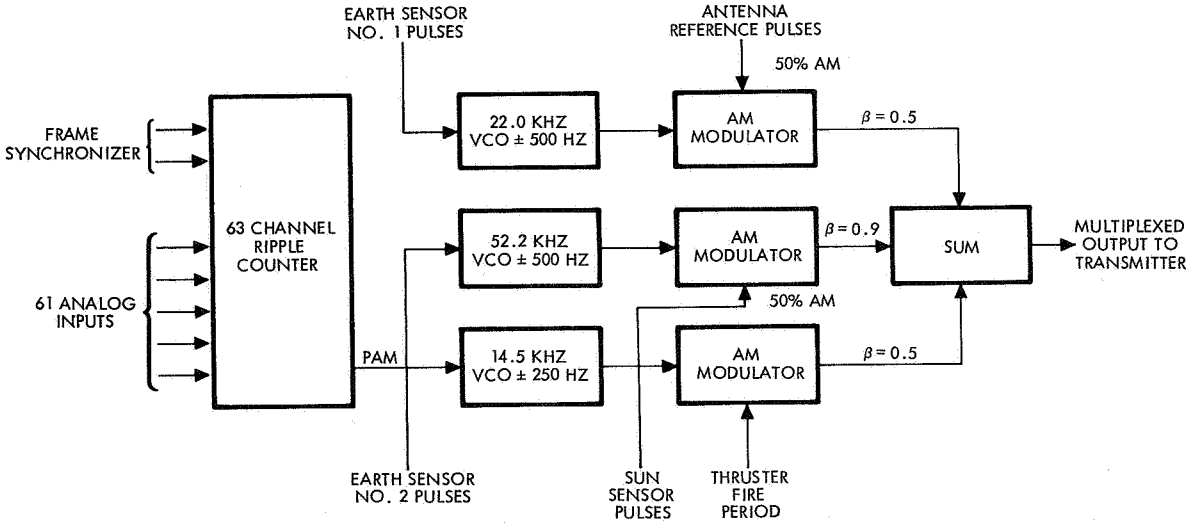

Figure 34. Telemetry Encoder Block Diagram

the subcarriers. The 63-channel PAM telemetry data frequency-modulates a third IRIG subcarrier while the attitude thruster firing period amplitude-modulates this subcarrier.

The numbers shown in the block diagram are the subcarrier and carrier (B's) modulation indices that are used for the telemetry link.

4.8.2 Telemetry Transmitter

The telemetry transmitter performs the following functions:

1. Accepts the telemetry encoder subcarriers and phase modulates them onto the S-band carrier.

2. Produces a minimum output power of 2 w at 2200 MHz.

It is proposed that the all-solid-state S-band transmitter, which was developed for the Space-Ground Link Subsystem (SGLS), be used for the telemetry transmitter. Excellent frequency stability is achieved by a temperature-compensated crystal oscillator, which is operated at low power (1/2 mw) and is isolated from succeeding stages by a buffer amplifier with high-input impedance. A simplified block diagram is shown in Figure 34a.

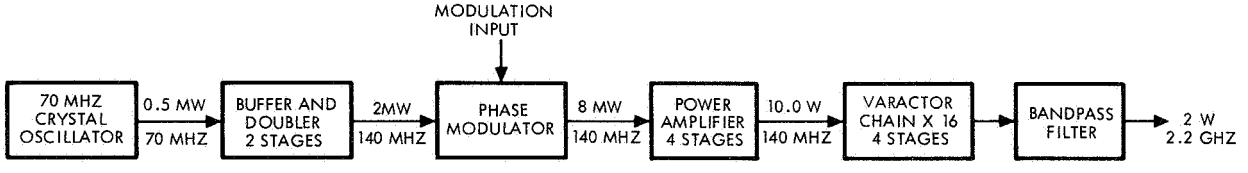

Figure 34a. Simplified Block Diagram of the S-band Telemetry Transmitter

Telemetry subcarriers are phase-modulated on a 140-MHz-RF carrier by a high-linearity varactor phase modulator. Only a small phase deviation is required, since the carrier and hence deviation are multipled by 16 for the final output frequency. RF power (10 w) is developed at a relatively low frequency (140 MHz) where efficiency is high, by means of four transistor stages, shown as the power amplifier block in Figure 33. A cascade of four high-efficiency, push-push varactor doublers multiplies the 140-MHz phase modulated carrier by 16 to obtain the 2200-MHz S-band frequency. Multiplier spurious frequencies are

removed by a high-Q cavity bandpass filter to achieve a high-purity S-band output spectrum having an average power of 2 w. The nominal efficiency (dc to RF) is 10.4 percent.

4.8.3 Diplexer

Functionally, the diplexer must provide for coupling the receiver and transmitter to a common antenna with minimum insertion loss between both units and the antenna while, at the same time, maintain adequate isolation between transmitter and receiver. Such a unit has been developed and space-qualified for the SGLS program and is proposed for the NAVSTAR diplexer. The measured parameters of the SGLS diplexer are as follows:

1)	Receiver-channel insertion loss	1.55 db
2)	Transmitter-channel insertion loss	0.65 db
3)	Receiver-image rejection	85 db (min)
4)	Transmitter-to-receiver isolation	80 db
5)	Transmitter second-harmonic attenuation	80 db

A block diagram of the proposed diplexer is shown in Figure 34b.

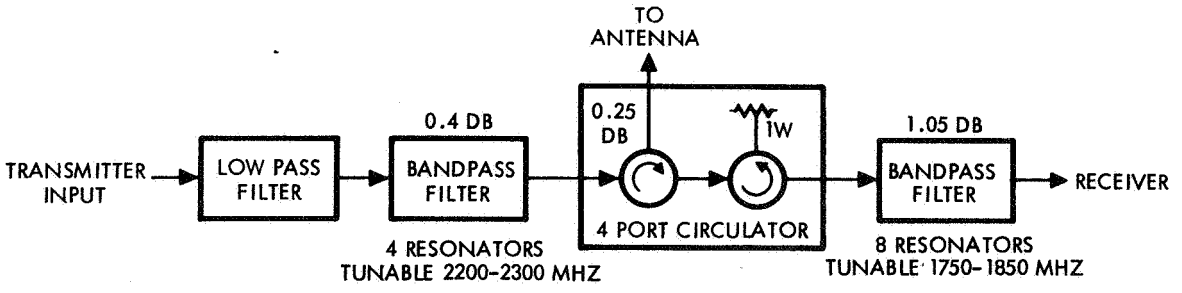

Figure 34b. Block Diagram for the S-band Diplexer

Both the transmitter and receiver bandpass filters are a cascade of optimally coupled cavity resonators having a typical unloaded Q of 2200. A combination of four capacitive sections and a quarter-wave stub, tuned to the second harmonic, provide the 80-db second-harmonic rejection with negligible insertion loss (low-pass filter in Figure 34). The four-port circulator of Figure 33 couples the spacecraft S-band antenna to the two diplexers and assures proper termination of the bandpass filters.

4.8.4 Command Receiver

A fully developed and flight-qualified S-band receiver performing the functions of the command receiver is available from the SGLS program. This all-solid-state, dual-conversion, phase-lock receiver is proposed for use as the NAVSTAR command receiver. A simplified block diagram of the 1800 MHz (1762 to 1842 MHz available by selecting the oscillator frequency) command receiver is shown in Figure 35.

Important features of this receiver design are coherent mixer injection frequencies, low-frequency IF amplifiers, and careful choice of local oscillator and product frequencies so that high-level subharmonics of the incoming frequency are not generated. The last design feature is of vital importance to a locked-loop receiver, since a self-locking mode is possible if a subharmonic of the received frequency is present and of threshold magnitude. Subharmonics were eliminated by means of of the dual conversion technique and by a prudent choice of local oscillator frequencies and multiplier ratios, based on a thorough analysis of all possible spurious mixing products. An added feature, obtained by dual conversion, is the division of IF gain over two frequencies thereby reducing the instability problem of a high-gain tuned amplifier cascade.

The receiver is designed to operate in a sweep mode until carrier phase lock is computed. This reduces the requirements on oscillator stabilities, doppler bandwidth allowance, and minimum loop bandwidth. After carrier phase lock, the sweep circuitry cuts off and a voltage is sent to the telemetry subsystem indicating that the receiver is in a position to demodulate command data.

The output of the receiver from the modulation phase detector are the two FSK command tones (2.0 and 2.9 kHz) keyed at 50 bits per sec. The output of the command tones goes to the command decoder for decoding of the ground station commands.

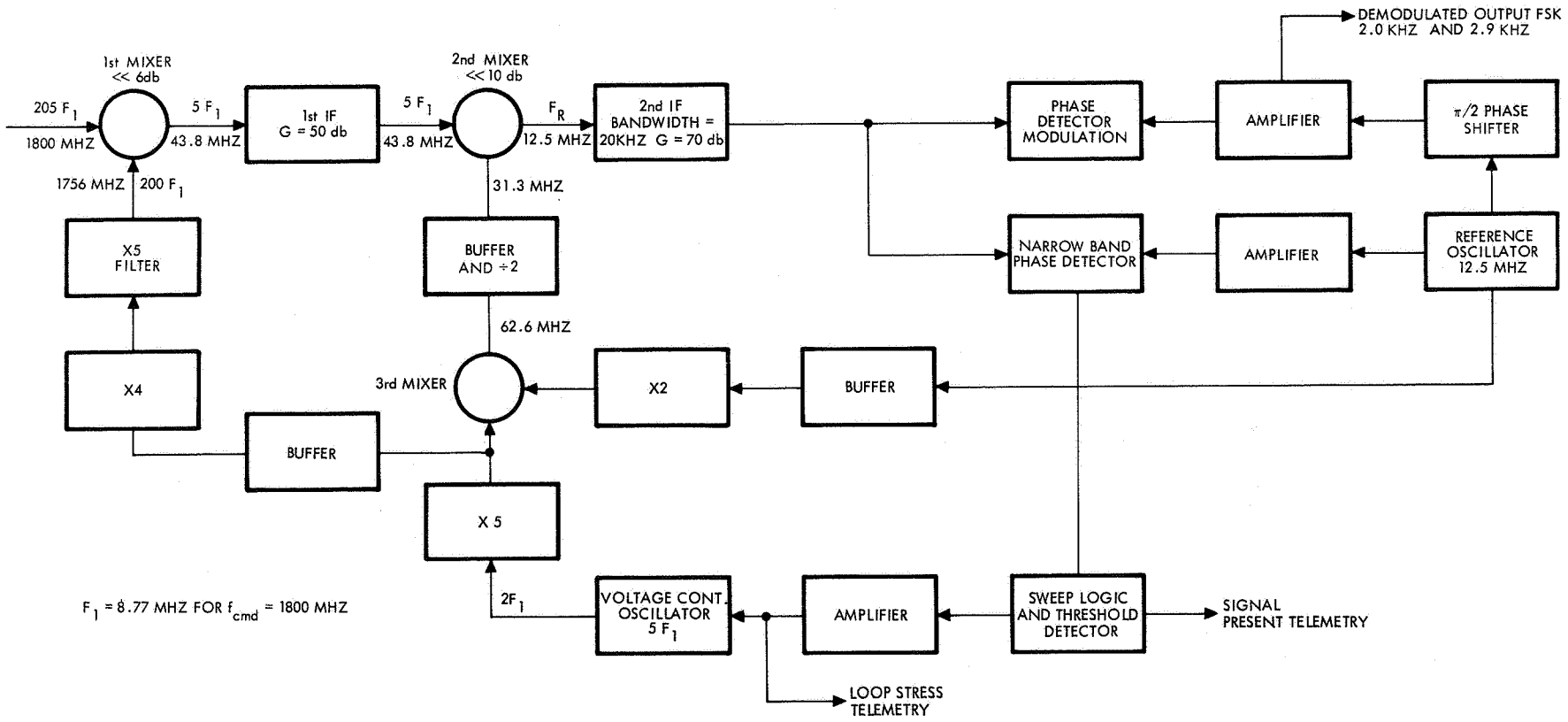

Figure 35. Simplified Block Diagram of the S-band Command Receiver

4.8.5 Command Decoder

The decoder is an advanced design of the type used on the Vela spacecraft with reduced parts count and weight and having power consistent with high reliability. It has two modes of operation, normal and alternate.

In the normal mode, the command decoder is to demodulate the FSK subcarriers (2.0- and 2.9-kHz tones) from the command receiver and process the 50 b/sec data stream into a 9-bit parallel readout corresponding to the command or update information. Each command or data word appears as binary information on these nine lines for 80 μsec at the end of the command sequence. A tenth line delivers an execute signal, which is 60 μsec long and occurs in the center of the command output interval. Whenever no tones are present, a squelch circuit in the input to the decoder disables it and turns off the power to most of its circuits. The nine data lines and the execute line are sent to the electrical integration assembly which provides command processing and distribution.

A preamble consisting of at least 16 zeros (320 μsec burst of the 2000-Hz tone) is required initially for squelch-circuit deactivation. Intercommand bits (all zeros) may be sent to defeat the squelch, thus allowing immediate transmission of a succeeding command without the inclusion of further preamble bits. The squelch circuit prevents inadvertent initiation of the decoding program cycle by noise from the receiver and minimizes standby power consumption.

A synchronizing bit, consisting of a single "1," initiates the decoding program cycle for analysis of the command message format. The data is then shifted into the shift register. A decoder address check is performed by comparing the eight address bits with an externally wired address. The nine command bits are checked, bit-by-bit, with their respective command complement bits for correctness. The worst-case probability of false interpretation of a command is calculated to be 3×10^{-6}.

The command decoding process is timed by a five-stage programmer and suitable gates. The programmer is reset by the loss of the command modulation tones (i.e., by the squelch circuit) or by power interruptions. The output lines are gated by buffer gates, which are enabled only when the command is correctly received, thereby avoiding an "on" failure of any line.

Upon satisfactory completion of the address and command checks, the nine bits stored in the shift register are transferred to the nine output lines via the buffer gates. Each of the output lines will be "high" (+2.5 v) or "low" (+0.4 v), depending on the received command.

The command decoder operates in its Alternate Mode in order to provide the periodic timing pulses required for firing of the positioning and orientation thrusters. In this mode, the decoder senses the "on" or "off" condition of the 2.0 and 2.9-kHz command tones and provides a discrete output corresponding to the pulse duration to the EIA.

The 2.9-kHz tone is considered "on" and the 2.0-kHz tone is considered "standby". By switching, through ground command, from the 2.0- to the 2.9-kHz tone for a specific duration and then switching back, a pulse of that duration is sent to the EIA.

A discrete type I command is sent to the decoder in order to transfer it from the Normal Mode to the Alternate Mode. Once in the Alternate Mode, the tones will be utilized as pulse duration commands to the exclusion of other commands or data as long as one of the two tones remains. To clear the system and revert to Normal Mode, it is necessary to remove both tones for at least 100 sec.

The command decoder also supplies artificial earth pulses to the control logic assembly in the event of failure of one earth sensor. The artificial earth pulse is used as a reference for despining of the navigation antenna as discussed in par. 4.5.2.1. The artificial earth pulses are derived by demodulating the 2.9-kHz tone which is frequency-modulated by ground station operation.

4.8.6 T And C Link Performance

The power budget for the telemetry and command links is given in Tables XVIII and XIX. A worst-case gain of -3.0 db was assumed for the satellite omnidirection antenna, including a linear-to-circular polarization loss of 3.0 db. A 30-ft ground-station antenna was also assumed. With these antennas, the command link has a large margin with only a 100-w transmitter. However, the telemetry link has a small margin with the 2-w telemetry. Consequently, stations receiving telemetry need at least a 30-ft antenna while stations transmitting commands can use a much smaller antenna.

TABLE XVIII

POWER BUDGET-TELEMETRY LINK, 2200 MHz
(PAM/FM/PM)

Parameter	Value
Satellite transmitter power (2 w)	+33.0 dbm
Circuit loss	1.50 db
Satellite antenna gain (omni)	0.0 db
Space loss (22,000 nmi) (2200 MHz)	189.9 db
Polarization loss (maximum)	3.0 db
Ground antenna gain (30-ft parabola)	43.0 db
Ground circuit loss	0.5 db
Net transmission loss	151.9 db
Total received power	-118.9 dbm
Receiver noise spectral density (T_s = 290° K)	-174.0 dbm/Hz
Received carrier-to-noise density ratio (C/Φ)	55.1 db
Required C/Φ	50.5 db
Performance margin	4.6 db

TABLE XIX

POWER BUDGET – COMMAND LINK, 1800 MHz
(PCM/FSK/PM-50 bps)

Parameter	Value
Ground transmitter power (100 w)	50.0 dbm
Circuit loss	2.5 db
Ground antenna gain (30-ft parabola)	43.0 db
Space loss (22000 nmi) (1800 MHz)	189.6 db
Polarization loss (maximum)	3.0 db
Satellite antenna gain (omni)	0.0 db
Satellite circuit loss	1.5 db
Net transmission loss	153.6 db
Total received power	-103.6 dbm
Receiver noise spectral density (N.F. = 6.0 db)	-168.0 dbm/Hz
Carrier Performance	
Carrier modulation loss (1.0 rad peak deviation)	2.3 db
Received carrier power	-105.9 dbm
Carrier loop noise BW ($2 B_{LO}$ = 1-KHz)	30 db
Threshold SNR in $2 B_{LO}$	6.0 db
Threshold carrier power	-128.0 dbm
Performance margin	+22.1 db
Data Performance	
Data modulation loss (1.0 rad peak deviation)	4.1 db
Received data power	-107.7 dbm
Data noise bandwidth (50 Hz)	17.0 db
Threshold SNR in data bandwidth ($P_e = 10^{-5}$)	19.0 db
Threshold data power	-132.0 dbm
Performance margin	+24.3 db

4.9 SATELLITE TRACKING DATA SUBSYSTEM

An L-band transponder has been added to the satellite to provide for a communication link between ground stations in the NAVSTAR network. This link will be used for relaying satellite tracking information from the ground tracking stations to a central station or stations where computations of satellite ephemeris and oscillator corrections are made from the received tracking data.*

The data links will be at L-band so that the navigation signal L-band despun antenna can also be used for this service. In addition, the 50-w navigation signal transmitter will also be used. The transmitter will be time-shared with the navigation signal by utilizing it between navigation signal broadcasts. The power subsystem capability of the satellite indicates that the transmitter can be on 1.1 sec between navigation signal broadcasts at the beginning of satellite life. The links are capable of a data rate of 400 b/sec so that 440 bits per satellite per broadcast frame is possible. Since there are eight satellites in a frame, a total of 3520 bits per satellite broadcast frame can be received by the central data-gathering station or stations, assuming that all eight satellites have a tracking data transponder. This number of bits is more than adequate for continuous updating of the network of satellites' ephermeris and oscillator corrections.

A tentative set of carrier frequency assignments is as follows:

1660 MHz: Uplink Tracking Data Carrier
1551 MHz: Downlink Tracking Data Carrier
1567 MHz: Downlink Navigation Signal Carrier

The two downlink carriers are separated by 16 MHz so that the tracking data carrier will not interfere with the navigation signal received by a user. However, the two carriers are within the 20-MHz bandwidth capability of the L-band transmitter, so that this transmitter can be used for both links as described above. The uplink carrier is at the high end of the L-band so as to ease diplexer requirements.

*Ground-station tracking data consist of the range (difference) measurements made from the L-band navigation signal transmitted to the network users.

4.9.1 Equipment Description

A block diagram of the data-tracking transponder is shown in Figure 36. The dotted lines enclose the equipment which must be added to the satellite to provide the tracking data relay function. Shown inside the dotted lines are a diplexer, plus a receiver which converts the uplink 1660-MHz carrier to an IF frequency for amplification and then up-converts the IF to 517-MHz frequency for driving the L-band navigation signal transmitter. The 517-MHz output at a 22.5 dbm power level serves as one of the inputs to a solid-state switch, which must be placed between the output of the X4 multiplier (which forms the other input to the switch) and the input to the 6-db amplifier in the transmitter (see transmitter block diagram, Figure 33. The 22.5-dbm power is the required level for the input to the amplifier following the switch. The transmitter then amplifies and X3 multiplies the 517-MHz signal from the receiver to 50-w power output and 1551-MHz carrier frequency. The solid-state switch connects either the X4 multiplier or the output of the receiver to the 6-db amplifier under command from a mode-control signal. The mode-control signal generated from the navigation signal subsystem in the satellite determines whether the transmitter is operating in the data-tracking-transponder mode or the navigation-signal mode.

The uplink signal out of the diplexer is fed to a preamplifier which provides enough gain to drive the mixer. The preamplifier can utilize one of the transistorized circuits that are now on the market.

The characteristics of a few of these units are given in the following tabulation:

Manufacturer	Minimum Gain	Noise Figure	Size (in.)	Weight
RHG Electronics	20 db	5.5 db	-	-
Aerotech	20 db	5.2 db	4.5 x 2.5 x 1	13 oz.
International Microwave	15 db	5.3 db	0.75 x 2.5 x 5.0	

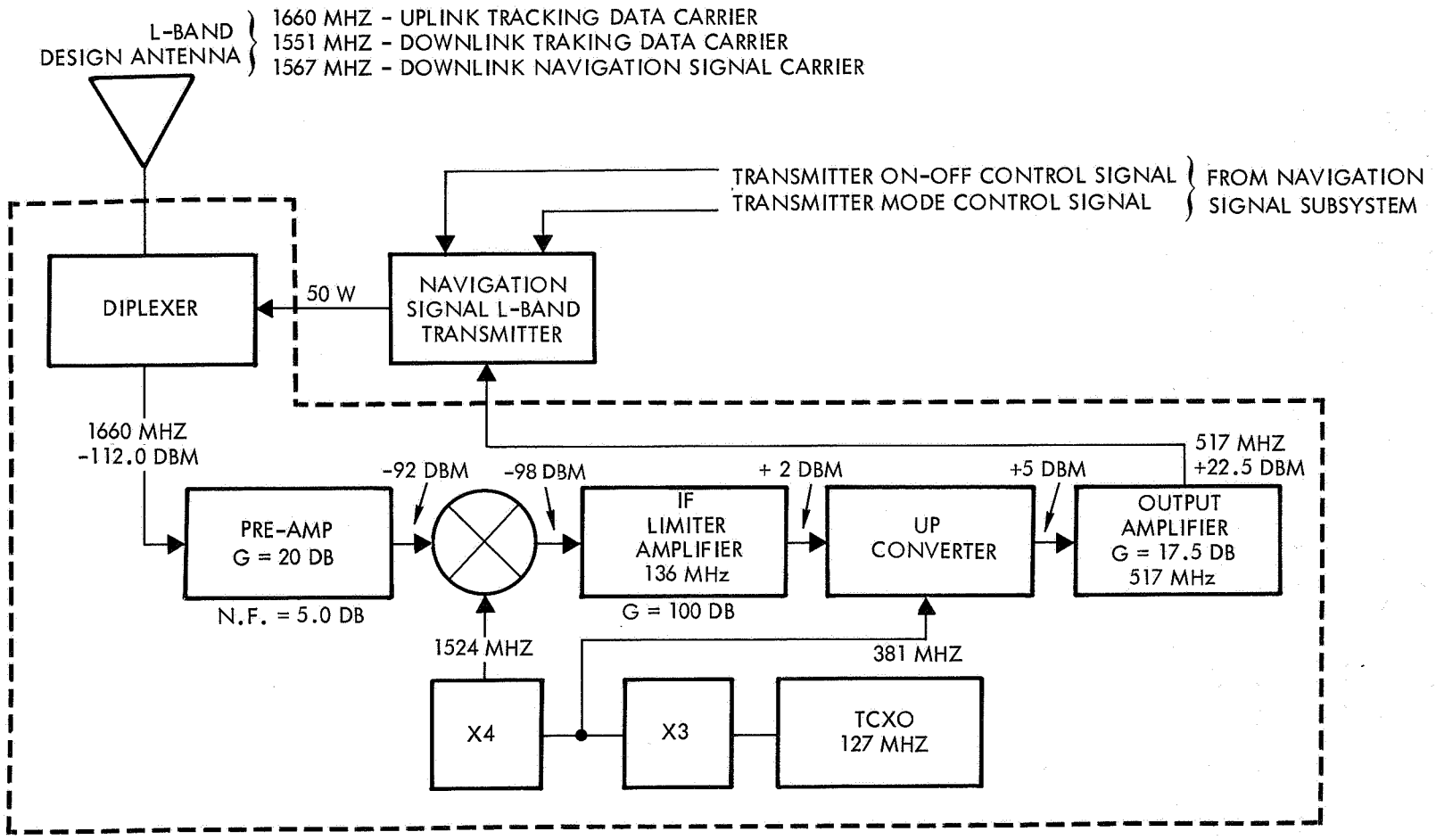

Figure 36. Tracking Data Transponder

A crystal oscillator, operating at 127 MHz, is multiplied by 12 in two multipliers, X3 and X4, to generate the local oscillator signal. These can be transistor multiplier stages using techniques and components that are available today.

The down converter will drive an IF amplifier and limiter circuit. This is a narrowband, 20-kHz, high-gain amplifier. It is needed to bring the signal level up to a level which can be converted to a frequency necessary to drive the low-level stages of the transmitter.

The up-converter will utilize a varactor to give the most efficient frequency conversion. The 381-MHz oscillator signal is obtained from the output of the X3 multiplier in the local oscillator chain. An output amplifier is needed to provide the 22.5 dbm required to drive the following stages in the transmitter.

All techniques required for circuitry in the transponding receiver are within the state-of-the-art. The receiver will require about three w of power. It will be approximately 9 x 2 x 3 in. in size and will weigh about 3 lb, including the preamplifier.

The diplexer provides about 0.5-db insertion loss. It is approximately 6 x 6 x 1 in. in size and will weigh about 1 lb.

4.9.2 Link Power Budgets

Power budgets for the tracking data uplink and downlink are shown in Tables XX and XXI. On the uplink, a signal-to-noise ratio of at least 14.0 db in the 20-kHz IF noise bandwidth of the receiver is specified so as to limit the downlink noise contribution. The downlink noise contribution is given by the following relationship and results in a 2.4 db downlink noise contribution. This value is large because of the X3 multiplication in the transmitter of the receiver output.

$$\text{Downlink noise contribution} = 10 \log\left[1 + N^2 \frac{S_g/\Phi_g}{S_v/\Phi_v}\right] \quad (1)$$

where

N = transmitter multiplication (X3)

Φ_v, Φ_g = noise spectral densities in satellite and ground station, respectively

S_v, S_g = received signal powers in satellite and ground station, respectively.

The downlink power budget assumes FSK modulation of the tracking data on the uplink carrier and noncoherent detection at the receiver. Noncoherent detection is assumed to eliminate carrier acquisition using phase lock receivers. Since the tracking data is received in short bursts (1.1 sec) between satellite navigation signal broadcasts, no time is available for carrier acquisition. Assuming that an 18.0-db signal-to-noise ratio in a bandwidth equal to the bit rate is required for a 10^{-5} bit error rate (about 4 db greater than ideal noncoherent FSK detection), the tracking data link can support a data or bit rate of 400 b/sec with 7.5-db margin.*

The ground stations can utilize the same L-band antennas used for receiving the navigation signal range (difference) data from the satellites. These antennas have been designed to provide 12-db gain (see subsec 4.1). The transmitting stations will require a 1 kw transmitter. The receiving station or stations will require a 5.0 db noise figure receiver and a noncoherent FSK demodulator.

TABLE XX

UPLINK POWER BUDGET TRACKING DATA LINK f_c = 1660 MHz

Parameter	Value
Ground station transmitter power (1 kw)	60.0 dbm
Circuit losses	1.5 db
Ground antenna gain	+ 12.0 db
Space loss (22,000 nmi)	189.0 db
Satellite antenna gain (despun)	+ 16.0 db
Circuit losses (including diplexer)	1.0 db
Net transmission loss	163.5 db

*Since doppler is very small, the FSK filters do not have to be much wider than that needed for the data rate.

TABLE XX

UPLINK POWER BUDGET TRACKING DATA LINK f_c = 1660 MHz (cont'd)

Parameter	Value
Received signal power	-103.5 dbm
Receiver noise spectral density (N.F. = 6.0 db)	-168.0 dbm/Hz
Receiver IF noise bandwidth (20 kHz)	43.0 db
IF noise power	-125.0 dbm
Required IF SNR	14.0 db
Required received signal power	-111.0 dbm
Margin	+ 7.5 db

TABLE XXI. DOWNLINK POWER BUDGET TRACKING DATA LINK f_c = 1551 MHz

Parameter	Value
Satellite transmitter power (50 w)	+ 47.0 dbm
Circuit losses (including diplexer)	1.0 db
Satellite antenna gain (despun)	+ 16.0 db
Space loss (22,000 nmi)	188.4 dbm
Ground antenna gain	+ 12.0 db
Ground circuit losses	1.5 db
Net transmission loss	162.9 db
Received signal power	-115.9 db
Receiver noise spectral density (N.F. = 5.0 db)	-170.0 dbm/Hz
Uplink noise contribution	2.4 db
Data noise bandwidth (400 b/sec)	26.0 db
Data noise power	-141.6 dbm
Required data SNR (b.e.r. = 10^{-5})	18.0 db
Required signal power	-123.6 dbm
Margin	+ 7.7 db

4.10 THERMAL CONTROL

Thermal control of the satellite and its equipment is accomplished by passive techniques. The system requires that an energy balance be made between the external heat sources, external radiant emission, and the internally generated heat at a temperature level within the temperature limits of the components. In sunlit operation, a radiative heat balance is established, while in eclipse the thermal inertia of the individual components serve to maintain the desired temperatures within the satellite.

4.10.1 Requirements

The thermal control subsystem is required to provide a desired thermal environment for the satellite and its components during five post-launch conditions, as follows:

1) Ascent
2) Transfer ellipse coast
3) Orbit injection
4) Orbital operation in eclipse
5) Orbital operation in sunlight

The thermal control system is required to provide the desired thermal environment for all the spacecraft components during any of the orientations obtained for the five conditions listed above. NAVSTAR is a spin-stabilized spacecraft with a mechanically despun antenna. The internal heat dissipation for NAVSTAR varies from approximately 80 to 40 w during its orbital operation. The maximum heat dissipation occurs during the sunlit orbital operation, while the minimum occurs during the eclipsed orbital operation with one battery failed.

4.10.2 System Description

The materials used to maintain the desired temperature range in the NAVSTAR satellite contain no active thermal control materials and are as follows:

1) Selected surface finishes and coatings
2) Multilayer insulation
3) Thermal interface fillers
4) Varying degrees of thermal structural coupling

The equipment platform is thermally isolated from the external structure by fiberglass structural attachments. The thermal radiation exchange between solar panels, equipment platform, and components is minimized by the selection of the coatings on the component and equipment panels. The surface of the solar-array substrates facing the interior of the spacecraft is covered with a high-emittance coating, providing the desired environment for the satellite components.

Interface filler materials of high-thermal conductance assure adequate thermal conduction to the equipment platform from the components with high-heat dissipation.

A careful selection of the components provides thermal balance so as to assure a reasonably uniform heat dissipation over the platform. The platform is made of aluminum honeycomb with metal-to-metal contact between the core and the face sheets to enhance thermal conduction. This type of mounting and support has previously been proved by TRW in the Intelsat III, Vela, and Pioneer programs.

The surfaces of the various components and equipment panels are treated by painting, anodizing, gold plating, or colorless chemical film, where necessary, to provide the desired local emittance. In some cases it is even desirable to just leave the metal bare. This variety of surface finishes or combinations of finishes can be used to achieve any specified temperature level.

Insulation of the apogee motor serves the purpose of maintaining the propellant within a specified range of temperature (30 to 90^{o}F) until

ignition, and prevents overheating of the satellite during apogee motor burning. Some thermal insulation of the apogee motor case from the satellite structure is provided by the use of titanium for the apogee motor adapter cone. This, together with multilayer insulation (five layers each, alternating 0.5 mil aluminum foil with dexiglass paper) wrapped around the motor case, provides protection of the spacecraft components from overheating during apogee motor firing. Figure 37 shows the insulation configuration which will be used on NAVSTAR.

Multilayer insulation also protects the apogee motor propellant from excessive temperature fluctuation during transfer ellipse coast, in combination with a multilayer aluminized Mylar blanket installed across the nozzle exit cone. This blanket, along with a polystyrene plug at the nozzle throat, is blown out at motor ignition. Both the blanket and plug are required to provide adequate thermal control for the engine.

To limit the heat leakage in space, it is necessary to have a cover on each end of the spacecraft. These covers limit the emittance to 0.15 from the top and bottom. Examination of the base-heating problem during apogee motor firing indicates the need for a high-temperature cover on the bottom of the spacecraft to survive apogee motor firing. The cover is made of 1-mil stainless steel with a vacuum-deposited coating and is covered with aluminized Kapton. The stainless steel provides the structural strength to withstand the back pressure from the apogee motor firing. Kapton gives the desired thermal radiation properties.

In a passive system, the electrical components are maintained within their temperature limits by component design requirements such as flatness, component location (equalized heat dissipation on platform), component orientation (maximum mounting area for heat dissipation densities greater than 0.3 w/in^2), baseplate area, and baseplate thickness sufficient to reduce heat densities to acceptable levels. It is desirable to keep the heat dissipation of a component below 0.3 w/in^2 and most of the NAVSTAR components have power densities equal to or less than this. However, certain components, e.g., power control units, exceed this limit. Local increases in baseplate thickness enhance the lateral conduction when required by these high heat-dissipation density units.

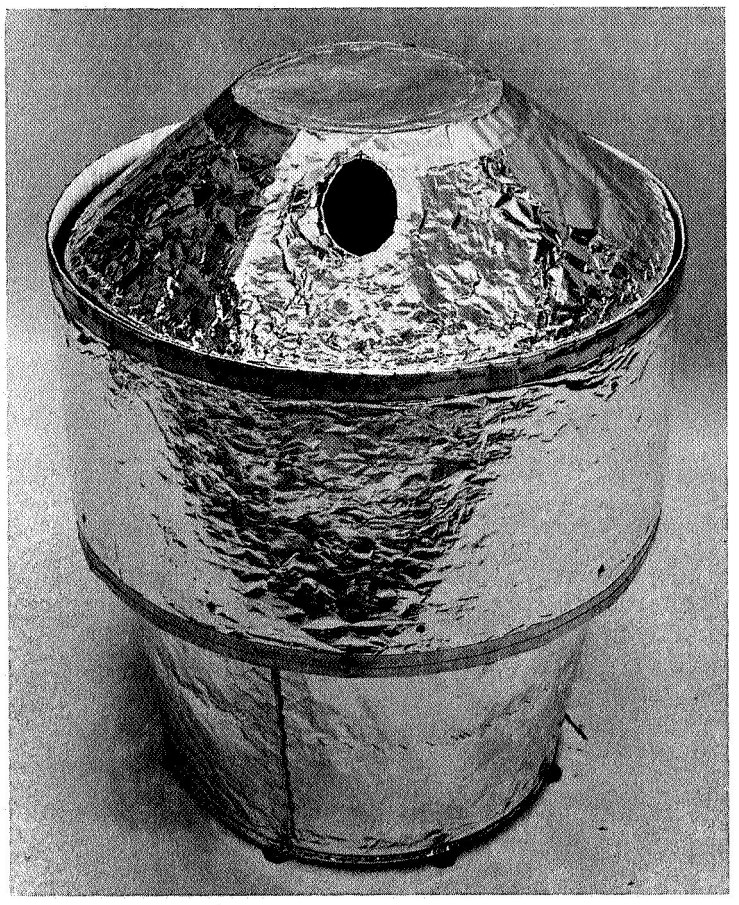

Figure 37. Apogee Motor Insulation

4.11 SYSTEM PERFORMANCE

The equipment, except for the shunt regulators, is located on the platform; the shunt regulators are mounted on the central cylinder.

Numerous studies and tests have been performed on Intelsat III (Ref. 1 through 4). During the thermal analysis of Intelsat III, a 188-node thermal model with 311 resistances was developed. The thermal model provides an analytical tool for evaluation of the thermal design. It divides the spacecraft into analytical nodes. Each of the nodes, representing a segment of the spacecraft, is connected to its adjacent node by thermal resistance to account for conduction and radiative heat transfer. The thermal model utilized the TRW Thermal Analyzer Program (TAP). TAP is an n-dimensional, asymmetric finite difference routine where the

thermal parameters are entered as their electrical analogies for solution on the high-speed digital computers. For this configuration, the results of the Intelsat III thermal analysis were used. Table XXII presents the predicted maximum and minimum temperatures for the NAVSTAR components. Table XXIII indicates the temperatures during eclipse for some of the critical satellite components.

The solar array temperature versus solar inclination angle are presented in Figure 38, and Figure 39 shows solar array temperatures during eclipse. The temperatures are the result of Intelsat III tests (Ref. 2) and analysis.

The propellant tanks have low-emittance finishes, which keep them near the temperature level of the satellite. The hydrazine supply in tanks, lines, and valves are maintained above its freezing point 34°F. The lines are insulated as shown in Figure 40 with 10 layers of aluminized Mylar insulation.

The antenna is despun. Its reflector is aluminum honeycomb with the backside polished to give a low emittance ($\epsilon = 0.05$) to maintain the antenna above its lower temperature limit during eclipse. The polarizer cannot be coated with thermal coatings due to its electrical requirements. The maximum antenna temperature is 150°F. The minimum temperature is -120°F which occurs during eclipse (Figure 41) because of the small amount of power being dissipated in the polarizers and the large heat leakage into space. It may be necessary to add a heater on the antenna to minimize its temperature band.

TABLE XXII

MAXIMUM-MINIMUM NAVSTAR COMPONENT TEMPERATURES

Component	Maximum Temperature (^{o}F)	Minimum Temperature (^{o}F)
Navigation Signal		
Oscillator	93	54
Time base unit	100	36
Data encoder	100	36
Transmitter	152	55
Tracking Data		
Diplexer	70	45
Transponding receiver	70	37
Telemetry and Command		
Telemetry encoder	127	36
Command decoder	127	49
Receiver	70	49
Transmitter	152	60
Diplexer	110	63
Attitude Stabilization		
Control logic	80	17
Valve driver	79	24
Earth-sun sensor package	104	62
Electrical Integration		
Electrical Integration Assembly	113	33
Electrical Power		
Solar array	212	-130
Battery	90	50
Power control unit	94	27
Converter	94	61
Shunt assembly	150	4
Positioning and Orientation		
Thrusters (axial)	120	60
Thrusters (radial)	105	48
Tanks	75	49
Structure		
Central cylinder	300	-31
Equipment platform	122	-10
End cover – top	300	-175
End cover – bottom	950	-175
Thermal Control		
Insulation	68	14
Apogee Motor		
Case	363	35
Nozzle	600	29
Propellant	60	42
Save and arm device	62	33

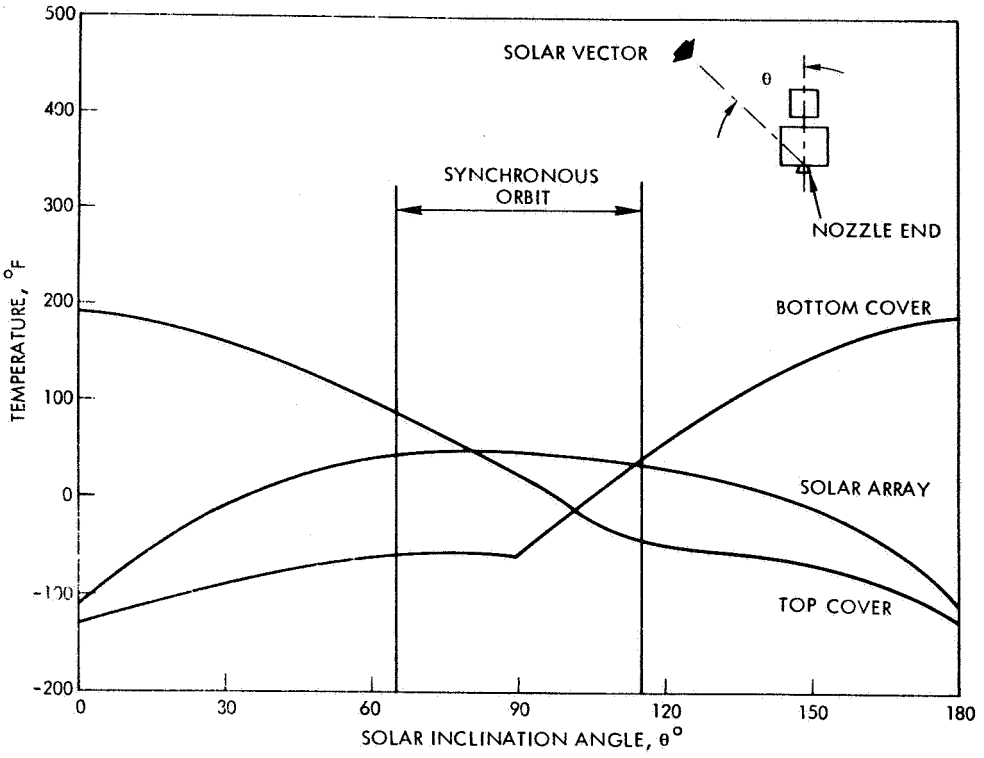

Figure 38. External Temperatures vs Sun Angle

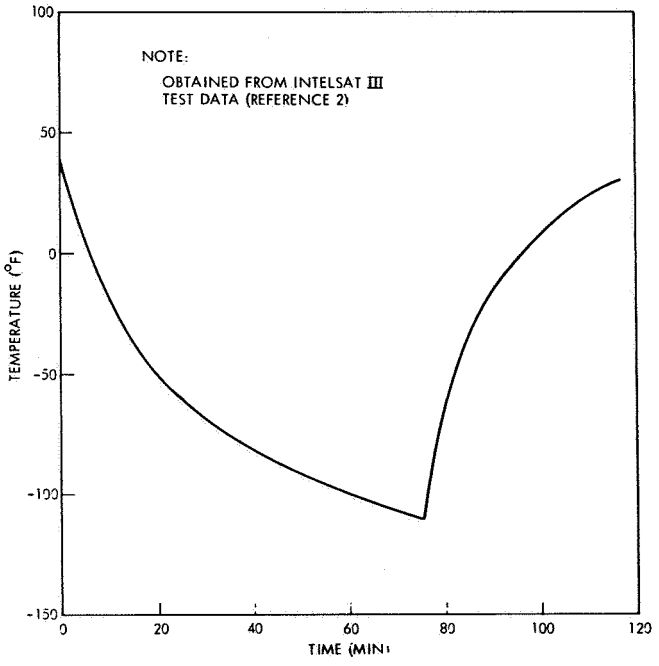

Figure 39. Solar Array Temperature During Eclipse

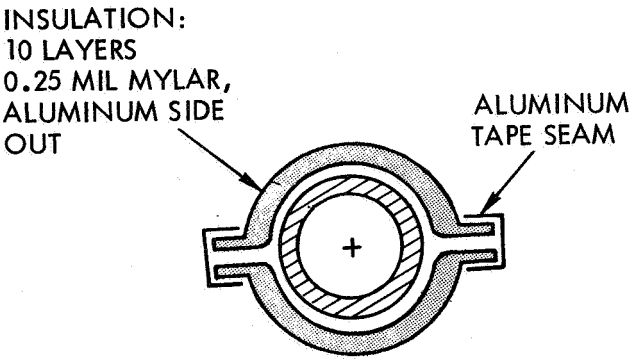

Figure 40. Line Insulation

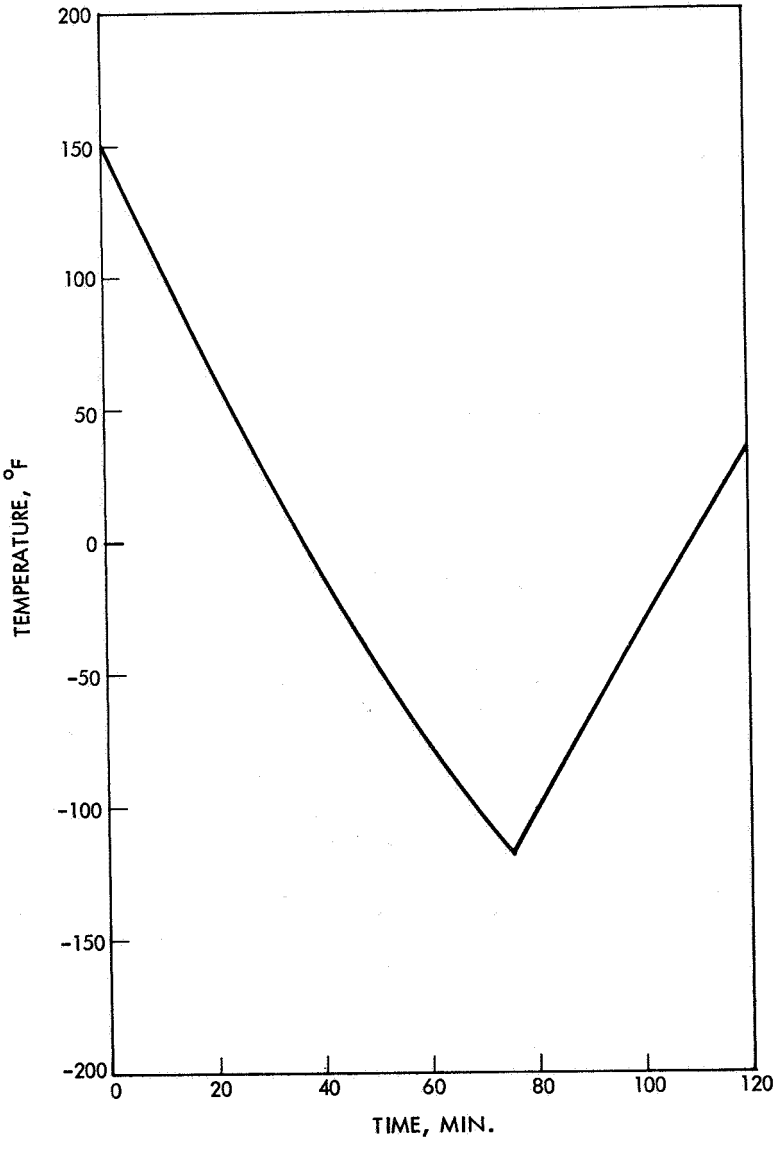

Figure 41. Antenna Temperature

TABLE XXIII

NAVSTAR COMPONENT TEMPERATURES DURING ECLIPSE

Component	Eclipse Temperatures (°F)		
	Start	End	Coldest
Navigation Signal			
Oscillator	76	58	54
Time base unit	81	40	36
Data encoder	81	40	36
Transmitter	112	58	55
Tracking Data			
Diplexer	54	47	45
Transponding receiver	83	41	37
Telemetry and Command			
Telemetry encoder	81	40	36
Receiver	86	53	49
Diplexer	106	63	63

REFERENCES

1. "Communications Satellite," Part I, Technical and Management; Volume 2, Design, 18 October 1965.

2. "General Report on Thermal Control Subsystem Development Test, Intelsat III," TRW IOC 67-3346.100-101, C. O. Meredith, L. E. Laaksonen, 27 September 1967.

3. "Summary Report on Thermal Control Subsystem Development Test, Intelsat III," TRW IOC 67-3346.100-93, C. O. Meredith, L. E. Laaksonen, 8 September 1967.

4. "Intelsat III Tandem Thruster Analysis," TRW IOC 67-3346.101-17, C. O. Meredith, F. Herzberg, 17 October 1967.

5. RELIABILITY

The question of orbiting vs spacecraft subsystem redundancy has been approached as follows. If a user knows his altitude, he needs to view three noncoplanar satellites in order to determine his position. Thus, the approach to the design of the constellation has been to provide four satellites visible at all times in the region of interest in case any satellite fails and causes a slight degradation in accuracy, but still permits the use of the navigation satellite system. The MTTF is sufficiently lon so that it is relatively straightforward to schedule a replacement for the failed satellite.

Given a ground rule of at least one redundant satellite, it remains to then design each satellite such that the overall MTTF is as large as possible consistent with launch physical constraints. This section presents the results of such a study.

5.1 INTRODUCTION

For reliability analysis purposes, NAVSTAR consists of 10 subsystems. These are structures, thermal control, apogee motor and safe/arm, position and orientation, attitude determination and control, antenna despin, and electrical power. These designs have been developed and are now undergoing test and reliability verification on other programs. This will provide some validation data against which future reliability estimates can be measured. In time, ground and orbit experience will provide substantial reliability data for use on the NAVSTAR program.

The three subsystems which are new designs for the NAVSTAR are navigation signal, telemetry and command, and electrical distribution.* These new designs can all be constructed using space qualified components and after suitable testing will exhibit the predicted reliability with substantial confidence.

---

*The tracking data communications subsystem is not included since it can fail without causing a system failure.

5.2 SUMMARY

The numerical reliability estimate for the NAVSTAR is 0.455 for a 5-year orbital mission including launch boost and deployment. This corresponds to a MTTF of 61.57 months. Table XXIV lists the equipment reliabilities per phase for the three mission phases for the 10 NAVSTAR subsystems.

The reliability values listed in Table XXIV were developed by employing the following conditional probability functions.

$$R_{(\text{Deployment})} = \frac{R_{(\text{Deployment plus Launch/Boost})}}{R_{(\text{Launch/Boost})}}$$

$$R_{(\text{Orbit})} = \frac{R_{(\text{Deployment plus Launch/Boost Plus Orbit})}}{R_{(\text{Deployment plus Launch/Boost})}}$$

TABLE XXIV

SUBSYSTEM RELIABILITY PER MISSION PHASE

Subsystem	Mission Phases		
	Launch/ Boost	Deployment	5-Year Orbit
1) Structures	$0.9^{3}488$	$0.9^{3}878$	$0.9^{5}36$
2) Thermal Control	$0.9^{8}550$	$0.9^{8}400$	$0.9^{7}105$
3) Apogee Motor & Safe/Arm	0.9984	0.9938	0.9922
4) Position & Orientation	$0.9^{5}545$	$0.9^{3}846$	0.9860
5) Attitude Determination and Control	$0.9^{3}886$	$0.9^{3}849$	0.9737
6) Antenna Despin Assembly	$0.9^{4}75$	$0.9^{4}62$	0.9437
7) Electrical Power	$0.9^{4}860$	$0.9^{4}82$	0.9940
8) Navigation Signal	$0.9^{5}80$	$0.9^{5}10$	0.8573
9) Telemetry & Command	$0.9^{5}0$	$0.9^{4}54$	0.7049
10) Electrical Distribution	$0.9^{3}677$	$0.9^{3}565$	0.8436
TOTALS:	0.99740	0.9928	0.4592

5.3 SYSTEM RELIABILITY CALCULATIONS

The reliability of NAVSTAR is computed for the launch/boost, deployment and 5-year orbit phases. The overall reliability of the satellite is computed by multiplying the probability of success for the three mission phases for each subsystem. Figure 42 depicts a simplified reliability block diagram of NAVSTAR, defining the total mission reliability for each subsystem. Detailed reliability block diagrams per subsystem, where appropriate, are incorporated in the subsystem reliability analysis, subsec. 5.5.

Most of the subsystems in the equipment incorporate considerable redundancy. Redundancy was incorporated in the design by employing the following approach. Each candidate assembly and its estimated weight were listed. Then the marginal increase in system reliability per lb of additional assembly weight was computed for each candidate. The particular assembly which resulted in the greatest system reliability improvement per pound was incorporated as redundant in the equipment. The procedure was then repeated with the initial redundant unit incorporated in the system, and a second redundant unit was added. The procedure was repeated until sufficient redundancy was introduced such that the reliability objectives were obtained, while still remaining within the weight constraints. This procedure of adding units whose contribution to system reliability per pound of additional weight is maximum will result in adding redundancy in an optimum manner since the marginal increase in reliability per pound of additonal weight will be decreasing. This means that, on a particular trial, the candidate selected for redundancy would be the optimum choice. This results in optimum selection for each trial and for the total system.

In most optimization approaches, more than one parameter requires tradeoff analysis. For example, it would be reasonable to optimize reliability as a function of cost, weight, performance, safety, etc. There are existing optimization techniques, such as dynamic programming, which can be effectively applied to reliability optimization problems. Future tradeoff optimization studies involving multiple parameters will be made employing dynamic programming techniques, considering multiple constraint parameters.

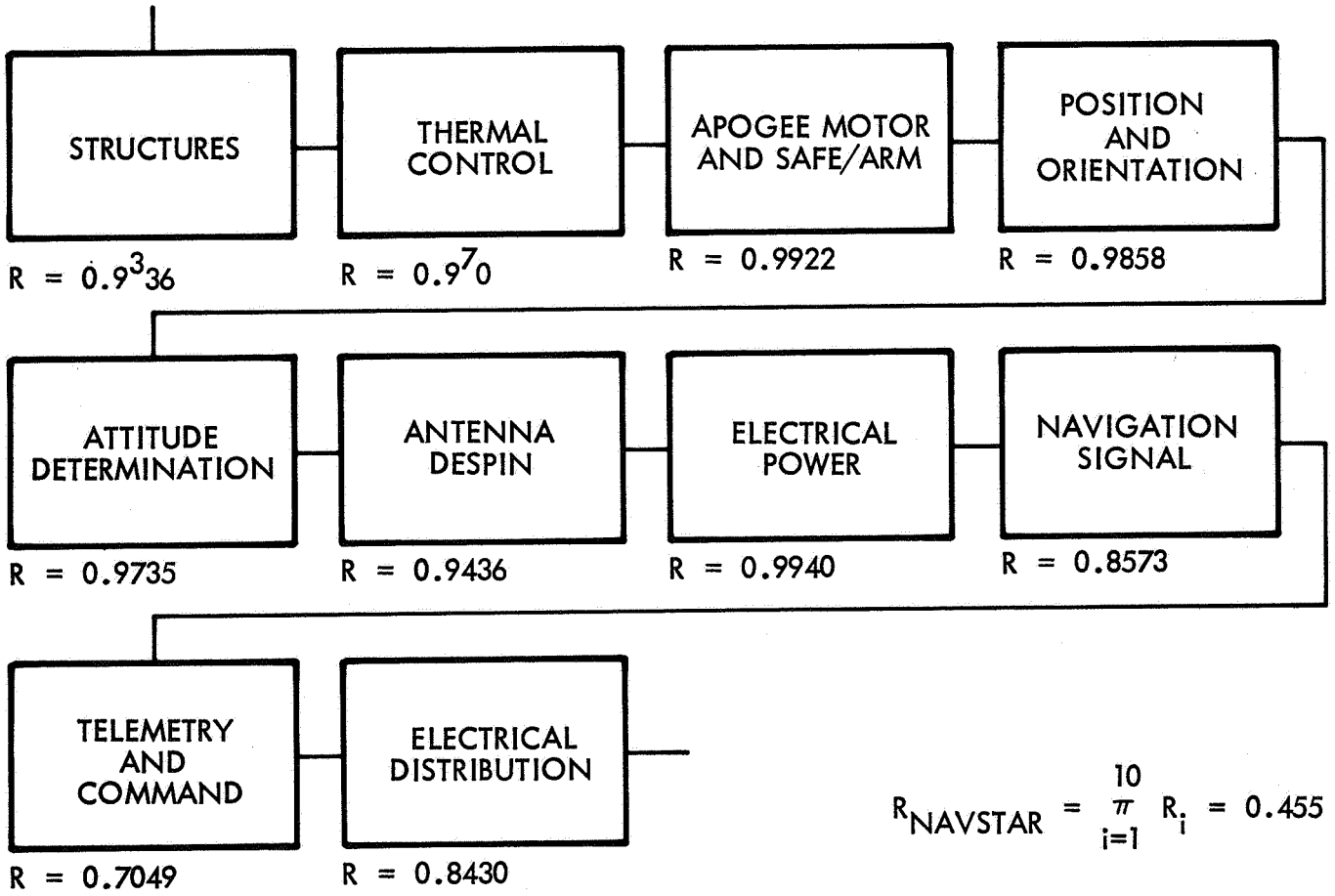

Figure 42. Simplified Reliability Block Diagram of NAVSTAR

5.4 MTTF CALCULATION

Since the NAVSTAR incorporates considerable redundancy, calculation of the MTTF requires special analysis techniques. The technique applied here is to divide the total spacecraft mission into two phases: launch/boost/deployment and orbit. The total launch/boost/deployment time is 265 hr (0.37 months) and the total orbit time is 43,800 hr, or 5 yr. Generally, different failure distributions will apply during these two phases. The satellite population may be divided into two mutually exclusive (but not independent) parts according to phase; i.e. those assemblies which fail during the early phase and those assemblies which fail during the orbital phase. The satellite MTTF in months may be computed as a weighted average of the MTTF's of these two populations.

$$MTTF_{NAVSTAR} = P_1 \, MTTF_1 + P_2 \, (MTTF_2 + 0.37) \qquad (1)$$

where

$MTTF_{NAVSTAR}$ = satellite MTTF in months

P_1 = proportion of the population failing in Phase I

P_2 = proportion of the population failing in Phase II

$MTTF_1$ = MTTF of the population failing in Phase I

$MTTF_2$ = MTTF of population failing in Phase II

0.37 months = mission time to the start of Phase II

The four unknowns (P_1, P_2, $MTTF_1$, $MTTF_2$) are estimated for several time points in the mission, (see Table XXV). From the table, P_2 = 0.99235; $P_1 = 1 - P_2 = 0.00765$. The estimate of $MTTF_2$ is obtained by employing estimation techniques using the Weibull distribution.

$$MTTF_2 = \alpha^{1/\beta} \, \Gamma \, (1 + 1/\beta) \qquad (2)$$

α = Weibull scale parameter

β = Weibull shape parameter

If the overall system distribution were exponential, β would equal unity. In this case $\beta = 1.46$ and $\alpha = 477.0$. Estimates of α and β were obtained by plotting satellite reliability vs time on Weibull probability paper and

TABLE XXV

SATELLITE AND SUBSYSTEM CUMULATIVE RELIABILITY VS TIME

Mission Times / Subsystem	Phase I - 265 hr	Phase II - Years in Orbit				
	Launch/ Boost/ Deploy-ment	1 year	2 years	3 years	4 years	5 years
Structures	$0.9^{3}37$	$0.9^{5}36$	$0.9^{5}36$	$0.9^{5}36$	$0.9^{5}36$	$0.9^{5}36$
Thermal Control	$0.9^{8}00$	$0.9^{7}11$	$0.9^{7}11$	$0.9^{7}11$	$0.9^{7}11$	$0.9^{7}11$
Apogee Motor & Safe/Arm	0.9922	0.9922	0.9922	0.9922	0.9922	0.9922
Position & Orien-tation	$0.9^{3}84$	0.9947	0.9941	0.9912	0.9884	0.9860
Attitude Determi-nation	$0.9^{3}73$	0.9951	0.9900	0.9847	0.9793	0.9738
Antenna Despin	$0.9^{4}37$	0.9963	0.9882	0.9763	0.9613	0.9437
Electrical Power	$0.9^{4}68$	0.9993	0.9983	0.9971	0.9957	0.9940
Navigation Signal	$0.9^{4}89$	0.9948	0.9782	0.9491	0.9082	0.8514
Telemetry & Command	$0.9^{4}44$	0.9800	0.9316	0.8646	0.7870	0.7049
Electrical Dis-tribution	$0.9^{3}2$	0.9812	0.9541	0.9210	0.8837	0.8436
Satellite Cumu-lative Reliability	0.9935	0.9345	0.8373	0.7143	0.5837	0.4592

then obtaining a least-squares fit for the plot of the probabilities. Substituting α and β into equation 2 yields $MTTF_2 = 61.6$ months.

$$MTTF_2 = (477)\, 0.685\, \Gamma\, (1.685)$$

$$= 61.6 \text{ months}$$

Since phase II actually starts 0.37 months after launch, the average time to failure for population 2 is 61.6 + 0.37 = 61.97 months. Substituting these values in Eq. 1,

$$MTTF_{NAVSTAR} = (0.00765)(MTTF_1) + (0.99353)(61.97)$$

$$= (0.00765)(MTTF_1) + (61.57)$$

$MTTF_1$ lies between zero and 0.37 months.

Therefore

$$MTTF_{NAVSTAR} \geq (0.00765)(0) + (61.57) = 61.57 \text{ months}$$

$$MTTF_{NAVSTAR} \leq (0.00765)(0.37) + (61.57) = 61.572$$

or $$61.57 \leq MTTF \leq 61.572.$$

An MTTF value of 61.57 months is thus estimated.

5.5 SUBSYSTEM RELIABILITY ANALYSIS

5.5.1 Structures Subsystem

The structures subsystem reliability analysis is based upon the Intelsat III reliability evaluation. The analysis did not incorporate the effect of micrometeoroid penetration. The overall reliability assessment for the structures subsystem is:

- Launch/Boost 0.9^3488
- Deployment 0.9^3878
- Orbit 0.9^536

Total structures reliability is the product of these three terms = 0.9^336.

5.5.2 Thermal Subsystem

The thermal subsystem is completely passive consisting of thermal blankets and thermal insulation. The reliability assessment for the thermal equipment is:

- Launch/Boost 0.9^8550
- Deployment 0.9^8400
- Orbit 0.9^7105

The thermal subsystem reliability is the product of these three terms = 0.9^70.

5.5.3 Apogee & Safe/Arm Subsystem

This equipment is comprised of the apogee motor and safe/arm devices. The safe/arm device provides ground safety and arms the apogee motor. Considerable testing has been performed on the motor and the reliability assessment for the motor, including the safe/arm assembly is 0.9922. This is apportioned as follows:

- Launch/Boost 0.9984
- Deployment 0.9938

The apogee motor is not required during the orbit phase.

5.5.4 Position and Orientation Subsystem

The position and orientation subsystem is simplified from the Intelsat by eliminating two propellant tanks, one pressure transducer, one fill and drain valve and one ordnance valve. The total number of components in the subsystem is reduced from 17 to 12, resulting in a slightly higher reliability, compared to the four tank configuration of Intelsat III. The reliability for the position and orientation subsystem is 0.9858. The reliability per phase is:

- Launch/Boost $0.9^{5}545$
- Deployment $0.9^{3}846$
- Orbit 0.9860

5.5.5 Attitude Determination & Control Subsystem

The attitude determination and control consists of four units, the control logic assembly, the valve driver assembly, the sun sensor and the earth sensor. The control logic assembly functions in one of three modes.

The control logic assembly is defined as operational if at least one of the modes of operation are successful. The block diagram for the subsystem is shown in Figure 43.

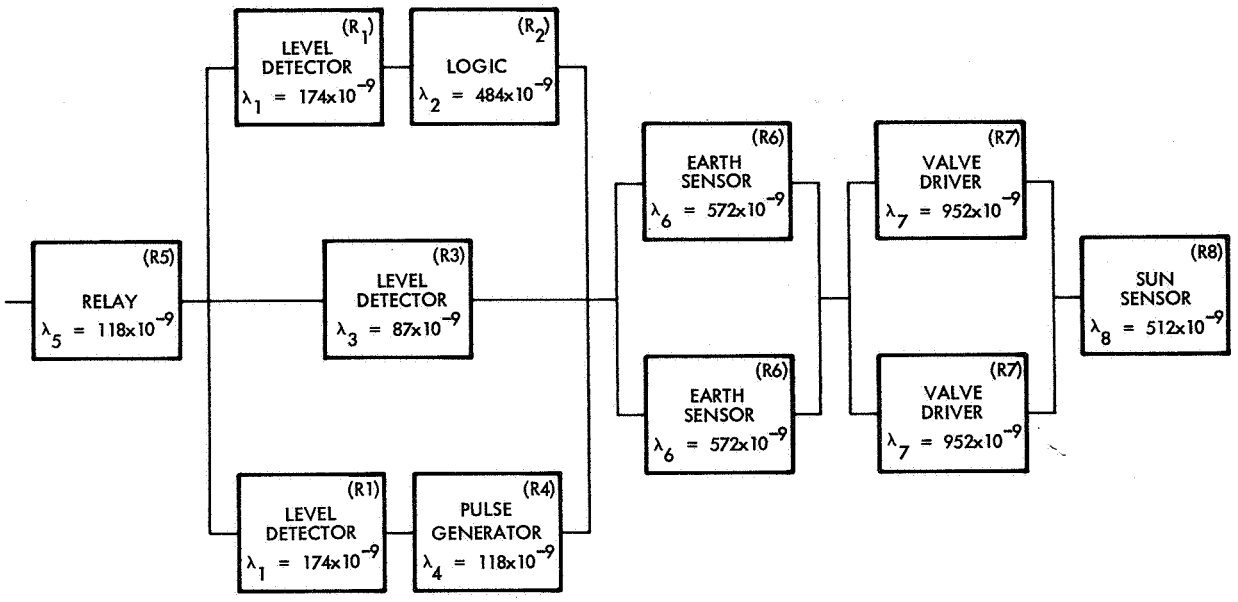

Figure 43. Reliability Block Diagram of Attitude Determination and Control Subsystem

$$R_{\text{Attitude Determination}} = [R_1R_2+R_3+R_1R_4-R_1R_2R_3-R_1R_2R_4-R_1R_3R_4+R_1R_2R_3R_4]\,[R_5]\left[2R_6-R_6^2\right]\left[2R_7-R_7^2\right]R_8$$

The reliability assessment per phase is:

- Launch/Boost 0.9^3886
- Deployment 0.9^3849
- Orbit 0.9737

The total reliability for the subsystem is 0.9735.

5.5.6 Antenna Despin Subsystem

The antenna despin subsystem is required to provide a highly directional despin mode antenna unit. The subsystem consists of active redundant control electronics and the despin motor. The reliability block diagram of this subsystem is shown in Figure 44.

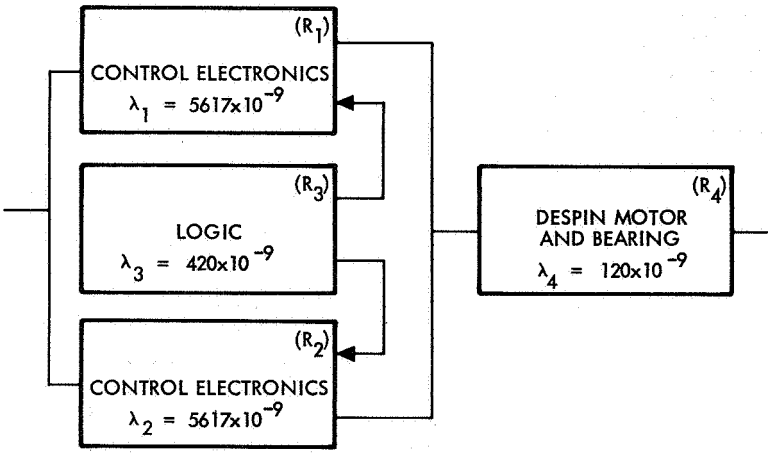

Figure 44. Reliability Block Diagram of Antenna Despin Subsystem

$$R_{\text{Antenna Despin}} = [R_1 + (1-R_1)R_2R_3]\ R_4$$

The reliability assessment for the subsystems

- Launch/Boost 0.99885
- Deployment 0.99849
- Orbit 0.9437

The reliability for the subsystem is 0.9436

5.5.7 Electrical Power Subsystem

The electrical power subsystem consists of four functional units, the solar array, battery, converter and power control unit (PCU) and shunt. The electrical power subsystem incorporates considerable redundancy. The batteries are redundant and one of the two batteries is sufficient to perform all mission functions. The converter is also redundant and the PCU incorporates considerable internal redundancy. Finally, the shunts are redundant. The reliability block diagram of the electrical power subsystem is shown in Figure 45.

$$R_{\text{Electrical Power}} = R_1 \left[2R_2 - R_2^2\right] [R_3 (1 + \lambda_3 R)]\ R_4$$

The reliability assessment per phase is:

- Launch/Boost $0.9^4 86$
- Deployment $0.9^4 82$
- Orbit 0.9940

The total reliability of the electrical power subsystem is 0.9940.

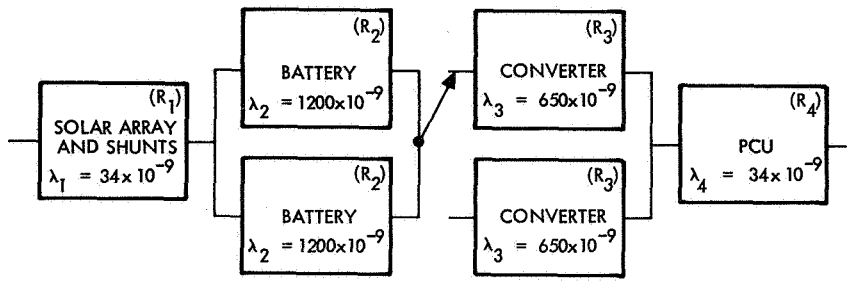

NOTE: THE SWITCH IN THE RELIABILITY BLOCK DIAGRAM INDICATES STANDBY REDUNDANCY. OTHERWISE, ACTIVE PARALLEL REDUNDANCY IS EMPLOYED.

Figure 45. Reliability Block Diagram of Electrical Power Subsystem

5.5.8 Navigational Signal Subsystem

The navigation signal subsystem consists of a highly stable oscillator, time base unit, data encoder and scanner and high power transmitter. This subsystem incorporates considerable redundancy as shown by the reliability block diagram presented in Figure 46.

$$R_{Navigation} = \left[2R_1 - R_1^2\right]\left[R_2(1+\lambda_2 T)\right]\left[R_3\left(1+\lambda_3 T + \frac{\lambda_3^2 T^2}{2}\right)\right]\left[R_4(1+\lambda_4 T)\right]$$

The reliability assessment per phase is:

- Launch/Boost $0.9^5 80$

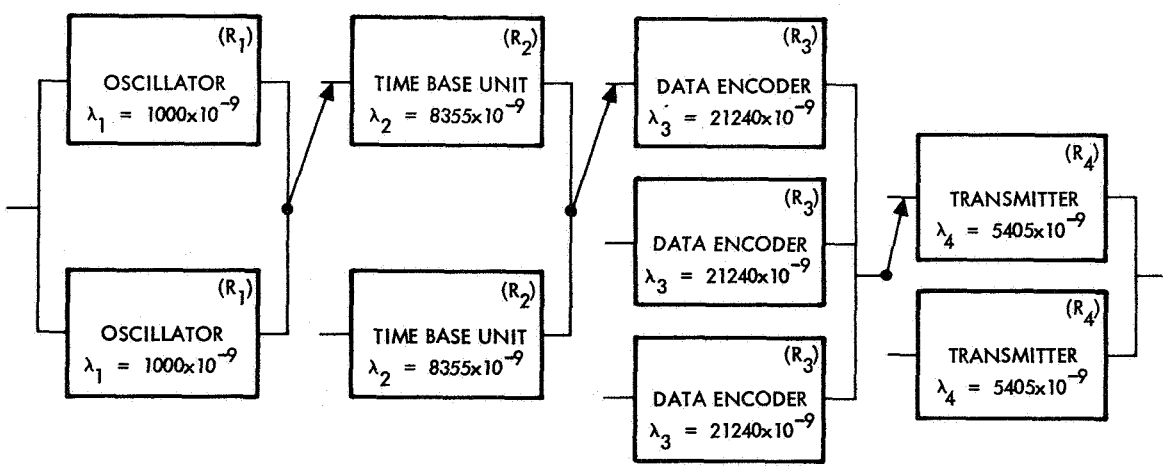

Figure 46. Reliability Block Diagram of Navigation Signal Subsystem

- Deployment $0.9^5 10$
- Orbit 0.8573

The total reliability for the navigation signal subsystem is 0.8573.

Note: The switch in the reliability block diagram indicates standby redundancy. Otherwise, active parallel redundancy is employed.

5.5.9 Telemetry and Command Subsystem

The telemetry and command subsystem consists of an S-band transmitter, receiver, encoder, and command decoder. Also a transponder for signal repeater functions is included, but this equipment is not considered in-line for reliability analysis purposes. The subsystem incorporates considerable redundancy; i.e., each unit incorporates parallel redundancy, either active or standby. The reliability block diagram for the subsystem is shown in Figure 47.

$$R_{\text{Telemetry \& Command}} = [R_1(1 + \lambda_1)T]\left[2R_2 - R_2^2\right]\left[2R_3 - R_3^2\right]\left[2R_4 - R_4^2\right]$$

The reliability assessment for each mission phase

- Launch/Boost $0.9^5 0$
- Deployment $0.9^4 54$
- Orbit 0.7049

The total reliability for the subsystem is 0.7049.

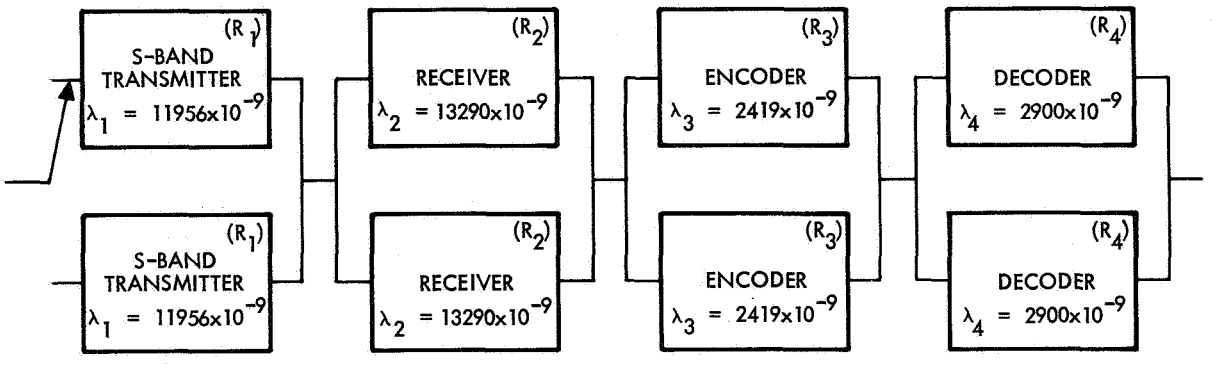

Figure 47. Reliability Block Diagram of Telemetry and Control Subsystem

5.5.10 Electrical Distribution Subsystem

The electrical distribution subsystem provides the interface between all the subsystems. The subsystem receives signals from the command decoder, converts them to discrete commands and sends the commands to the other subsystems. The basic electrical distribution sequencer is redundant, while the output gates are considered in-line. The reliability block diagram for the electrical distribution subsystem: is shown in Figure 48.

$$R_{\text{Electrical Distribution}} = \left[2R_1 - R_1^2\right][R_2]$$

The reliability assessment for the electrical distribution subsystem is:

- Launch/Boost 0.9^3677
- Deployment 0.9^3565
- Orbit 0.8436

The total reliability for the subsystem is 0.8430.

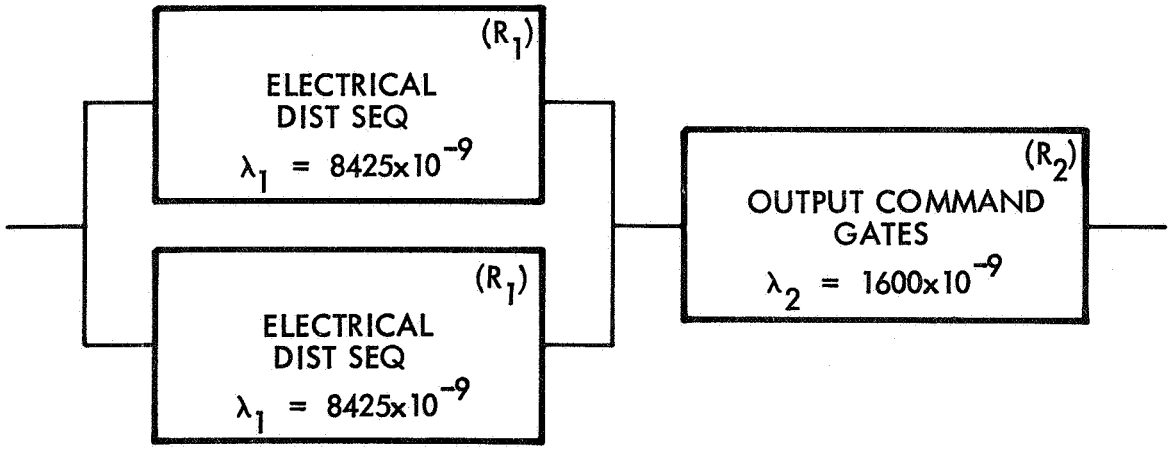

Figure 48. Reliability Block Diagram of Electrical Distribution Subsystem

APPENDIX A

NEW TECHNOLOGY

New technology and innovations developed under this contract are discussed in the appendix to vol. I.

APPENDIX B
VERY STABLE OSCILLATORS – A SURVEY

by

J. M. Andres

August 1967

QUANTUM ELECTRONICS DEPARTMENT
PHYSICAL RESEARCH CENTER

TABLE OF CONTENTS

I. INTRODUCTION

This report is a survey of some of the more important very stable oscillators or frequency standards. Included in the survey are quartz crystal oscillators, rubidium gas cell and cesium atomic beam frequency standards, and the atomic hydrogen beam maser. The principles of operation and the frequency stability characteristics of these devices are treated, and the physical characteristics, i.e., weight, dimensions, of several commercially available oscillators, are presented.

The quartz crystal oscillator was developed in the early 1920's and is the stable oscillator in widest use. The atomic frequency standards were developed in the 1950's and became commercially available in that decade as the ammonia maser and the cesium beam frequency standard. The optically pumped rubidium standards became commercially available in the early 1960's and the hydrogen beam maser became a commercial product in the mid-60's.

Each of these devices has its virtues and limitations as will become evident in the discussion that follows. It is hoped that this report will enable the reader to make an intelligent decision as to which stable oscillator is best suited to his particular needs.

II. OPERATING PRINCIPLES

A. Quartz Crystal Oscillators

Quartz crystal oscillators are basically mechanically vibrating elements driven by electrical means. They are invariably for fixed-frequency operation and are capable of a very high degree of frequency stability. These quartz oscillators belong to the same family of oscillators as the electrically driven tuning fork oscillator, but the unique physical properties of quartz give it a tremendous advantage over other mechanical oscillators.

Crystalline quartz has great mechanical and chemical stability, and a very small amount of power is required to overcome mechanical losses and maintain the oscillation. As a consequence the mechanically oscillating system can be decoupled considerably from the environment. The piezoelectric properties of crystalline quartz provide a convenient means of coupling the mechanical oscillations to an electrical circuit. Thus, an electric field gives rise to a mechanical deformation of the crystal, and conversely, crystal deformation results in surface charges on the crystal faces, allowing energy to be transmitted to an electrical circuit.

In use, a quartz crystal resonator is mechanically supported at points chosen to avoid inhibiting the desired vibrations and to suppress unwanted modes of vibration. Thin metallic electrodes are evaporated directly upon the opposite faces of the crystal, and an alternating voltage applied across the crystal causes it to vibrate in the desired manner. A number of different vibrational modes are posssible for a plate of quartz including flexural, face-shear, thickness-shear and others. In the case of the best precision crystal oscillators a fifth-overtone thickness shear mode of vibration is used in which the resonant frequency is either 5 MHz or 2.5 MHz.[1/]

A mathematical analysis of the mechanical oscillation, taking into account the piezoelectric coupling mechanism gives rise to the equivalent circuit for the quartz resonator shown in Figure 1. The capacity C_1 represents the electrostatic capacity of the quartz plate between the metal electrodes. The resistance R corresponds to elastic wave losses in the crystal and any energy losses through the crystal mounts. The L and C_2 represent the resonance parameters associated with the mass and spring constant of the

vibrating quartz. In general $C_1 >> C_2$, L is many henries, and R is very small, so that the Q of the circuit is very high ($>10^5$). The high ratio C_1/C_2 implies very loose coupling between the tuned circuit and the other parts of the oscillator circuit. The resonance frequency depends upon temperature through the linear expansion coefficient, the variation in density with temperature and the variation in modulus of elasticity with temperature. It is possible to cut the crystal so that the orientation of the crystalline faces assume any arbitrary angle with respect to the crystalline axes. By choosing the orientation in a suitable manner, it is possible to obtain a very small frequency-temperature coefficient over a fairly wide temperature range. The effects of any remaining temperature dependence can be further reduced by placing the crystal in a well insulated temperature-controlled box.

In order to ensure oscillation stability the oscillator circuit elements are also often included within the temperature controlled oven, and care is taken so that the drive level in the oscillator circuit is maintained constant through the use of negative feedback and A.G.C. techniques. In addition, a "buffering" stage is added to minimize the influence of the load on the oscillations. Figure 2 is a schematic diagram of a commercially available precision crystal oscillator. A number of circuits have been invented for use with quartz crystal oscillators; for example, Ref. 2 discusses several.

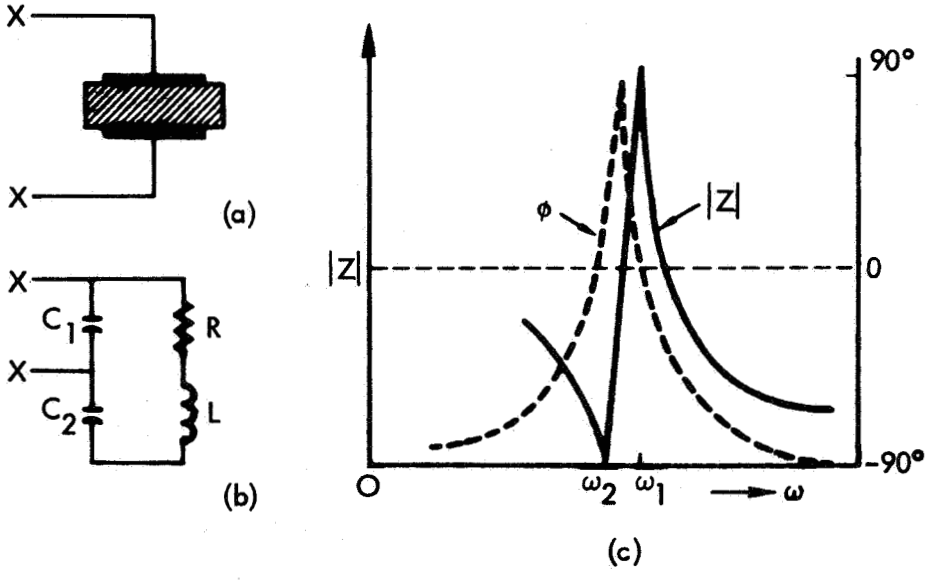

Figure 1. a) Quartz resonator, b) equivalent circuit, and c) magnitude and phase angle of impedance. $\omega_2 = 1/\sqrt{LC_2}$, $\omega_1 = \omega_2\sqrt{1+C_2/C_1}$.

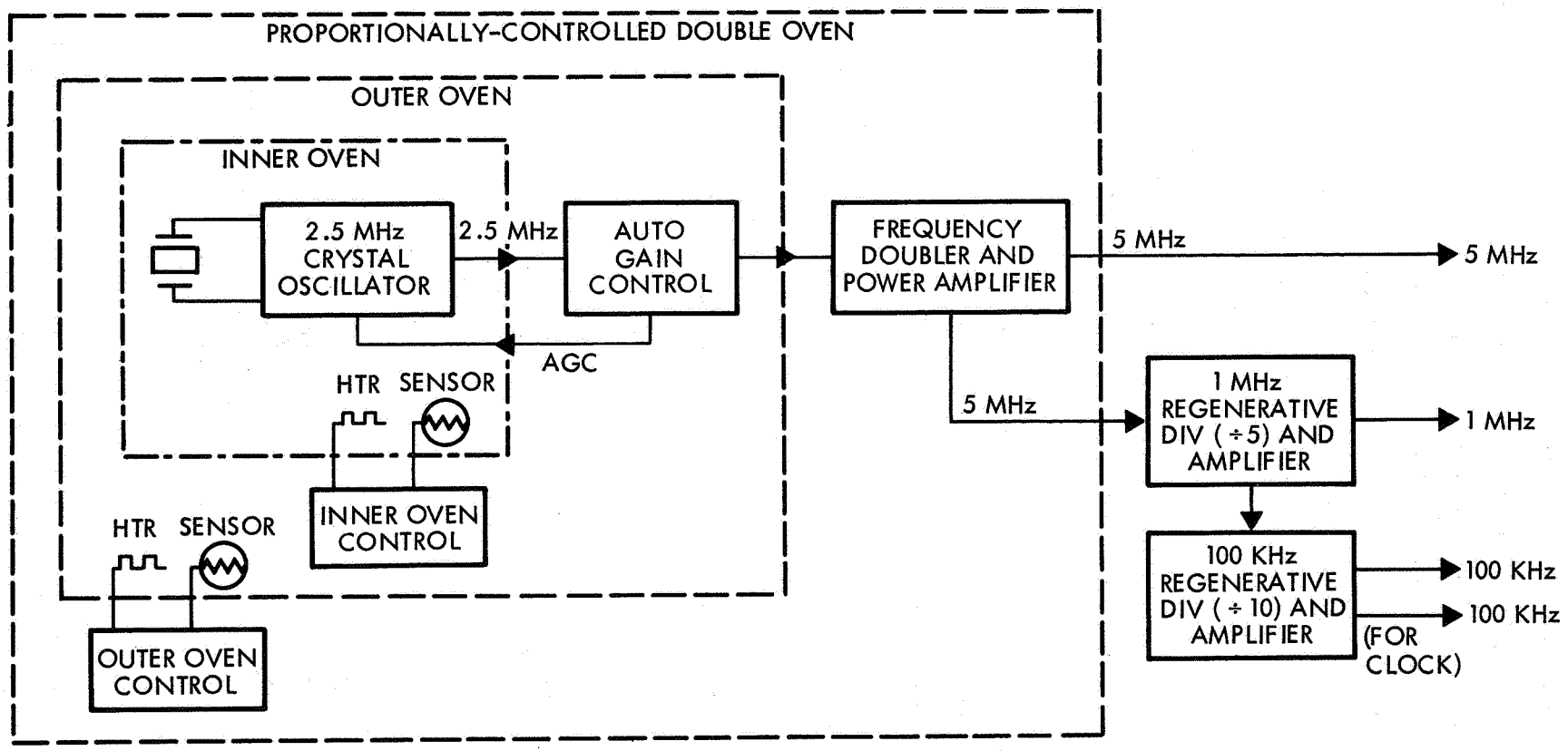

Figure 2. Block Diagram of Commercial Quartz Oscillator (Hewlett Packard Model 106 A, B).

B. Passive Atomic Frequency Standards

General Properties

In order to eliminate or reduce the frequency shift associated with the aging of quartz crystal oscillators, or to improve the performance of such oscillators in non-optimal environments, one is led to consider the use of an atomic oscillator or frequency standard. In such oscillators, an atomic resonance, corresponding to a transition between two atomic or molecular energy levels is used as the basic standard of frequency. The resonance frequency f_o is related to the energy level separation by $\Delta E = hf_o$, where h is Planck's constant. The atomic resonance frequency can be almost completely decoupled from the environment, and thus, even under relatively severe environmental conditions atomic oscillators will exhibit excellent frequency stability characteristics.

There are two general classes of atomic oscillators or frequency standards. One, which we shall call passive, includes those standards in which a quartz crystal oscillator is slaved or locked to the atomic resonance. The other, the active atomic oscillator class, includes the maser oscillators in which the atomic system is incorporated into a regenerative system. Such systems do not require a quartz oscillator as they are self-oscillating at the atomic resonance frequency. In this section the passive atomic frequency standards are discussed.

In order for a passive atomic frequency standard to improve upon the stability of crystal oscillators the sensing system linking the atomic resonance to the crystal oscillator and the resonance itself should exhibit several characteristics. In Figure 3 a "differentiated" resonance signal is reproduced such as would be observed at the output of an atomic resonance detection system as the input frequency to the detection system is slowly swept through the resonance. When the input frequency is at resonance center, f_o, (or also far from resonance) the output signal is zero except for noise. As the input frequency deviates slightly from f_o,

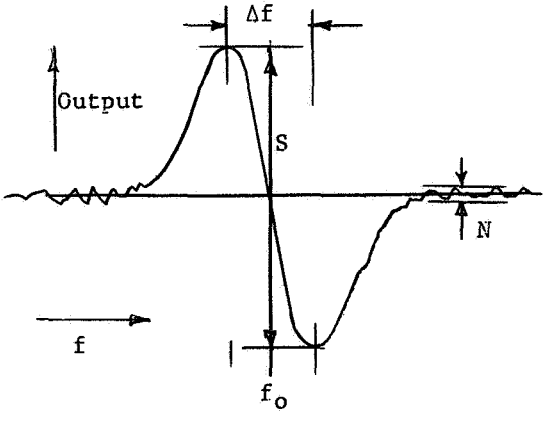

Figure 3. Typical Control Signal.

the output either increases or decreases depending upon whether the frequency deviation δf is positive or negative. The magnitude of the output signal corresponding to a deviation δf is $\delta f \cdot S/\Delta f$. (See Figure 3). It is evident from the figure that there is a minimum $\delta f = \delta f_{min}$ that can be detected, and that this minimum is determined by the magnitude of the noise N. Thus, when the output signal is approximately equal to the noise it is impossible to discern whether in fact a frequency deviation exists. Thus: $\delta f_{min} S/\Delta f \simeq N$ defines δf_{min}. Thus $\delta f_{min} = \Delta f/(S/N)$, or in fractional terms, $\delta f_{min}/f_o = \Delta f/f_o(S/N)$. It is evident that for good control $\delta f_{min}/f_o$ should be small. This requires that the atomic resonance width Δf, or more particularly $\Delta f/f_o$ should be small, and that the method of detecting the controlling atomic resonance should exhibit a large S/N ratio.

Quantum Properties of Alkali Atoms

The two most commonly used passive atomic frequency standards are the cesium atomic beam standard and the rubidium gas cell frequency standard. Both types are manufactured for commercial sale and both exhibit good frequency stability. Before discussing the basic operating principles of these devices it is instructive to examine the atomic energy level diagram characteristic of the alkali metals. Rubidium and cesium are both members of this class of metals which includes those atoms having a single electron outside of a closed shell noble-gas configuration. Other alkali metals include lithium, potassium, and sodium. (A laboratory model sodium frequency standard was built in 1958.)

Figure 4 is an energy level diagram for rubidium which is characteristic of the energy level structure of all the alkali metal atoms. The gross features of the energy level diagram characterize the permitted energy configurations of the single electron in a spherically symmetrical electrostatic potential. The small deviations from the gross structure are due to small perturbations of this energy. The energy separation between the $5P_{3/2}$, $5P_{1/2}$ levels is due to so-called LS or spin orbit interaction between the orbital motion of the electron and the characteristic spin of the electron. Classically it can be looked upon as due to the energy of interaction of the magnetic moment associated with the electron spin and the magnetic field seen by the electron due to its orbital motion around the central electrical charge. The

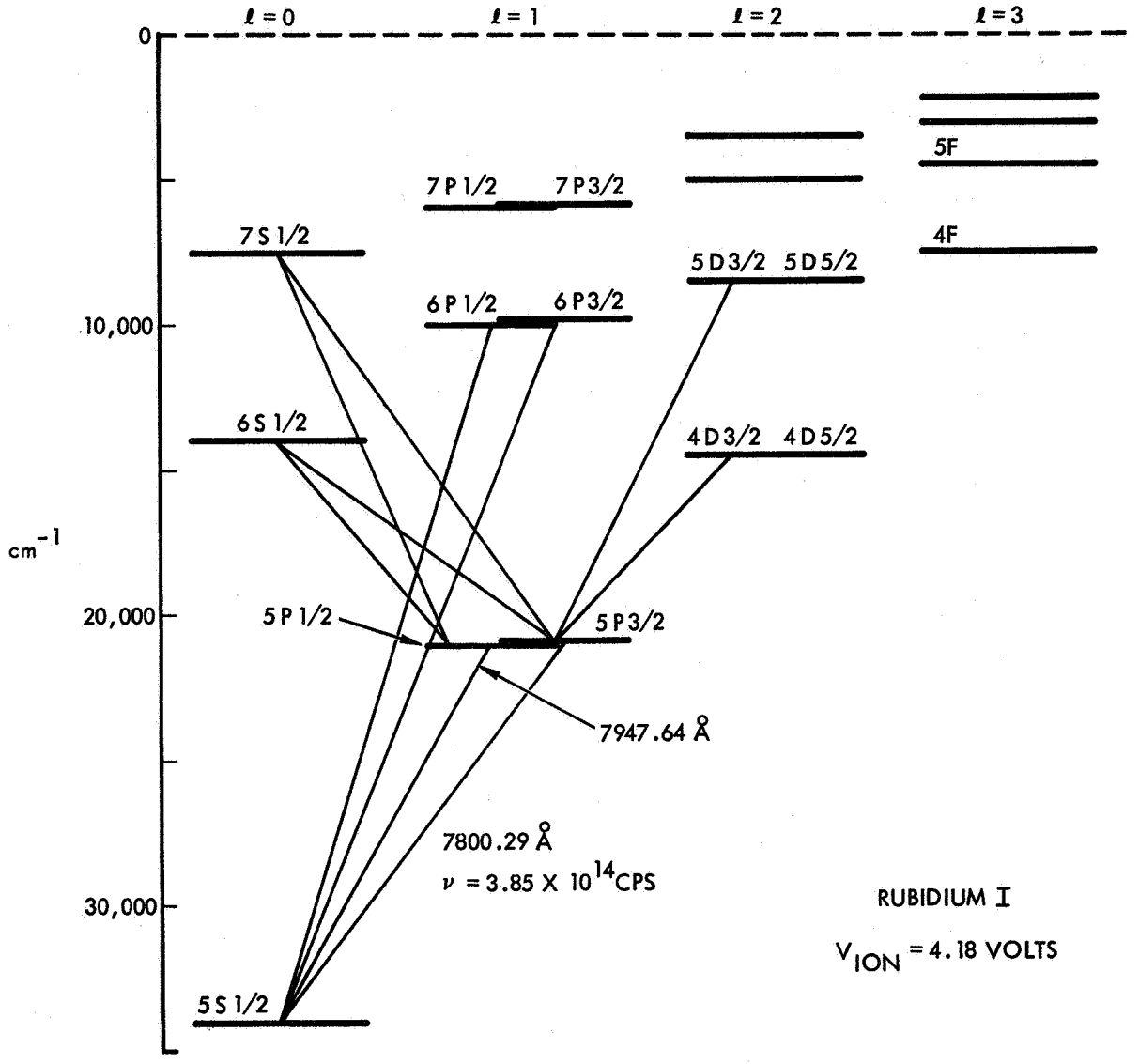

Figure 4. Atomic Energy Level Diagram for Rubidium Atom

strongest optical spectral lines for rubidium and for the other alkalis are those coming from transitions between the $5P_{1/2}$ and $5P_{3/2}$ states and the $5S_{1/2}$ ground or lowest energy state. These spectral lines are the so-called D lines and for rubidium they are 7947 Å and 7800 Å. In the case of sodium these D lines are at the wavelength of 5890 Å, and produce the characteristic yellow sodium light. The resonance in which we are interested for use with the atomic frequency standard corresponds to an energy level separation not shown in this figure. The $5S_{1/2}$ ground energy state of the alkalis is split with an energy separation ranging from 228.2 Mc for lithium 6 to 9193 Mc for cesium 133. Figure 5 shows this splitting for rubidium 87 and indicates a further level splitting which takes place in the presence of a weak magnetic field. The zero field hyperfine splitting, as this splitting is called, is due to the energy of interaction between the electron spin magnetic moment and the nuclear spin magnetic moment. One energy state corresponds to the case when the two magnetic moments are parallel and the other to the case when the two moments are antiparallel. The labels F = 2 and F = 1 in the figure are characteristic of the rubidium 87 case and are labels indicating the total angular momentum of the electron spin and nuclear spin. When the nuclear spin angular momentum of 3/2 is parallel with the electron spin momentum of 1/2, the total spin angular spin momentum of F = 2 is obtained. When they are antiparallel the total spin angular momentum F = 1 is obtained. In the presence of an external magnetic field the total spin magnetic moment associated with the coupling of the individual electron and nuclear magnetic moments may assume different positions with respect to the magnetic field, and each position gives rise to a slightly different energy. Thus, the different levels labeled m_F correspond to these different energies. When $m_F = +2$ the parallel combination of angular momenta is aligned parallel to the applied field and when $m_F = -2$ the angular momentum combination is anti-parallel to the applied magnetic field. The transition of special importance in Figure 5 for use in atomic frequency standards is that between the F = 2, $m_F = 0$ and the F = 1, $m_F = 0$ levels. It is seen from the figure that the energy level separation, and hence, the frequency of the resonance is virtually independent of the applied magnetic field strength when this magnetic field strength is small, and exhibits only a quadratic dependence upon the field strength. For this reason the transition is often referred to as the

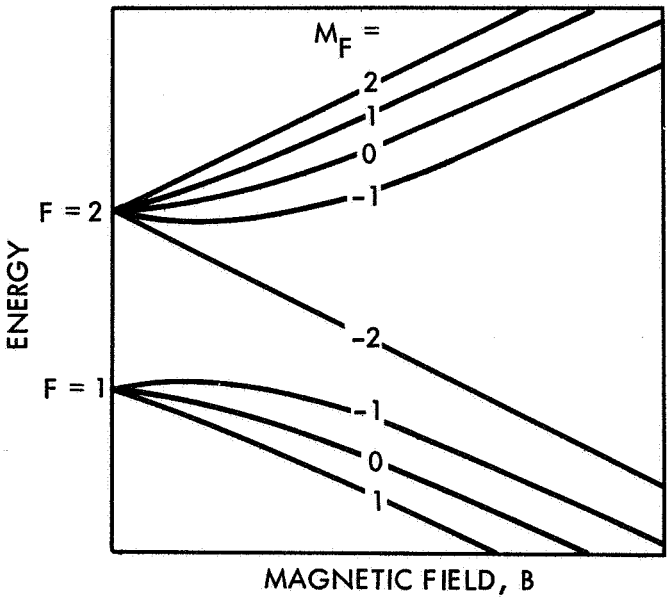

Figure 5. Splitting of lowest energy state of rubidium 87 atom with applied external magnetic field.

TABLE 1

CHARACTERISTICS OF ALKALI METALS AND HYDROGEN

MATERIAL	f_o = RESONANT FREQUENCY, MHz	QUADRATIC MAGNETIC TERM Hz	NUCLEAR SPIN	SUBLEVELS
H 1	1420.406	+ 2750 B^2	1/2	4
Na 23	1771.6	+ 2210 B^2	3/2	8
K 39	461.72	+ 8500 B^2	3/2	8
K 41	254.02	+15,400 B^2	3/2	8
Rb 85	3035.7	+ 1290 B^2	5/2	12
Rb 87	6834.68	+ 573 B^2	3/2	8
Cs 133	9192.7	+ 427 B^2	7/2	16

field-independent hyperfine transition. A small magnetic field is thus seen to be needed to resolve the energy levels of interest from the other levels, but it must be small enough so that one operates near the zero slope portion of the curves. Table 1 contains a list of the zero field hyperfine resonance frequencies for the isotopes of the alkali metals and hydrogen. Also tabulated are the corresponding nuclear spin angular momenta and the number of sublevels into which the hyperfine levels split in the presence of a magnetic field. The number of sublevels is given by quantity $2(2I + 1)$ where I is the nuclear spin.

1. Rubidium Gas Cell Atomic Frequency Standard

General Operation

Let us now examine the operation of the rubidium gas cell standard. Figure 6 is a functional diagram of this device and shows the crystal oscillator which is slaved to the rubidium resonance frequency. The heart of the device is the unit containing the rubidium lamp, filter cell, cavity, gas cell and photosensor. The gas cell contains the rubidium atoms used to control the crystal oscillator. The remaining blocks are circuit elements used to link the crystal to the rubidium atoms.

The operation of the device is briefly as follows. The output of the crystal oscillator (an exact subharmonic of the rubidium resonance frequency) is multiplied to a higher frequency and frequency modulated at an audio frequency. This signal is supplied to the microwave resonant cavity through a harmonic generating crystal, and sufficient oscillating magnetic field strength is generated within the cavity to couple to the magnetic moments of the rubidium atoms at the atomic resonance frequency. The atomic resonance is monitored by observing the intensity of the light transmitted through the gas cell. At resonance this intensity goes through a minimum. Since the signal exciting the atoms is frequency modulated at an audio frequency, an audio signal is picked up by the photodetector. This audio signal is amplified and compared with the modulation oscillator in the phase detector. The output of the detector has a waveform of the type shown in Figure 3, i.e., it is positive on one side of resonance, negative on the other, and zero at resonance. This control voltage is applied to a variable capacitor in the crystal oscillator circuit to maintain the oscillator at the exact subharmonic frequency of the atomic resonance.

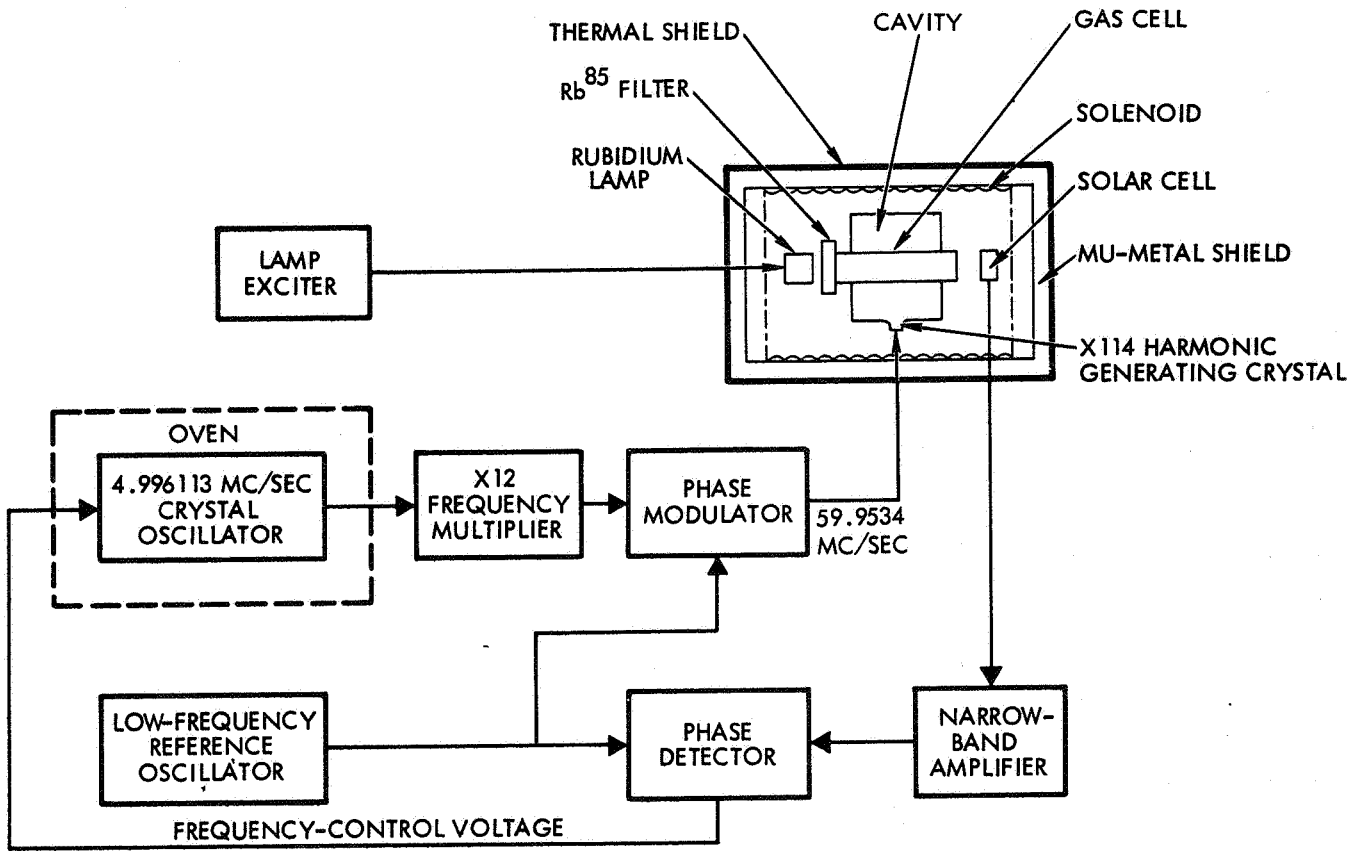

Figure 6. Functional Block Diagram, Rubidium Gas Cell Frequency Standard

Let us examine the processes occurring in the gas cell to determine the factors affecting the signal-noise ratio and the resonance width. The strength of the atomic resonance control signal is proportional to the quantity $n_1 - n_2$ which is the difference in the number of atoms in the two levels involved in the resonance transition. Thus, for Rb87, n_1 would represent the number of atoms in the F = 1, $m_F = 0$ sublevel, and n_2 would represent the number of the F = 2, $m_F = 0$ sublevel (See Figure 5). The "optical pumping" action of the rubidium lamp serves to make the control signal larger by making n_2 larger than n_1. This pumping and the associated optical detection process result in the excellent signal/noise ratio of gas cell frequency standards, and are discussed in the following paragraphs.

Optical Pumping and Detection

Suppose that the five sublevels included in the F = 2 level are illuminated with light of wavelength λ_2 characteristic of the transition from one of the P states to the F = 2 sublevels of the ground state, and that the F = 1 sublevels are illuminated with light of the slightly different wavelength λ_1 corresponding to transitions from the same excited P state to the F = 1 sublevels of the ground state. (See Figure 7 - left half). If it were possible to filter out either one of the components, λ_1 or λ_2, one would obtain very effective optical pumping action. Let us consider what would happen were it possible to eliminate the λ_1 component from the optical radiation. The atoms in the five F = 2 sublevels are capable of absorbing the light of wavelength λ_2 and would be excited to one of the excited P states. From this excited P state they decay spontaneously in a matter of 10^{-8} seconds with remission of light and would fall back into one of the eight sublevels of the F = 2 or F = 1 levels. In general, they will enter any of the eight sublevels with equal probability. The atoms present in the three F = 1 sublevels are not optically excited to an upper energy level since the λ_1 radiation exciting them to the higher state has been filtered out. Thus, atoms are being pumped into the F = 1 sublevels through the action of the light of wavelength λ_2, but they are not being pumped out of the F = 1 sublevels since there is no light of wavelength λ_1 present. As a consequence, under the influence of the λ_2 light alone all of the atoms in the container illuminated by this light will soon be in the three F = 1 sublevels.

Through the influence of this action we have thus populated the F = 1, m_F = 0 sublevel and completely emptied the F = 2, m_F = 0 sublevel, and in so doing we have increased the difference $(n_1 - n_2)$ which is the population difference between these levels until it is now equal to 1/3 the total number of atoms present in the cell. In practice the optical pumping action must compete with what are called thermal relaxation processes which in the absence of the light would restore the populations of the sublevels to the values determined by the Boltzmann equation. However, if the optical pumping light is made sufficiently intense the optical pumping action can be made the dominant process and the population difference can be made to approach the ideal just obtained.

The optical detection process can now be easily understood. Under the action of microwave energy having a frequency equal to that of the atomic resonance, atoms in the state F = 1, m_F = 0 will be induced to make transitions to the state F = 2, m_F = 0. (If the strength of this electromagnetic radiation is sufficiently great the result will be to equalize the populations of these two sublevels and the number of transitions from state 1 to state 2 will equal the number of transitions from state 2 to state 1.) Thus, when the microwave energy is present the difference $(n_1 - n_2)$ is altered and there are now atoms present in the F = 2, m_F = 0 level where they can absorb the pumping light at wavelength λ_2. When the microwave energy at the resonance frequency is turned on, the amount of pumping light at wavelength λ_2 transmitted through the cell will decrease since more of the light is absorbed by the atoms in the cell. The amount of light transmitted through the cell thus measures the number of atoms present in state 2 and monitors the action of the microwave signal. If the microwave signal is slowly swept in frequency through the resonant frequency the light transmitted through the cell will exhibit the characteristic resonant line shape, and will have a minimum when the microwave frequency corresponds to the atomic resonant frequency.

We now turn to the question of how one accomplishes the filtering of the pumping light which permits us to pump with only light of wavelength λ_2. Figure 7 also shows the position of the hyperfine levels in the ground state of the isotope rubidium 85. The wavelengths connecting these levels labeled F = 3 and F = 2 are designated λ_2' and λ_1'. It is noted that the center

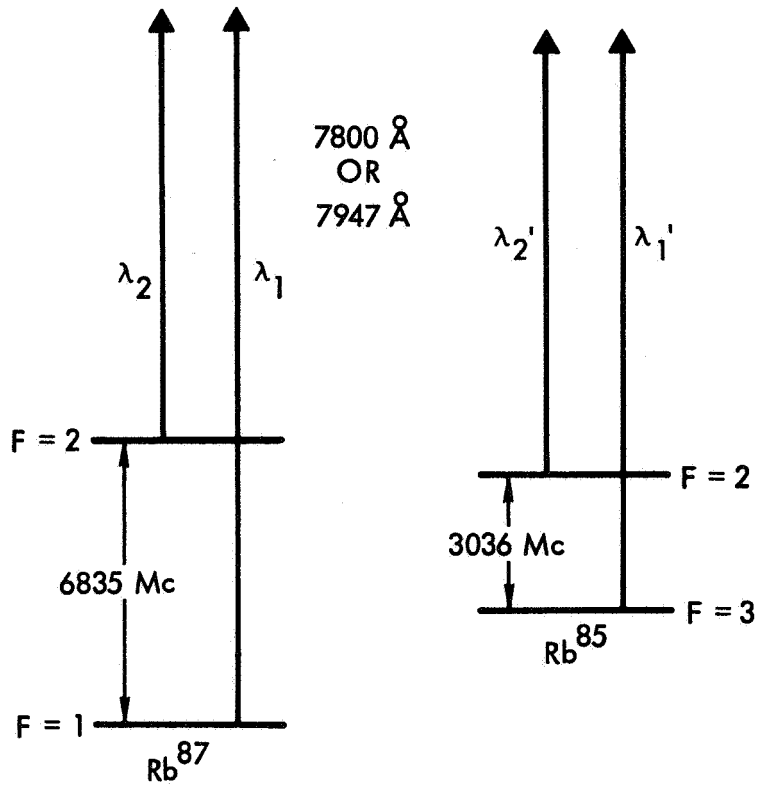

Figure 7. Schematic diagram, optical pumping of rubidium atoms.

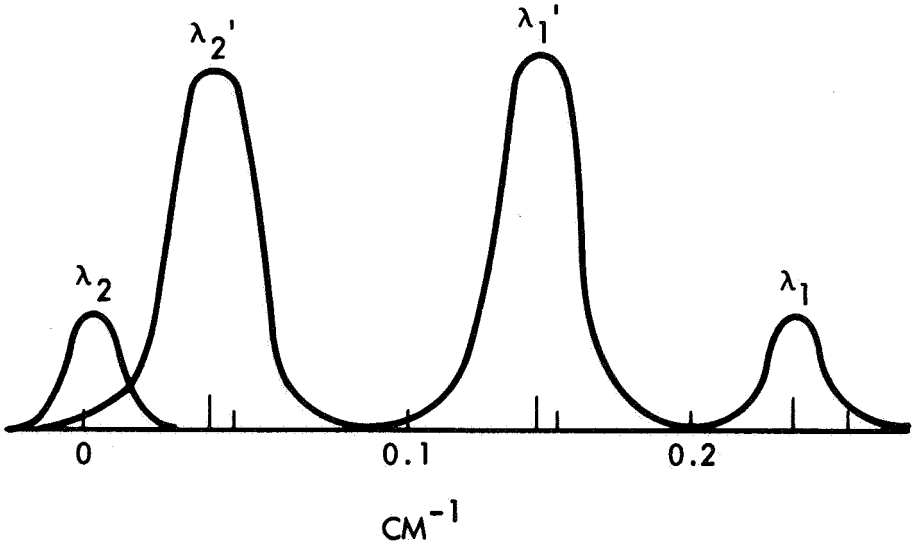

Figure 8. Emission spectrum from rubidium lamp containing natural rubidium (72% Rb85, 28% Rb87).

position of the rubidium 85 levels is shifted with respect to the center position of the rubidium 87 levels. Figure 8 shows the spectrum obtained from a natural isotopic mixture of rubidium atoms in which approximately 72% of the atoms are rubidium 85 atoms and 28% are rubidium 87 atoms. It is seen that the λ_2' component of light produced from the rubidium 85 atoms overlaps the λ_2 component from the rubidium 87 atoms and that the λ_1' component similarly overlaps, but to a lesser degree, the λ_1 component. This difference in the degree of the overlap provides a means of obtaining the difference in intensity of the λ_2 and λ_1 components necessary for optical pumping action. If a cell containing rubidium 87 atoms is illuminated with light from a lamp containing only rubidium 85 atoms there is sufficient overlap of the λ_2' component of the λ_2 component that the λ_2' component is capable of exciting rubidium 87 atoms in the F = 2 sublevels to the optically excited state. Since the λ_1' component emitted by the rubidium 85 lamp overlaps the position the λ_1 component of the spectrum to a lesser degree, there will be relatively little excitation of the rubidium 87 atoms from the F = 1 sublevels. Thus, the differential pumping action desired by which atoms are pumped out of the F = 2 sublevels but not out of the F = 1 sublevels can be obtained by using a rubidium 85 lamp to pump the rubidium 87 atoms. Alternatively, it is possible to obtain the reverse type of pumping by placing a filter cell containing rubidium 85 atoms in front of a rubidium 87 lamp. If the temperature of the filter cell and the lamp are suitably adjusted, the filter cell will absorb the λ_2 component of light from the rubidium 87 lamp, leaving only the λ_1 component.

From this brief discussion of the optical pumping and optical detection process in rubidium 87 we have seen how these techniques are useful in enhancing the population difference between the two levels involved in the atomic resonance, and how the microwave resonance can be monitored through observing the transmission of the pumping light through the gas cell.

Resonance Width and Frequency Shifts

Let us now examine the factors determining the width of the atomic resonance, Δf, and any frequency shifting mechanisms. We have seen earlier that it is important to have a small Δf for control purposes. The magnitude of Δf depends upon the length of time T, that the resonating atoms spend,

on the average, interacting with the oscillating microwave field, and the apparent frequency that the atoms "see." It is evident that a fast moving atom will experience a doppler shift and will interact most strongly with a microwave field shifted slightly from the resonant frequency characteristic of a stationary atom. The fact that there is a distribution of atomic velocities in a bottle containing rubidium atoms gives rise to a broadening of the resonance width. This "doppler width" is 9 KHz for the atomic resonance of Rb87 at room temperature. By adding a buffer gas of neon, argon or a mixture of several such noble gases, the normal high speed thermal motion of the rubidium atoms is reduced to a slow diffusion and the doppler broadening is reduced to a value more nearly 100 Hz. As a consequence, the line width Δf is almost completely determined by the interaction time T which is the mean time between collisions which remove the atom from the resonating energy state. Collisions between rubidium atoms, collisions with the wall, and absorption of the pumping light all interrupt the interaction with the microwave radiation and give rise to a line width of the order of 200-400 cycles at normal operating temperatures (~38°C.).

Collisions with the buffer gases are not interruptive since the buffer gas is not magnetic, but such buffer collisions distort the atoms slightly and give rise to a frequency shift or offset, which is proportional to the amount of buffer added to the gas cell and is typically 3 parts in 10^7 or several KHz. In addition, the presence of the buffer gas introduces a temperature dependent shift which is also proportional to the amount of buffer gas. By mixing several noble gases it is possible to minimize these buffer shifts since the magnitude and sign of the buffer shift and associated temperature dependence is different for different buffer gases. The presence of the pumping light also perturbs the atomic energy levels slightly and the perturbation depends upon the spectrum and intensity of the pumping light. For the commerical rubidium standards the typical frequency shift is of the order of 50 Hz.

Summary

The optically pumped rubidium gas cell is seen to exhibit the features required in a passive frequency standard, namely a good signal-to-noise ratio and a narrow resonance line width. We will see later that gas cell frequency

standards exhibit good frequency stability and can be quite compact in size. These standards must be calibrated against other standards because of the buffer shift and pumping light intensity shift, but once calibrated remain quite stable.

2. The Cesium Atomic Beam Frequency Standard

General Operation

The operation of the cesium atomic beam frequency standard can be understood in terms of the functional diagram in Figure 9. This diagram is seen to be nearly identical with Figure 6, the diagram for the rubidium standard. The cesium beam resonator has replaced the microwave optical unit of Figure 6. It is also noted that the quartz oscillator in Figure 9 is operated at a frequency of 5 MHz and is not an exact subharmonic of the Cs133 resonance frequency 9192.631770 MHz. A frequency synthesizer is thus required to generate 12.631 MHz which is added to the 9180 MHz signal obtained by multiplication from the crystal. It is possible to operate the cesium device using a crystal which is an exact subharmonic of the resonance frequency and avoid the use of the synthesizer in the main control loop.

Cesium Beam Resonator

Let us examine the operation of the cesium beam resonator to determine the parameters affecting the signal-noise ratio and the resonance width, Δf. We recall that the S/N ratio for the gas cell device was determined by the optical pumping and detection, and the width Δf by the mean time between rubidium disorienting collisions.

A schematic of the cesium beam resonator apparatus is shown in Figure 10. A collimated beam of Cs133 atoms is generated in the cesium oven, and the directed motion is due to the thermal translational energy of the atoms. Such a beam of thermal atoms is characterized by a mean velocity and a distribution about this mean. Cs133 has an energy level diagram similar to those in Figure 4 and 5, but since the nuclear spin is 7/2 vs. 3/2 for Rb87, the ground state is characterized by the total momentum quantum numbers $F = 4$ and $F = 3$. Accordingly, these levels split into 9 and 7 sublevels respectively in a weak magnetic field. For stronger magnetic fields the curves again extend as shown in Figure 5 with a group of 8 sublevels increasing

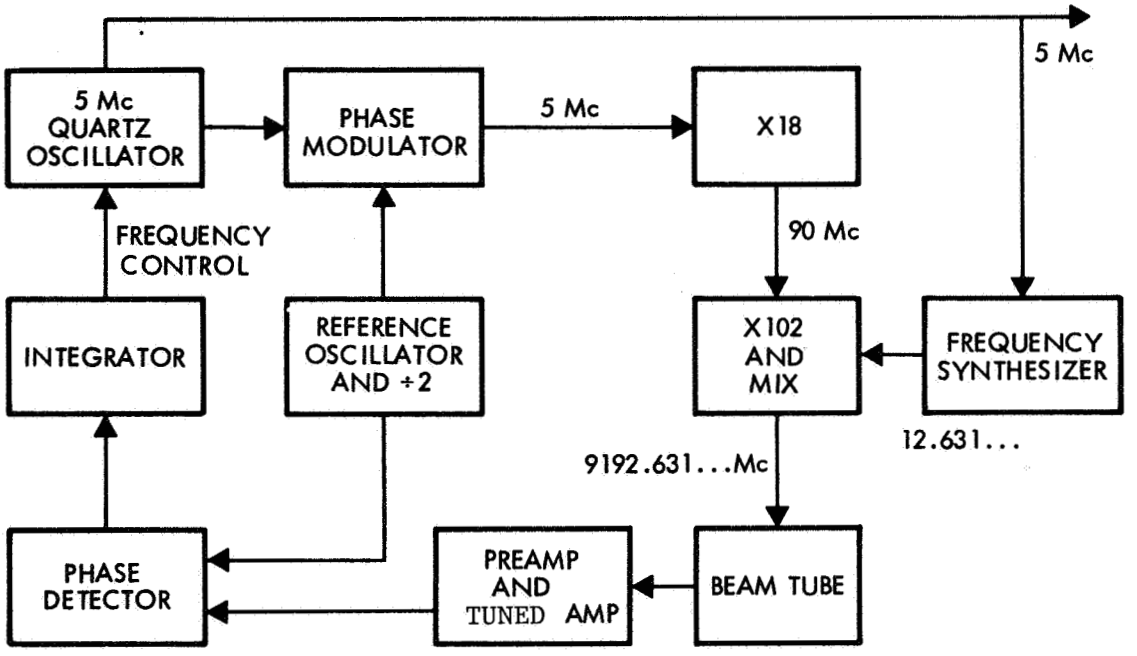

Figure 9. Functional block diagram, cesium atomic beam frequency standard (Hewlett Packard, Model 5060A).

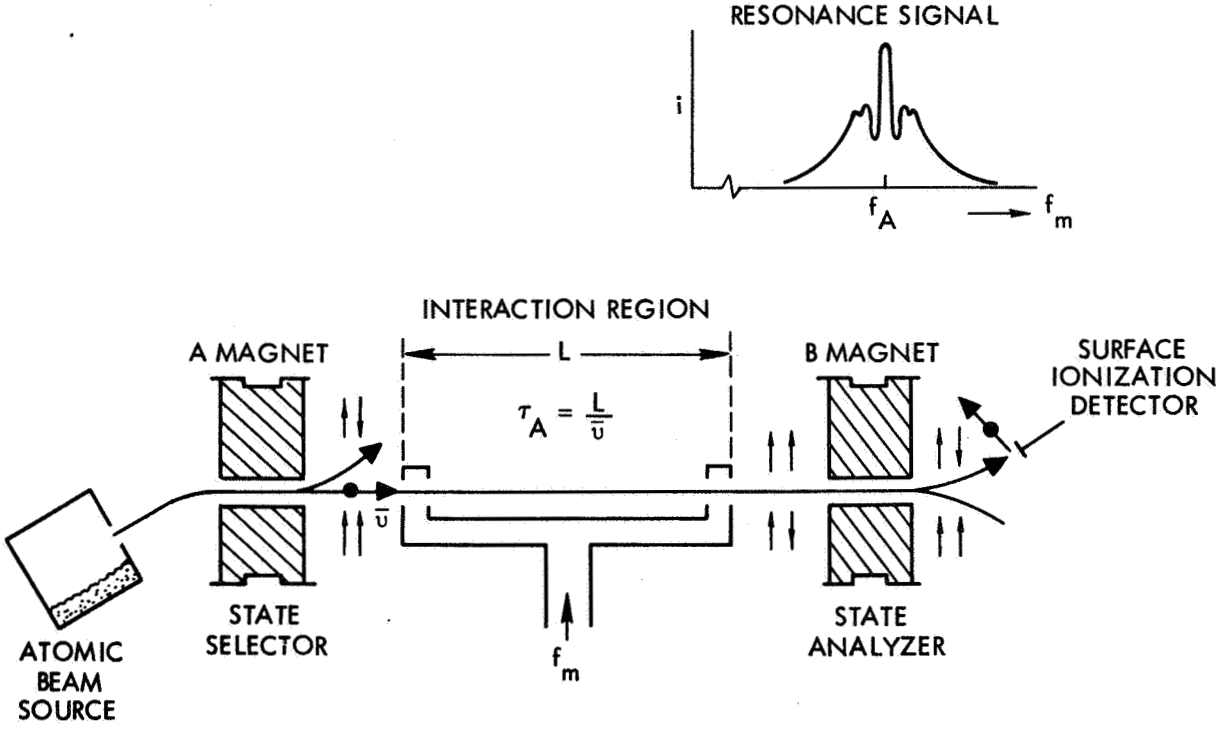

Figure 10. Schematic diagram of atomic beam resonator. The C field magnet providing a uniform magnetic field throughout the interaction region is not shown.

in energy with field and a group of 8 sublevels decreasing in energy. The magnetic moment associated with these two groups is either $+\mu_o$ or $-\mu_o$, where μ_o is the magnetic moment of a free electron. By directing the atomic beam coming from the oven through a strong magnetic field (the A magnet) having a field gradient, the beam will split into two components, corresponding to the two magnetic moments, as each group will experience an equal and opposite force from the field gradient. In particular, atoms in the levels labeled by $F = 4$ and $m_F = 4, 3, 2, 1, 0, -1, -2, -3$ will be deflected in one direction, and the remaining eight sublevels deflected in the opposite direction.

Those atoms in the particular sublevel $F = 4$, $m_F = 0$ are, of course, the ones of interest since we are again interested in the field independent transition. (See Table 1 for field dependence of frequency). After leaving the region of the A magnet, the atoms enter a region of small magnetic field, the C magnet, and are allowed to enter the resonant cavity to interact with the microwave field. If the microwave field is in resonance with the atomic resonance frequency a number of atoms will "flip" or be induced to make a transition to the $F = 3$, $m_F = 0$ state. Atoms making such a "flip" will be directed by the B magnet to the detector. The B magnet operates in the same manner as the A magnet, splitting the beam into two groups again. The detector consists of a hot wire ionizer (which serves to give the cesium atoms a positive charge) a mass spectrometer and an electron multiplier. The output of the beam tube is the output current of the multiplier. The resonance curve of the cesium beam resonator is shown in the inset of Figure 9. (More accurately when the frequency microwave signal is modulated at an audio rate, the output current of the multiplier will be an audio frequency signal, and the phase detector output will resemble the derivative of the resonance curve of Figure 9, similar in nature to Figure 3.)

Comparing with the rubidium gas cell device we see that the signal is again proportional to $n_2 - n_1$, but here $n_1 = 0$, since all of the $F = 3$, $m_F = 0$ atoms have been removed from the atomic beam. The signal strength is thus proportional to n_2 which is approximately 1/16 the number of atoms, n, in the collimated beam emanating from the oven. The more intense the atomic beam the greater the resonance signal. A greal deal of effort has gone into

the design of magnets A and B to obtain better beam optics making use of a greater solid angle of atoms from the oven. The statistical fluctuation in beam currents are proportional to $\sqrt{n}$, so that the S/N ratio will be proportional to $\sqrt{n}$.

Resonance Width

The resonance line width, Δf, depends upon the quantity $\bar{v}/L$, where L is the length of the microwave interaction region and $\bar{v}$ is the most probable velocity of the atoms in the beam. The "interference" pattern nature of the resonance shown in Figure 9 results from the use of two short interaction regions separated by length L rather than a single long interaction region. The result is a narrower resonance width, but some care must be used to avoid locking the crystal oscillator to the wrong resonance peak. Care must also be taken to maintain a uniform homogeneous magnetic field throughout the entire microwave interaction region, or additional line breath will result.

It is to be noted that in the resonator tube the atoms drift in an evacuated environment having a pressure from 10^{-7} to 10^{-8} Torr (mm of Hg). The expended atoms condense on the wall surface. As a consequence no atomic collisions occur, and during the interaction with the microwave energy the atoms approach the free state more completely than in any other apparatus. Such cesium beam units are the present basis for the U.S. Frequency Standard. In order to obtain the sharpest resonance the apparatus must be long, and practical considerations lead to a compromise length. It is to be appreciated that vibrational motions or large angular accelerations might seriously degrade the performance of the cesium resonator.

Summary

The cesium atomic beam frequency standard can be regarded as a primary standard, in that independently constructed beam tubes compare in frequency to a few parts in 10^{12}. The signal-to-noise ratio is generally smaller than the case for the rubidium gas cell device, and whereas the rubidium device can improve upon the short term stability of the "flywheel" crystal oscillator, the cesium device is at its best for very long performance periods. We shall see later that the dimensions of the cesium beam standard are determined by the necessity of providing a long interaction region in order to obtain a narrow resonance width.

C. Masers, Active Atomic Oscillators

General Discussion

In the maser oscillators the atomic system itself is made to oscillate at the resonance frequency by placing the atoms within a low loss resonant structure tuned to the atomic frequency. In the discussion of the passive oscillators it was pointed out that radiation having a frequency corresponding to the energy separation between two energy levels, $f = \Delta E/h$, can induce atomic transitions between the two levels. For example, atoms can absorb energy from the radiation field and be excited from the lower energy level to the upper. Atoms in the upper level can also be stimulated by the field to give up energy to the field and drop to the lower level. In general, a net absorption of energy will occur if $n_1 > n_2$, i.e., the number of atoms in the lower level exceeds the number in the upper, and a net emission if $n_2 > n_1$. The processes of induced absorption and induced emission occur with equal probability, thus, the basic requirement for maser oscillation is the maintenance of a population differential between the two energy levels, with a greater number present in the upper state.

When the atoms are placed in a low loss resonant cavity structure, and if $n_2 > n_1$, oscillations will build up if the rate of induced emission of energy is sufficient to overcome the losses in the cavity plus any energy coupled to external circuits. The frequency of oscillation will be determined primarily by the atomic resonance frequency, but the resonance frequency of the cavity structure will also affect the oscillation frequency since these two resonant systems are coupled.

In terms of the resonant cavity Q, the atomic resonance width Δf, and $n_2 - n_1$ one can write the condition for oscillation in the form:

$$\frac{1}{Q} \leqq K \frac{(n_2 - n_1)}{\Delta f} ,$$

where K is a proportionality constant. Thus, oscillation is more likely to occur for a given Q for large $n_2 - n_1$ and narrow line width, Δf.

The oscillation frequency, f, will be determined by the expression:

$$f = f_o + (f_{cav} - f_o)Q \frac{\Delta f}{f_o} \quad ,$$

where f_o = the atomic resonance frequency and f_{cav} is the cavity resonance frequency.

The pulling of the oscillation frequency by the cavity, given by the second term, will be minimized if the atomic resonance is sharp, i.e., if $f_o/\Delta f$, is large compared with the cavity Q.

It is now possible to examine the operation of the hydrogen maser, specifically the means for making $n_2 > n_1$ and Δf small.

1. The Hydrogen Maser Oscillator

General Operation

The hydrogen maser bears a certain resemblance to the cesium atomic beam frequency standard. In Figure 11 the maser is shown schematically. Atomic hydrogen is produced by dissociation of hydrogen gas in an rf discharge. A collimated beam of these hydrogen atoms is passed through the inhomogeneous field of a state selecting magnet. This magnet is similar to the A and B field magnets discussed earlier. The nuclear spin of hydrogen is 1/2 so that the ground state hyperfine levels are labeled by the total angular momentum quantum numbers F = 1 and F = 0. The selector magnet directs atoms in states F = 1 m_F = 0 and 1 through an aperture into the quartz bulb in the resonant cavity. Atoms in states F = 1 m_F = -1 and F = 0 m_F = 0 are rejected. The cavity in which the quartz bulb is located is tuned to the field independent hyperfine resonance frequency of hydrogen at 1420.4 MHz. This corresponds to the energy separation between the F = 1, $m_F = 0 \rightarrow F = 0$, $m_F = 0$ sublevels. The magnetic beam deflection system produces a population difference, $n_2 - n_1 = n_2 = n/4$, in the atomic beam entering the cavity, where the quantity n is the number of atoms in the beam before entering the magnetic selector. These n_2 atoms are subjected to the oscillating field within the cavity and induced to give up energy to this field.

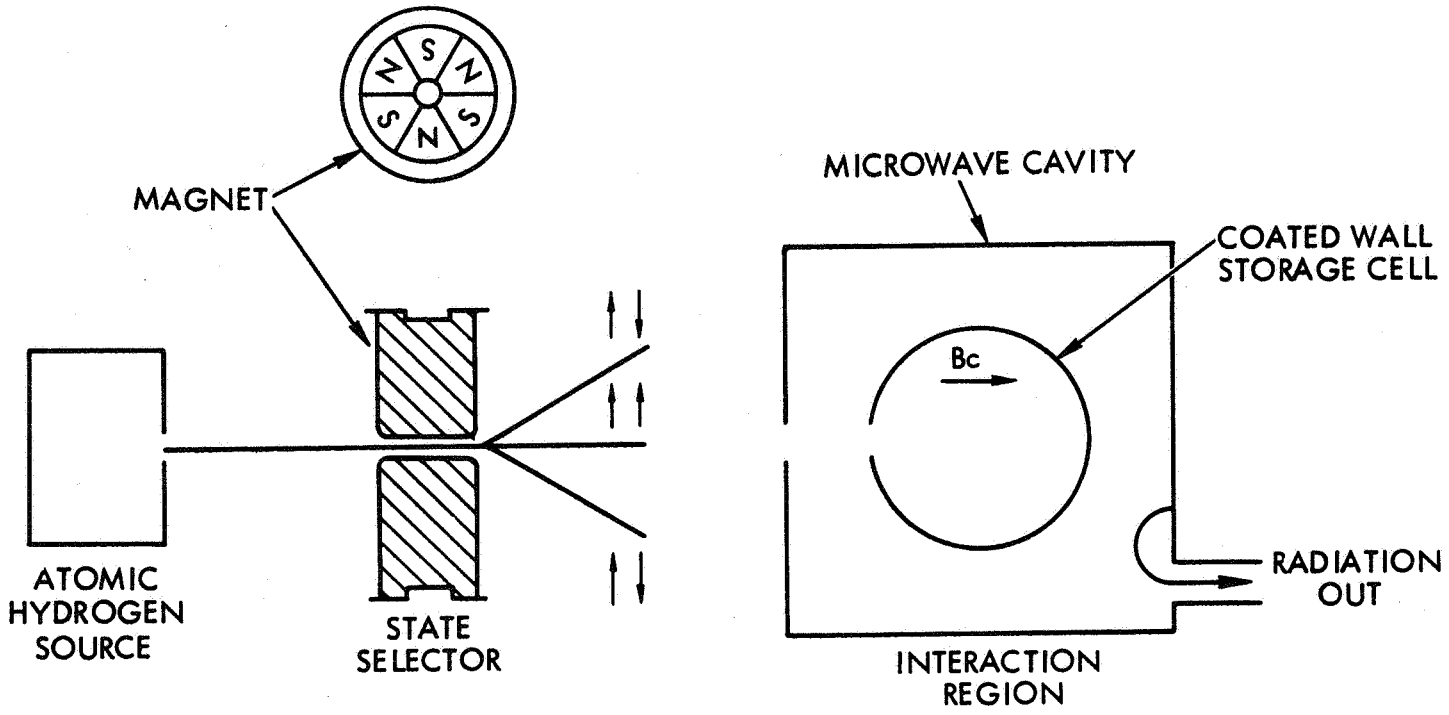

Figure 11. Schematic diagram of the atomic hydrogen maser. The C field magnet providing a uniform magnetic field throughout the interaction region is not shown.

Resonance Width

The resonance width, Δf, is determined by the length of time, T, the atoms interact, undisturbed, with the rf field, thus $\Delta f = 1/T$. The quantity T is related to the rates at which interruptions occur. Thus, $1/T = R_1 + R_2 + R_3$. The first, R_1, is the rate at which atoms diffuse out of the cavity through the entrance aperture. The second, R_2, is the rate at which hydrogen - hydrogen collisions take place. The third, R_3, is the rate of occurrence of disorientation by wall collisions. (The walls of the bulb are coated with special coatings, e.g., teflon, in order to permit a large number of wall collisions before disorientation occurs.) Typically, the rate of H - H collisions is 1 sec^{-1}, the rate of disorienting wall collisions is 0.5 sec^{-1} and, the average number of escapes is 0.7 sec^{-1}. Thus, $1/T \simeq 2$ sec^{-1}.

The quantities $n_1 - n_2$ and the resonance width, Δf, entering into the expression for oscillation threshold are not independent quantities. The quantity $n_2 - n_1$ (or n_2 here since $n_1 = 0$) may be increased by increasing the beam flux, but such an increase will increase the atomic concentration in the bulb and hence, the number of H - H collisions. The concentration can be reduced by increasing the size of the aperture, but this will in turn increase Δf by increasing the rate of escape from the bulb. An optimal balance between these different quantities is usually sought. It is seen that the line width $\Delta f \sim 1$ Hz for the hydrogen maser is considerably less than that for the cesium and rubidium standards discussed earlier. Line widths of the order of 200 Hz are characteristic of these two devices.

Frequency Shifts

The collisions of the hydrogen atoms with the wall coating material gives rise to a resonance frequency shift on the order of parts in 10^{11} and is similar to the buffer shifts in rubidium. The shift depends inversely upon the bulb diameter as this determines the number of collisions per second. A second-order doppler effect also produces a frequency shift of parts in 10^{11} which is slightly temperature dependent. The quadratic magnetic field dependence of the resonance frequency is given by $f = f_o + 2750\ B^2$ (gauss), so that considerable care in maintaining a constant and relatively uniform

magnetic field is required. The cavity pulling effect is significant for maser oscillators inasmuch as a cavity Q of 10^3 - 10^4 and a resonance Q of 10^9 is required for oscillation. This large cavity Q for hydrogen leads to the requirement that the cavity resonance frequency be stable to a part in 10^7 to obtain oscillation stability of 1 in 10^{13}. These various sources of frequency shift are quite reproducible, so that variations between different hydrogen masers produced to the same specifications is on the order of parts in 10^{13}. The hydrogen maser is classified as a primary frequency standard.

The signal power level of the hydrogen maser is quite low, on the order of 10^{-12} watts. A complete hydrogen maser frequency standard is shown in the block diagram of Figure 12, showing how a crystal oscillator is phase locked to the maser oscillator output. The dynamics of such a phase locked system differ from those of the passive systems discussed above. In one case, the frequency of the crystal oscillator is locked to the frequency of the resonance. In the case of the masers the crysal oscillator is phase locked to the maser oscillator.

2. Other Maser Oscillators

Before turning to a discussion of the frequency stability characteristics of the various frequency standards, brief mention should be made of the operation of other types of maser oscillators.

The first maser developed (in 1956) was the ammonia beam maser. The ammonia beam maser is not currently being produced commercially. It has been studied extensively and exhibits excellent short term stability and spectral purity. The long term stability is not as good as that of the standards discussed above. The oscillation frequency is approximately 24 GHz.

The rubidium maser oscillator is the oscillator counterpart of the passive rubidium frequency standard. It has only recently (1965) been operated successfully and is not currently being produced commercially. The population inversion $n_2 - n_1$ is maintained by optical pumping as in the passive rubidium standard. By using intensity pumping as described earlier a limiting value of $n_2 - n_1 = n/5$ can be obtained. The line width Δf depends upon the rate of Rb-Rb collisions, the optical pumping intensity, buffer gas and wall collisions.

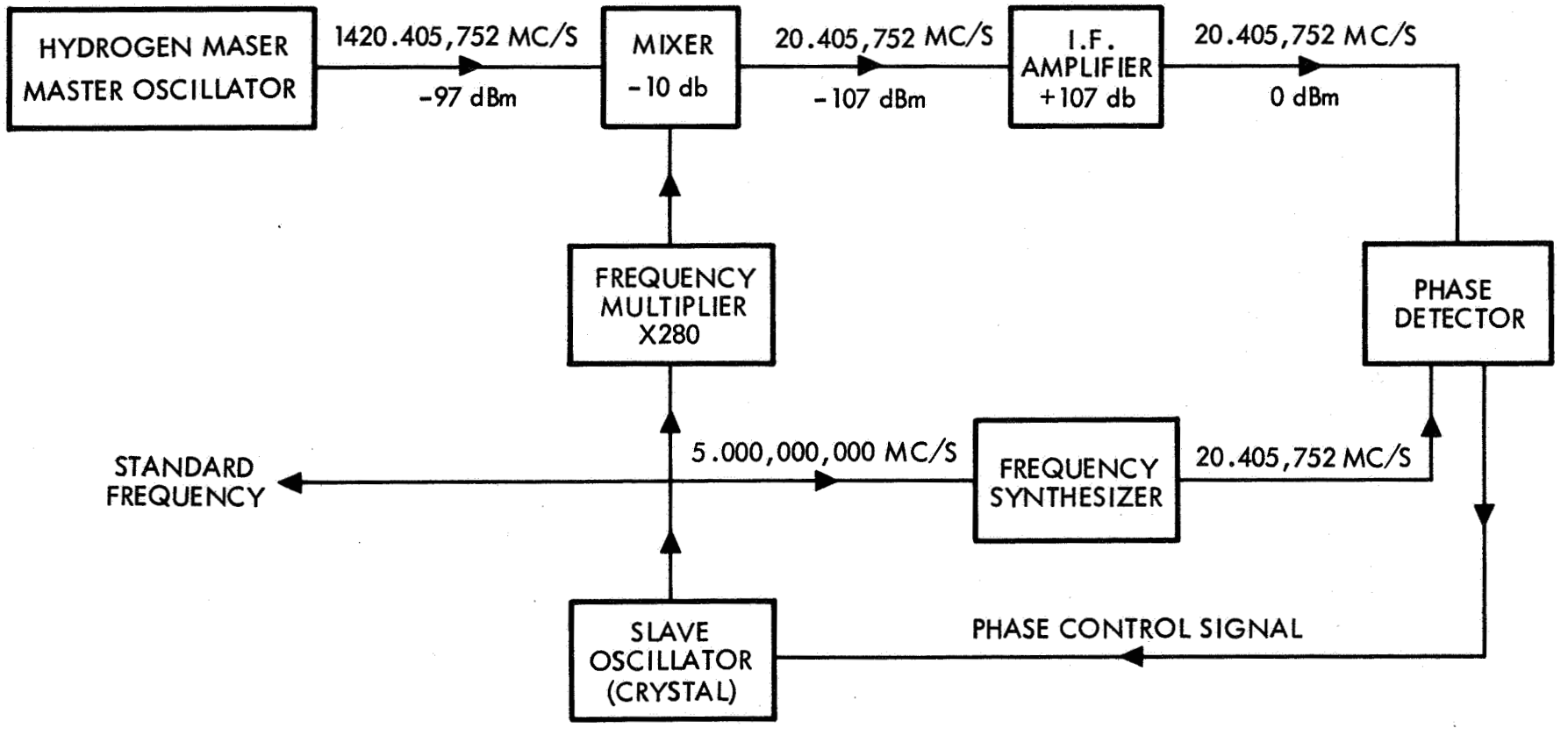

Figure 12. Block diagram of hydrogen maser frequency standard.

Again, as in the hydrogen maser, an optimal balance between the factors determining $n_2 - n_1$ and Δf is required. In this case the rubidium vapor density and pumping lamp light intensity must be optimized. The relatively larger collision cross section for rubidium over hydrogen requires the use of a higher Q resonant cavity (Q ~ 50,000) in order to obtain oscillation. This in turn increases the cavity pulling problem. The refinement of the rubidium maser oscillator is expected to lead to a short term stability comparable with that of the hydrogen maser in a much smaller device.

D. Summary

By way of summary, the characteristics of the three commercially developed atomic frequency standards are presented in Table 2.

TABLE 2

Summary of Important Characteristics of Three Atomic Frequency Standards (Ref. 5)

Characteristic		Atomic Hydrogen Maser	Rubidium Gas Cell Controlled Oscillator	Cesium Atomic Beam (24-inch) Controlled Oscillator
Nominal Resonance Frequency		1420.405751 Mc/s	6834.682608 Mc/s	9192.631770 Mc/s
Resonance Width		1 c/s	200 c/s (typical)	250 c/s
Atomic Interaction Time, τ_A		0.5 seconds	2×10^{-3} seconds (typical)	2.5×10^{-3} seconds Interaction length, $L=25$ cm (typical)
Atomic Resonance Events per Second		10^{13}	10^{12}	10^{9}
Principal Frequency Offsets	Magnetic	$f-f_0=2750\ B^2$ (gauss) 5×10^{-13} (typical)	$f-f_0=574\ B^2$ (gauss) 1×10^{-9} (typical)	$f-f_0=427\ B^2$ (gauss) 1×10^{-10} (typical)
	2nd Order Doppler	$4\times10^{-11}(\partial f/\partial T=1.4\times10^{-13}/°K)$	8×10^{-13}	3×10^{-13}
	Collisions	2×10^{-11}	3×10^{-7} (typical)	none
State Selection Method		Atomic Beam Deflection in Hexapole Magnets	Optical Pumping	Atomic Beam Deflection in Dipole or Multipole Magnets
Resonance Detection Method		Atomic Microwave Radiation (active maser oscillation)	Optical Absorption	Surface Ionization of Deflected Atoms
Temperature of Resonating Atoms		300°K	330°K	360°K

III. PERFORMANCE CHARACTERISTICS

A. Definitions and Measurements

1. Definitions

The specification of the performance of the various atomic frequency standards is difficult and no universally accepted method of describing performance exists. A number of terms are used to describe performance, including spectral purity, frequency stability, accuracy and reproducibility. The following definitions of these quantities have received general acceptance.

Accuracy: Accuracy refers to comparison with an accepted standard, thus the frequency accuracy of an oscillator is measured by the deviation of the mean frequency of the oscillator from a standard such as the U.S. Frequency Standard. The particular standard must be named and a definition of mean frequency given to completely specify the accuracy.

Reproducibility: The term reproducibility commonly refers to the ability of an oscillator to return to a previously measured value of frequency after having been turned off and on, or to operate within specified limits of the operating frequency of other members of the class of similar oscillators. For example, a set of cesium beam standards built to the same specifications, tuned-up and checked out using a standard procedure will each oscillate at a slightly different frequency. The mean or average frequency can be determined and the standard deviation about this mean is a measure of the reproducibility.

Frequency Stability: The frequency stability is a measure of the time behavior of the frequency of the oscillator. The frequency refers to the average frequency of the oscillator during the time interval of measurement. For example, the frequency of oscillation may be measured over a large number of successive one second intervals. The measured frequencies will generally exhibit a random scatter about a mean frequency. The standard deviation about the mean is thus a measure of the stability. Typically one hears "the standard deviation is 5 parts in 10^{12} for 1 second averaging times." Over longer periods a time dependent drift or shift in frequency may be observed, and the individual measurements will scatter about this trend line. Such a drift or "aging rate" is commonly specified in terms of fractional parts per day or per week.

Spectral Purity: The spectral purity is a way of expressing the stability performance in the frequency domain rather than the time domain. Thus, it is

customarily the Fourier Transform of the frequency time series. For particular applications this spectral information is of more interest than the temporal behavior.

2. Measurements

Frequency stability measurements can be made over a range of averaging periods using several methods. Short term stability measurements have been made at TRW by observing the stability of a low frequency beat derived by mixing 10 GHz signals obtained by multiplying the 5 MHz frequency standard outputs as shown in Figure 13. Multiplication to 10 GHz was chosen for ease in data interpretation since a 1 Hz change in the beat frequency corresponds to a shift of 1 part in 10^{10}. Normally the frequency of one unit is offset with respect to the other by a constant amount to provide a convenient beat frequency of 100 to 500 Hz. The beat frequency can be counted and printed or converted to a voltage and displayed on a strip chart. When using a counter a quantization error of 1 Hz limits the accuracy of the system to 1 pp 10^{10} for a 1 second averaging period, and is correspondingly more accurate for 10, 100, 1000 second or longer counting periods. Use of the strip-chart presentation and the frequency to voltage conversion permits shorter averaging periods limited by the response time of the recorder. (This is typically 0.01 sec for a Sanborn Recorder). Stability measurements over a period of hours or days can be made with the beat frequency and counter equipment, but continuous recording of the relative phase between two oscillator units provides data which is readily interpreted for long-term information. A constant difference frequency results in a straight line relationship between phase and time; deviation from linearity indicates a time varying frequency difference or frequency instability. By proper choice of frequency difference and chart speed, frequency shifts as small as 1 pp 10^{12} are easily measured.

Long term stability and accuracy measurements can be made relative to the National Bureau of Standards U.S. Frequency Standard by way of station WWVL located in Boulder, Colorado. Commercial VLF receiver and servo phase shifters automatically shift the phase of a 100 KHz signal derived from the local frequency standard in order to zero the phase of a 40 KHz signal synthesized from the 100 KHz local signal relative to a 40 KHz signal obtained

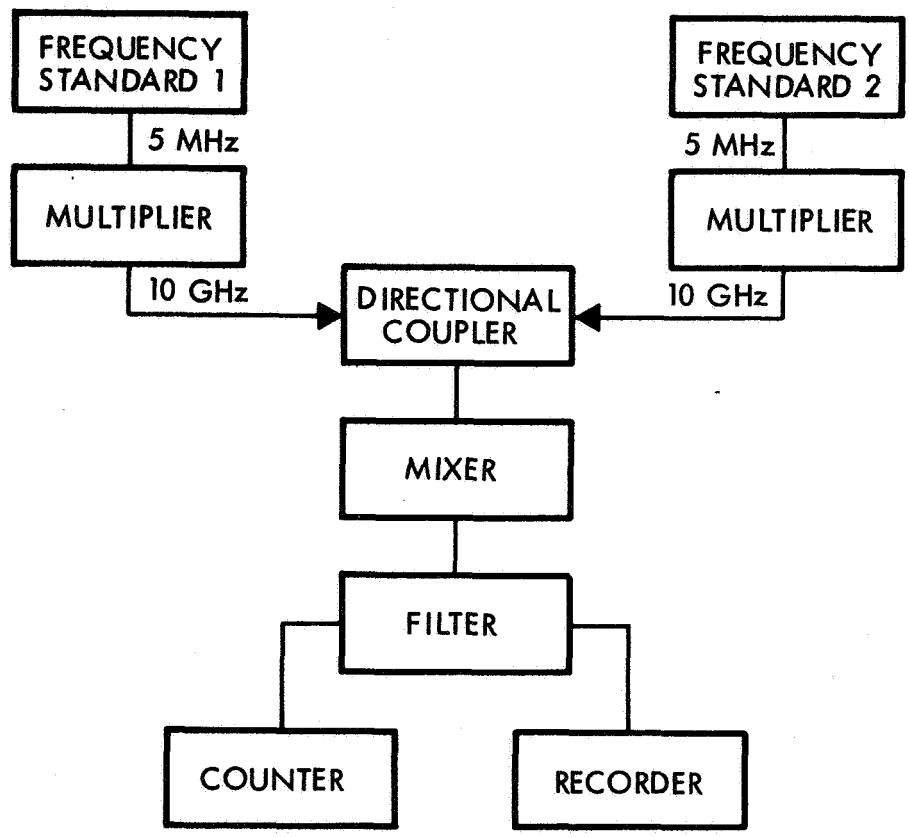

Figure 13. Schematic of apparatus for frequency stability comparisons.

by doubling the 20 KHz received WWVL signal. The phase shift required to maintain zero relative phase is recorded on a strip chart. A frequency difference of 1 pp 10^{10} can be observed in a three-hour period with little difficulty if the observation is made during midday or midnight hours. During sunrise and sunset periods at both transmitter and receiver sites, a large shift in phase occurs because of slight changes in the VLF propagation path with changes in the ionosphere. Averages over 8 to 24 hours are preferred for accuracy. Measurements over a period months are required to detect frequency drifts of atomic frequency standards. Measurements relative to these VLF broadcasts must be corrected for station frequency changes. The WWVL broadcast frequency variations are published periodically.

B. Frequency Stability Characteristics of Quartz Oscillators

The best quartz crystal oscillators reflect the most advanced design in precision frequency sources. Their signal stability and spectral purity are excellent. These oscillators incorporate all the features mentioned in the earlier discussion of crystal oscillators. Thus, the crystal is housed in a proportionally controlled double oven; automatic gain control maintains the drive level to the crystal constant; all outputs are carefully buffered to minimize the effect of load on frequency. Most of the electronic circuitry is also placed within the temperature controlled ovens. Each particular crystal is operated at its point of minimum temperature coefficient, that is, where the rate of change of frequency with temperature is a minimum.

The stability performance of the best commercial laboratory units (for example Hewlett-Packard 106 A, B) is better than ± 5 pp 10^{11} per 24 hours (drift). The short term stability is 1.5 pp 10^{11} rms fractional deviation for 0.1 sec and for 1 sec and is 8 pp 10^{10} rms for 1 msec. A frequency shift of ± 1 pp 10^{10} is specified for an ambient temperature range of 0° - 40°C.

A precision quartz oscillator packaged for spacecraft operation by Johns Hopkins Applied Physics Laboratory and described in Ref. 3 exhibited a frequency drift of 6 pp 10^{11} per day in orbit. This drift rate agreed with previous ground measurements. Other ground measurements indicated a short term rms fractional fluctuation of 1 pp 10^{11} for 2 sec averaging and

3 - 6 pp 10^{12} for 200 sec averaging. Temperature sensitivity is quoted as 1 pp 10^{11} per degree C, but improved temperature control circuitry is planned.

Another precision oscillator has been packaged by Bell Telephone Laboratories in a portable unit intended for field use and is described in Ref. 4. The long term stability (or drift) is less than 1 pp 10^{10} per day after the first four hours of operation. After a week of operation the drift decreases to less than 1 pp 10^{10} per week. The rms deviations of frequency are 1 pp 10^{10} for 0.2 second averaging-decreasing to 1.5 pp 10^{12} for averaging times greater than 10 seconds. The temperature sensitivity is ± 7 pp 10^{13} per degree C over a range of 10°C to 40°C.

These frequency stability performance characteristics reflect the best in packaged crystal oscillator units. The crystal oscillators used at the U.S. Naval Observatory which have been operated in an optimum environment continuously for months have drift rates as low as a few parts in 10^{13} per day. A temporary shut down of any crystal oscillator of the oven will produce a change of frequency, and a new period of stabilization is required. The new operating frequency will be several parts in 10^{9} different from the operating frequency before shut down. Sensitivity to vibration can be minimized by shock mounting, but static acceleration is more of a problem. Typically a shift of 10^{-9} per g will occur when a static acceleration is applied.

In summary, the stability performance of quartz crystal oscillators is quite good when they are operated in a carefully maintained environment. Such environments should be constant temperature, constant acceleration, vibration free and operation should be continuously maintained.

C. Frequency Stability Characteristics of Passive Atomic Standards

The results of frequency stability measurements of commercially manufactured cesium atomic beam standards and rubidium gas cell standards are shown in Figure 14. The data are the result of beat frequency and phase difference measurements of the type discussed earlier. Each point is the result of a number of measurements of frequency and is the calculated standard

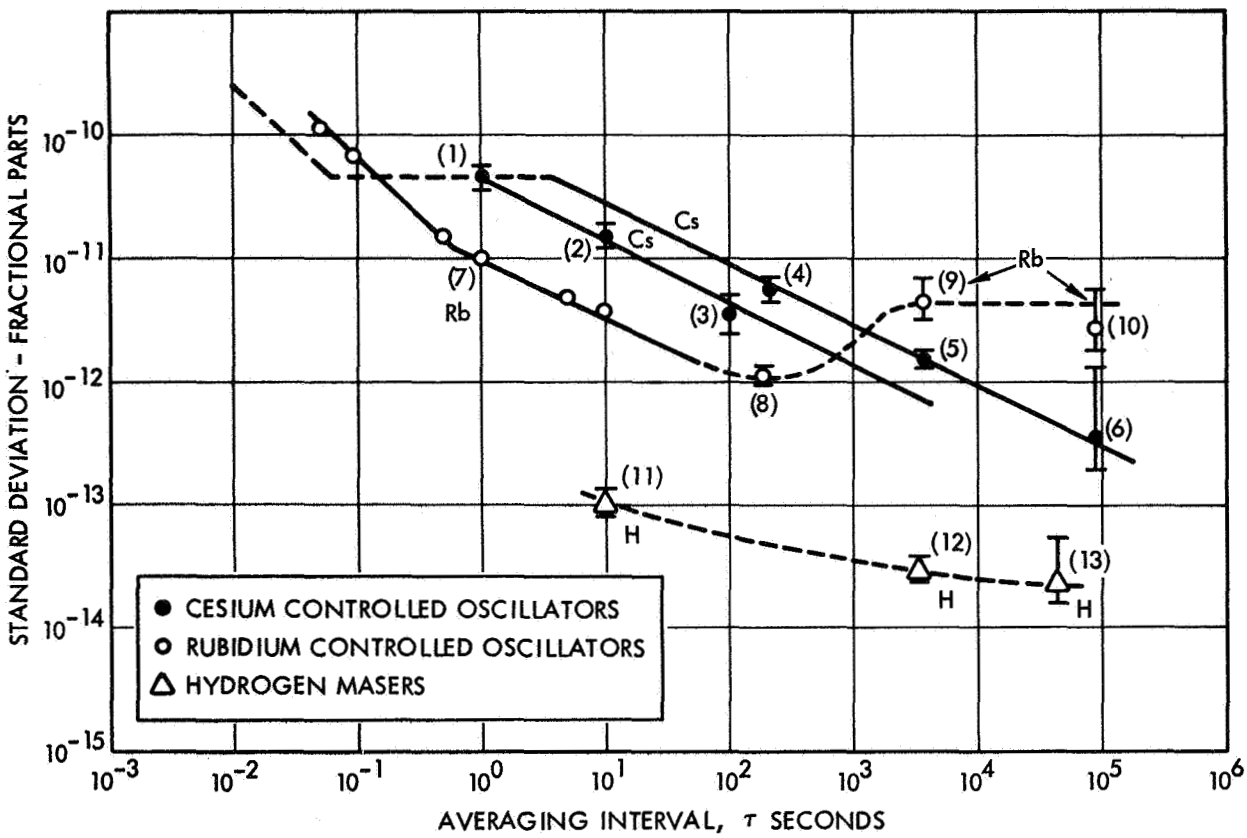

Figure 14. Atomic oscillator stability plot from Ref. 5. The symbols Cs, Rb, H identify the type of oscillator for which data taken. The numbers next to the data points refer to the data source listed in Table 3. The uncertainty limits on the measurement points indicate the degree of uncertainty in stability measurements (95% confidence intervals) and generally reflect a small number of samples. The solid curves indicate theoretically calculated stabilities.

TABLE 3

Sources of Data Plotted in Figure 14. (Ref. 5)

Data Point Identification	Atomic Standard	Source
(1), (2), (3)	Cesium Beam	Laboratory Standard—Varian BLR-2 Tube.
(4)	Cesium Beam	Hewlett-Packard Model 5060A (Varian BLR-3 Tube)—NBS Report of Calibration No. 805894, February 2, 1965.
(5), (6)	Cesium Beam	Two Hewlett-Packard Model 5060A Standards—Continuous phase difference record.
(7) Group of six points	Rubidium Gas Cell	Two Varian Model R-20 Standards.
(8)	Rubidium Gas Cell	Varian Model R-20 Standard—NBS Report of Calibration—pooled estimate 20 samples 202 measurements.
(9), (10)	Rubidium Gas Cell	Two Varian Model R-20 Standards—Continuous phase difference record.
(11)	Hydrogen Maser	Two Varian Model H-10 Masers—Beat frequency measurements.
(12), (13)	Hydrogen Maser	Two Varian Model H-10 Masers—Beat frequency measurements.

deviation in frequency computed from this (finite) number of measurements. The vertical bars represent the 95 percent confidence interval on the standard deviation and reflect the limited number of samples. The numbers on the curves identify the data sources and refer to Table 3.

Continuous phase difference plots for cesium and rubidium are shown in Figure 15 and 16. The data in Figure 15 is provided by General Technology Corporation and that in Figure 16 is replotted from data in Ref. 5. The time resolution in Figure 16 is approximately 10 nanoseconds reflecting the jitter in the recorder trace.

In addition to this data, long term performance of a number of commercial frequency standards has been measured at the National Bureau of Standards in Boulder, Colorado. These measurements are made by beating the 5 MHz output of the standard with the output of the standard NBSII (a cesium beam standard). The frequency offset is such as to give a beat note having a period of approximately 208 seconds. Period measurements are made for approximately 20 minutes, i.e., 10 periods, and an average period and beat frequency calculated. This beat frequency is then recorded, approximately one reading a day, and the result plotted for a longer period of time. Figure 17 shows the results of such measurements and Figure 18 shows a similar record taken in 1962 with the TRW (STL) Rubidium Frequency Standard.

In appraising all of this data it must be stated that the statistical support is meager, especially for the long-term frequency stability measurements. Statistical significance, of course, implies a larger number of samples, and a large number of long measurement intervals implies either long periods of time or a large number of simultaneous long term experiments. Inasmuch as large quantities of atomic frequency standards do not exist and are not in widespread use, there is a good explanation for the scarcity of long term data.

The physical origin of slow drifts or very low frequency fluctuations is not well understood. Phenomena such as rubidium lamp deterioration, changes in buffer gas composition, outgassing of sealed atomic beam tubes, and other such long term effects need further study before meaningful predictions of very long term performance can be made. At present, there is no meaningful basis for extrapolating the apparent drifts of particular classes of frequency

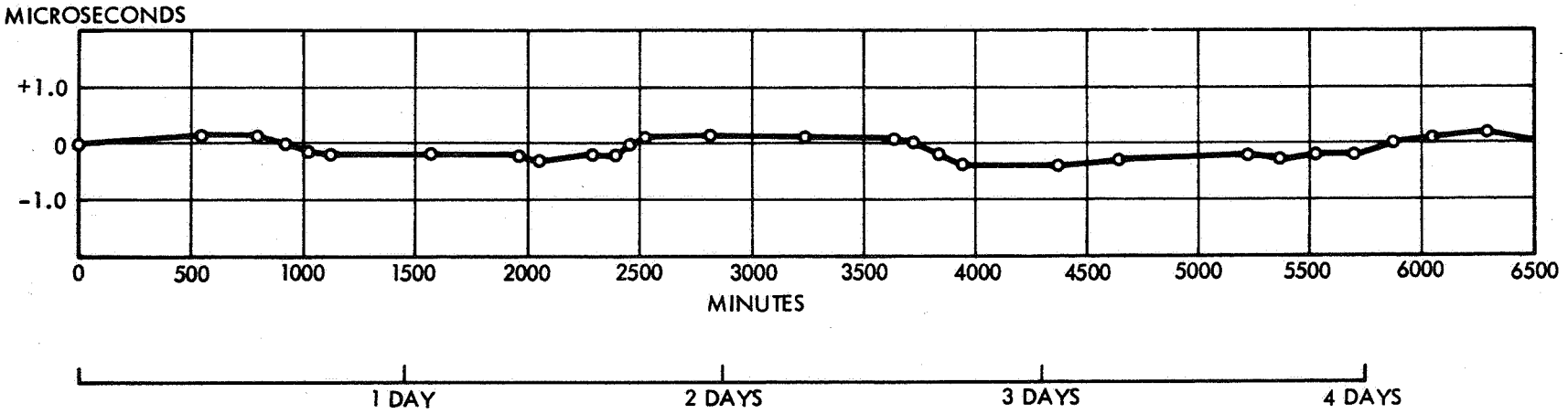

Figure 15. Phase difference measurements, in microseconds, between two General Technology Corporation rubidium gas cell frequency standards.

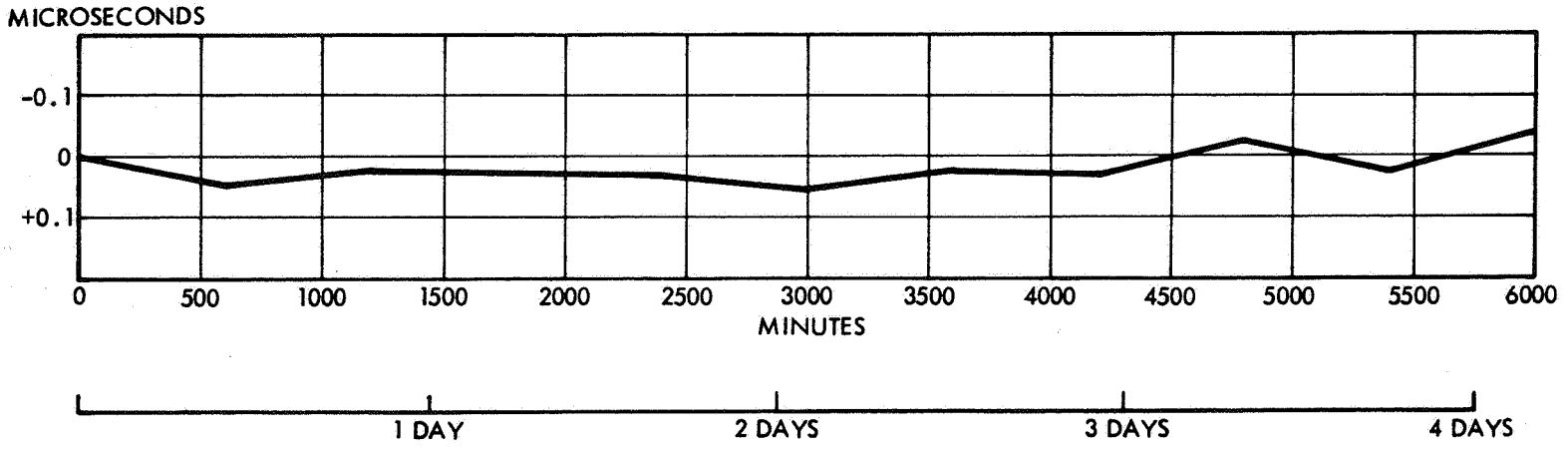

Figure 16. Phase difference measurements, in microseconds, between two Hewlett Packard cesium beam atomic frequency standards (from Reference 5).

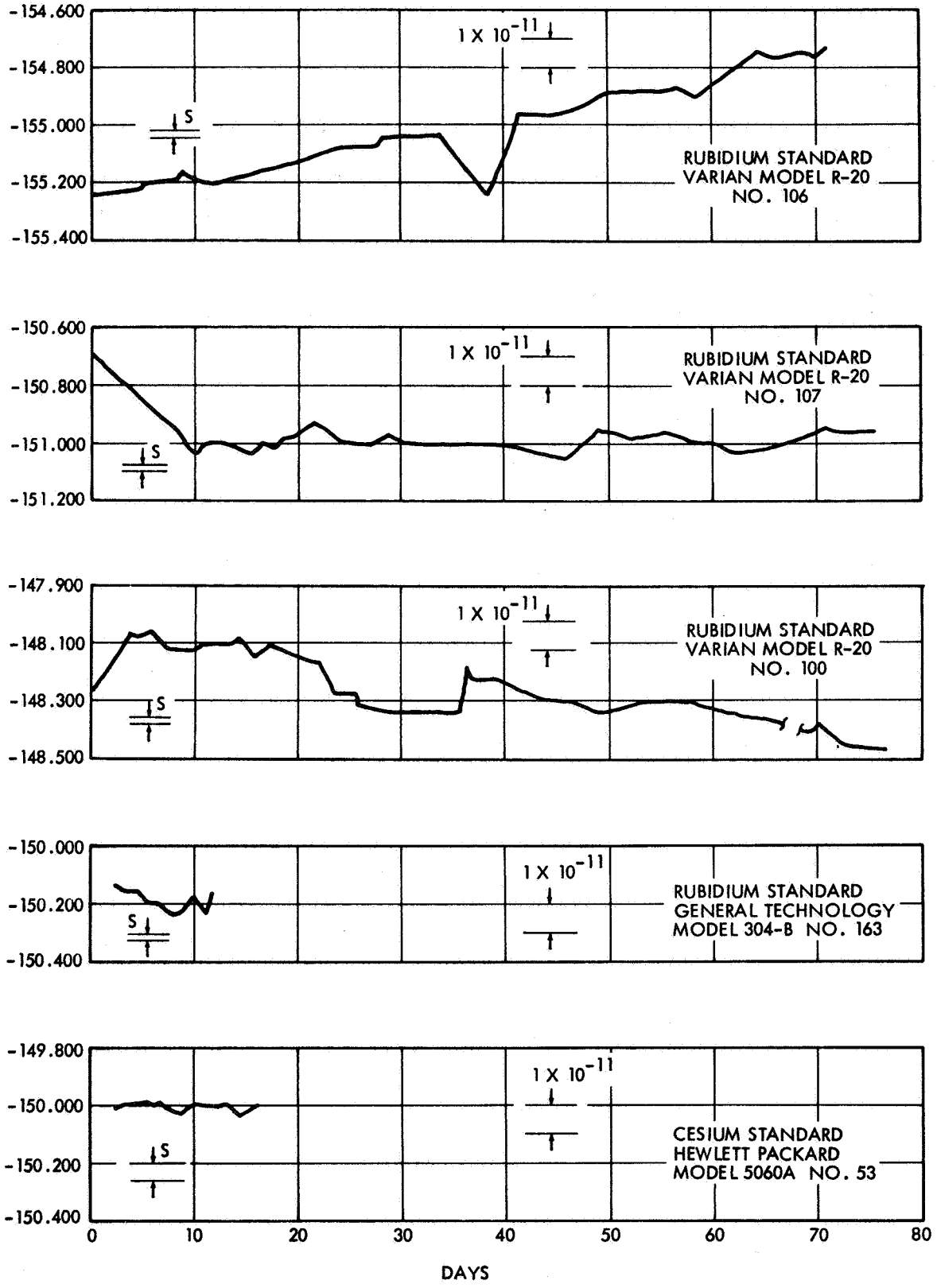

Figure 17. Frequency stability data taken from National Bureau of Standards Calibration Reports for various frequency standards. (from Ref. 5). See text for description of data taking process.

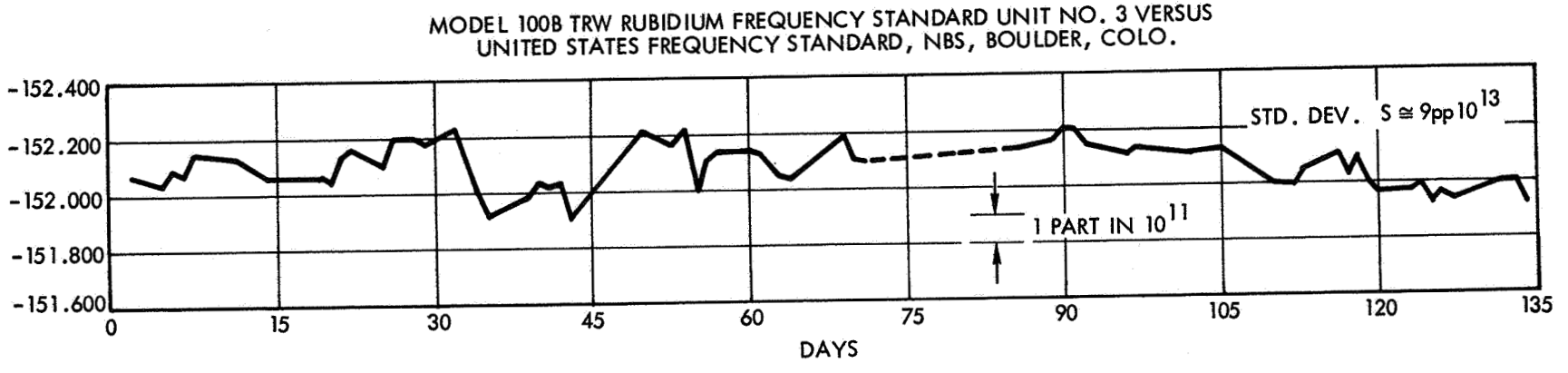

Figure 18. Frequency stability data taken from NBS report on TRW (STL) rubidium frequency standard.

standards for periods beyond those for which experimental data exists. There is some evidence to indicate that these apparent drifts can change sign occasionally in an unpredictable manner.

D. Frequency Stability Characteristics of Maser Oscillators

A relatively small number of measurements have been published of the frequency stability of commercial hydrogen maser oscillators. Figure 14 shows the results of these data which were obtained by beat frequency measurements. It is evident from the data shown that the hydrogen maser is currently the most stable frequency standard in existence.

There is some indication that the rubidium maser oscillator, which is not commercially available, will exhibit better very short term stability performance. It is expected that for larger periods it will exhibit the aging and low frequency fluctuations associated with the passive rubidium frequency standards.

E. Summary

In summary of the frequency stability characteristics of the three commercially available atomic frequency standards, Table 4 is presented here.

TABLE 4

Summary of Frequency Stability
Characteristics of 3 Atomic Frequency Standards (Ref. 5)

Characteristic	Atomic Hydrogen Maser	Rubidium Gas Cell Controlled Oscillator	Cesium Atomic Beam (24-inch) Controlled Oscillator
Intrinsic Reproducibility of Present Devices	$\pm 5\times10^{-13}$	does not apply	$\pm 3\times10^{-12}$
Stability (rms deviation from the mean): One second	5×10^{-13}	1×10^{-11}	5×10^{-11}
One minute	6×10^{-14}	2×10^{-12}	6×10^{-12}
One hour	3×10^{-14}	5×10^{-12}	8×10^{-13}
One day	2×10^{-14}	5×10^{-12}	2×10^{-13}
Systematic Drift*	None detectable with resolution of 1×10^{-12} per year	less than 3×10^{-11} per month	None detectable with resolution of 3×10^{-12} per year

IV. PHYSICAL CHARACTERISTICS OF STABLE OSCILLATORS

A. Introduction and Tabular Summary

In order to decide whether a particular type of stable oscillator is best suited to a particular application it is necessary to consider various physical characteristics of the apparatus. In many applications the weight, volume, power consumption, ability to operate in extreme temperature ranges and harsh vibrational environments and other factors are extremely important. The instrument lifetime or mean time between failures is another important characteristic. Typical physical characteristics are presented in this section for the various oscillators we have considered, and are summarized in Table 5. It is evident that many trade-offs are possible, e.g., better thermal shielding can be obtained by increasing the weight.

B. Quartz Crystal Oscillators

The three quartz crystal oscillators discussed earlier, i.e., the Hewlett-Packard 106 A,B, the Johns Hopkins and Bell Laboratories units, have each been well packaged for their intended application. (See Table 5). The HP oscillator is intended for general laboratory and industrial use. The unit weighs 25 pounds and its dimensions are 7" x 16-3/4" x 16-3/8". The operating temperature is 0°C to 40°C. Power required is approximately 8 watts.

The Johns Hopkins unit described in Ref. 3 is packaged for operation aboard the Geos A spacecraft, and provides signals for a doppler measurement system. The complete oscillator package was 3.6 inches in diameter, 5 inches long and weighed 2.75 pounds. The crystal itself was placed in a thermally massive inner flask surrounded by aluminized Mylar and fiberglass-paper layer insulation. This is surrounded by a heater flask, more insulation and an outer flask (or can).

The oscillator reported by the Bell Telephone Laboratories in Ref. 4 was packaged as a portable unit and intended for field use. The assembly is 8.5" x 8.5" x 16" and weighs 25 pounds. The unit is powered by 24 volts D.C. and requires 24 watts in operation 25°C after warm-up. The package is of the usual double oven design consisting of an outer oven, with polyurethane foam insulation, containing an inner oven with more insulation housing the oscillator unit. Electrical filters provide noise insulation and electrostatic and mechanical isolation is provided by the outer enclosure.

TABLE 5

PHYSICAL CHARACTERISTICS OF SELECTED STABLE OSCILLATORS

	Weight, Lbs.	Volume, Ft.^{3}	Power Required, W	$\Delta f/f$ in Earths Mag. Field	Operating Temp. Range	Warm-Up Time	Comments
CRYSTAL OSCILLATORS							
HP 106 a,b	25	1.11	8	-	0°-40° C	-	-
Geos. A,(Ref. 3)	2.75	51in^3	<1.3	-	-23°- +47°C	8 Hrs. (Thermal Time constant)	-
Bell Labs, (Ref.4)	25	0.67	24	-	10° - 40° C	4 Hrs. (Initial Stabilization)	-
ATOMIC STANDARDS							
Varian, R-20 Rb Gas Cell	40	0.6	42, A.C.	$\pm 5 \times 10^{-12}$	0 - 50° C	1 Hour	Standby power supply available
Gen. Tech. 304B Rb Gas Cell	39	0.95	35 A.C. or D.C.	$<5 \times 10^{-12}$	0 - 45° C	1 - 2 hours before	"
Gen. Tech. 305A Rb Gas Cell	44	1.95	48	"	"	full frequency	Incl. interal batteries good for 15 minutes
Gen. Tech. 306A Rb Gas Cell	14	0.3	28	"	-35° - +45°C	specs. met	No Freq. synthesizer f_{out} = 5.273 MHz
HP 5060 A Cesium Beam	63	1.42	50 A.C. or D.C.	$<\pm 5 \times 10^{-12}$	0 - 50°C	1 Hr. (If oscillator warm) 4 hrs. otherwise	16" Beam Tube
National NC 3501 Cesium Beam	70	1.38	45 A.C. or D.C.	$<5 \times 10^{-12}$	0 - 50° C	20 - 30 minutes	Internal battery capable of 20 min. oper. optional
Varian, H-10, H - Maser	800	16.4	200	-	-	-	Continuous vacuum pumping system

These three units illustrate that small physical size is compatible with quality crystal oscillator performance. No reliability data are quoted, but reliability performance is believed good.

C. Passive Atomic Frequency Standards

1. Rubidium Gas Cell Standard

It is seen from Table 5 that the rubidium standard is the most compact and lightweight of the atomic frequency standards. The high signal to noise ratio gives it a high degree of short term stability, and it is consequently best suited to a rugged environment. The atomic reference is able to compensate for the effects of vibration upon the crystal oscillator.

It is to be noted from Table 5 that for space/power/weight limited situations it is possible to operate the rubidium standard without the frequency synthesizer and obtain a rather compact unit. (Dimensions 9" x 6" x 11" for G. Tech. 306A). The military and missileborne units have been tested for performance under shock, vibration, humidity and other harsh conditions as specified by the military.

Lifetime data on rubidium frequency standards has been accumulated since 1961 by Varian Associates and General Technology Corporation. The original Varian units used vacuum tube lamp exciters and these units exhibited a MTBF of between 4000 and 5000 hours. Later models using solid state exciters exhibited an MTBF of 7500 hours, and this was increased to 24,000 hours in units engineered for reliability. The General Technology Corporation device has been all solid state since first sold in 1961. Their data also indicates a MTBF in excess of 22,000 hours.

2. Cesium Beam Frequency Standard

Also included in Table 5 is the Hewlett Packard Model 5060A cesium beam standard and the National Company NC 3501 cesium beam standard. The increased weight and volume is associated with the geometry of the beam tube and the necessity of providing magnetic shielding over its length. The beam tube used in the HP 5060A is 16 inches long, 5-1/2" in diameter and weighs 16 pounds. This compares with the lamp-cavity-detector unit of the rubidium frequency standards which is typically 10" long, and 5-1/2" in diameter, and

weighs approximately 7 pounds. It is possible to imagine a missileborne unit equivalent to the Gen. Tech. 306A which would include only the beam tube and basic electronics without the frequency synthesizer. A volume of approximately one-half cubic foot and a weight of approximately 25 pounds should be possible.

The lifetime of the cesium beam frequency standard is determined by the lifetime of the atomic beam tube. The commercial units offer a 10,000 hour guaranteed operating lifetime on the beam tube. The electronic circuitry is expected to exhibit a much longer expected lifetime.

D. Active Frequency Standards

1. Hydrogen Maser

The only active standard which is commercially available at this time is the Varian Associates Atomic Hydrogen Maser, Model H-10. By its nature the hydrogen maser is a large and heavy device. The principle reason for the size is the long wavelength (21cm) of the hydrogen resonant frequency, and the need for a high Q resonant cavity to sustain self oscillation. In addition, magnetic shielding of the structure is required and continuous pumping of the system is required to maintain a high vacuum. The weight and volume information for the H-10 maser is included in Table 5. The dimensions are 24" x 24" x 79". Reliability and lifetime data does not seem to be available at this time.

V. CONCLUDING REMARKS - FUTURE

A. The Choice of an Oscillator

At this point the reader will appreciate that each of the stable oscillators discussed has its virtues and faults. For many applications the performance of the crystal oscillator will be adequate and an atomic frequency standard will not be required. In cases where extreme stability is required, one may wish to use the expensive and bulky hydrogen maser. The advantages and limitations are reviewed at this time.

Quartz Crystal Oscillators:

Advantages: Compact, light weight, inexpensive, good short term stability and capable of predictable long term performance if in continuous operation.

Disadvantages: If operation interrupted or if subject to change in temperature, stress or vibration, the frequency will shift unpredictably.

Rubidium Gas Cell Standard:

Advantages: Most compact, light weight and least expensive of atomic standards. Good short term stability (better than uncontrolled quartz oscillator). Capable of good performance even when subjected to vibration and temperature change.

Disadvantages: Not a primary standard. Must be calibrated after manufacture. May be subject to small, slow long term drifts.

Cesium Atomic Beam Standard:

Advantages: Good long term stability and reproducibility. Primary standard. Most compact of primary standards.

Disadvantages: Short term stability not as good as rubidium standard. Loop gain not able to overcome rapid environmental changes such as vibration or sudden accelerations. Beam tube expires (~10,000 hours).

Atomic Hydrogen Maser:

Advantages: Greatest intrinsic reproducibility, long and short term stability. Primary standard capability.

Disadvantages: Size, weight and expense.

It is possible to approach the choice of a stable oscillator in a logical manner by asking a sequence of questions. In answering these questions, one will pretty well have determined which oscillator he must use. These questions are:

1. What is the frequency stability required, both long term and short term? Is a long term stability of 1 part in 10^{10} required, or a part in 10^{13}?

2. What is the operating environment? Is the temperature constant? Is there a great deal of vibration? Will the oscillator be tended or will it be required to operate for long periods unattended?

3. What are the important physical constraints? Are there limitations on weight, power, size, etc.?

4. Is cost important? There is a strong correlation between frequency stability and expense, and between operating convenience and expense.

As an example, suppose that an oscillator is required to operate aboard an earth satellite to provide a timing signal. The frequency stability requirement is a part in 10^{10} and operation for 10,000 hours is required. The weight, volume and power constraints are rigid, and reliability of operation is important. The choice is thus between a crystal oscillator and a rubidium frequency standard. The environment is free of vibration and the temperature can be maintained constant within narrow limits. The crystal oscillator will drift slowly - but generally in a predictable manner. The atomic standard will drift exhibit a very much smaller long term drift. The system designer would probably choose a crystal oscillator and make the final choice on how difficult it is to predict the oscillator frequency and what additional equipment such a prediction would make necessary.

B. Future Developments

It is possible to predict the following developments in stable oscillators.

Quartz Crystal Oscillators

Reduced initial stabilization periods; reproducible drift rates; improved short term stability; exploration of effects of nuclear radiation, shock and vibration.

Rubidium Frequency Standards

Further size reductions as pumping source improve and more efficient generation of power at high frequencies enables elimination of cavity. Short term stability will improve as better crystal oscillators evolve.

Cesium Beam Frequency Standard

Better short term stability as crystal oscillators evolve and increased beam tube currents improve atomic beam control signal. Corresponding improvements in tube dimensions and tube lifetime are to be expected.

Atomic Hydrogen Maser

Reductions in size and weight are to be expected. Automatic control of cavity tuning and other functions now requiring a human operator.

Other

Further improvements are to be expected in the rubidium maser oscillator, and the availability of a commercial unit. Such a device will improve upon the short term stability of the rubidium frequency standards, but will still be subject to the long term limitations of these devices.

REFERENCES

1. E. A. Gerber and R. A. Sykes, "State of the Art - Quartz Crystal Units and Oscillators," Proc. IEEE, 54, 103 (February 1966).

2. "A Handbook of Selected Semiconductor Circuits," NObsr 73231, NAVSHIPS 93484, Bureau of Ships, Dept. of the Navy.

3. J. B. Oakes and R. A. Mauck, "A High Stability Crystal Oscillator for the Geos Spacecraft," From IEE Conf. Publication No. 31, "Frequency Generation and Control for Radio Systems." The Institution of Electrical Engineers, London, W.C.2, England.

4. H. S. Pustarfi, "An Improved 5 MHz Reference Oscillator for Time and Frequency Standard Applications," IEEE Trans. on Instrumentation and Measurement, Vol. 1M-15, No. 4, Page 196, December, 1966.

5. A. O. McCoubrey, "A Survey of Atomic Frequency Standards," Proc. IEEE, 54, 116 (February 1966).

FIGURE CAPTIONS

Figure 1. a) Quartz resonator, b) equivalent circuit, and c) magnitude and phase angle of impedance. $\omega_2 = 1/\sqrt{LC_2}$, $\omega_1 = \omega_2\sqrt{1+C_2/C_1}$.

Figure 2. Block diagram of commercial quartz oscillator (Hewlett Packard Model 106 A,B).

Figure 3. Typical control signal for passive atomic frequency standard.

Figure 4. Atomic energy level diagram for rubidium atom.

Figure 5. Splitting of lowest energy state of rubidium 87 atom with applied external magnetic field.

Figure 6. Functional block diagram, rubidium gas cell frequency standard.

Figure 7. Schematic diagram, optical pumping of rubidium atoms.

Figure 8. Emission spectrum from rubidium lamp containing natural rubidium (72% Rb85, 28% Rb87).

Figure 9. Functional block diagram, cesium atomic beam frequency standard (Hewlett Packard, Model 5060A).

Figure 10. Schematic diagram of atomic beam resonator. The C field magnet providing a uniform magnetic field throughout the interaction region is not shown.

Figure 11. Schematic diagram of the atomic hydrogen maser. The C field magnet providing a uniform magnetic field throughout the interaction region is not shown.

Figure 12. Block diagram of hydrogen maser frequency standard.

Figure 13. Schematic of apparatus for frequency stability comparisons.

Figure 14. Atomic oscillator stability plot from Reference 5. The symbols Cs, Rb, H identify the type of oscillator for which data taken. The numbers next to the data points refer to the data source listed in Table 3. The uncertainty limits on the measurement points indicate the degree of uncertainty in stability measurements (95% confidence intervals) and generally reflect a small number of samples. The solid curves indicate theoretically calculated stabilities.

Figure 15. Phase difference measurements, in microseconds, between two General Technology Corporation rubidium gas cell frequency standards.

Figure 16. Phase difference measurements, in microseconds, between two Hewlett Packard cesium beam atomic frequency standards (from Reference 5).

Figure 17. Frequency stability data taken from National Bureau of Standards Calibration Reports for various frequency standards. (from Reference 5). See text for description of data taking process.

Figure 18. Frequency stability data taken from NBS report on TRW (STL) rubidium frequency standard.

APPENDIX C
SATELLITE OSCILLATOR RESET

Left to itself a good crystal oscillator will age at a rate of the order of 1 to 5 parts in 10^{10} per day, i.e.,

$$\frac{\Delta f}{f}(t) \approx kt$$

where

$$k = \begin{cases} 1.10^{-10} \\ 5.10^{-10} \end{cases} \text{ per day}$$

$$= \begin{cases} 1.10^{-15} \\ 5.10^{-15} \end{cases} \text{ per sec}$$

As a clock then

$$\frac{d}{dt}(\Delta t) = kt$$

or

$$\Delta t = k_o + \frac{1}{2} kt^2$$

The effect of this aging characteristic on accuracy is not of concern here since it is assumed that the user has available to him calibration information essentially equivalent to k_o and k and the residuals from such a calibration have already been considered in Reference 1. Rather we are concerned with the time station-keeping problem of insuring that each satellite maintains its transmission within its assigned time multiplex slot with a tolerance, T, of the order of ±0.2 sec. If we assume frequency control only, the optimum (minimum) control strategy is as shown in Figure C-1. Discrete frequency change commands are issued at the time the error just reaches the positive limit, and in such amount as to

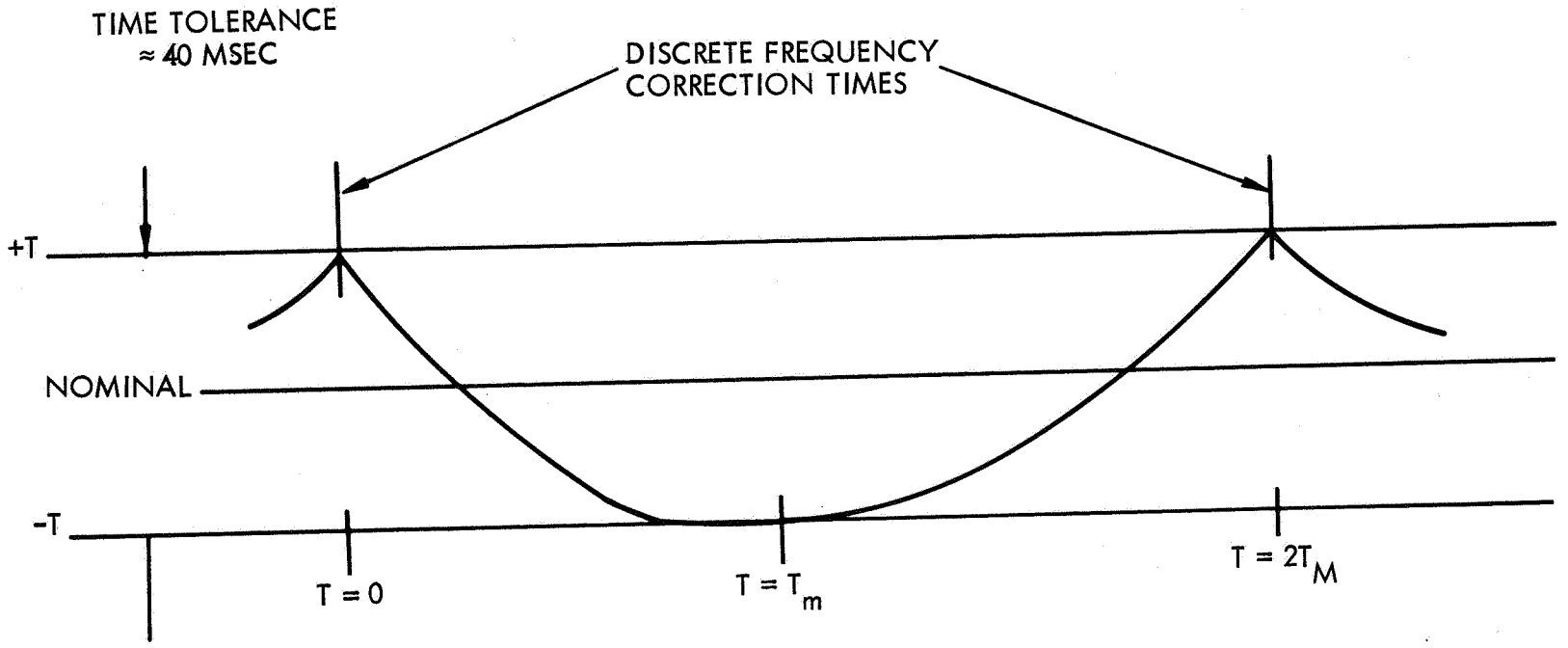

Figure C-1. Optimal Frequency Correction to Maintain Time Error within a Specified Band in the Presence of Crystal Ageing

just cause the negative error to reach the negative limit. Δt then follows a path given by:

$$\Delta t(t) = a + bt + \frac{1}{2} kt^2$$

in which the constants can be evaluated from the boundary condition:

$$\Delta t(0) = +T$$

$$\Delta t_{min} = -T$$

Thus $a = T$. Then the minimum is given by

$$\frac{d}{dt} \Delta t(t_m) = 0 = b + kt_m$$

or

$$t_m = -\frac{b}{k}$$

and

$$\Delta t_{min} = T - \frac{b^2}{k} + \frac{b^2}{2k}$$

$$= -T$$

or

$$b = -2\sqrt{Tk}$$

and

$$t_m = 2\sqrt{\frac{T}{k}}$$

The reset time is

$$\tau = 2\, t_m = 4\sqrt{\frac{T}{k}}$$

In confirmation of which the error at reset time is:

$$\Delta t(\tau) = T - \left(2\sqrt{Tk}\right) \cdot \left(4\sqrt{\frac{T}{k}}\right) + \frac{k}{2}\left(16\frac{T}{k}\right)$$

$$= T$$

Thus with typical numbers $k = 5.10^{-15}$ and $T = .02$ sec., the reset interval is:

$$\tau = 4\sqrt{\frac{.02}{5.10^{-15}}}$$

$$= 8 \cdot 10^{6} \text{ sec.}$$

$$\approx 100 \text{ days}$$

The maximum frequency error corresponding to reset times is then

$$\left(\frac{\Delta f}{f}\right)_{max} = \left[\frac{d}{dt}(\Delta t)\right]_{max}$$

$$= \pm b$$

$$= \pm 2\sqrt{Tk}$$

$$= \pm 2\sqrt{.02.5.10^{-15}}$$

$$= \pm 2.10^{-8}$$

which corresponds to a velocity correction of ±20 ft/sec. The frequency control should provide a resolution of the order of 2 parts in 10^9 at least.

Over a maximum postulated 10 year lifetime, the total frequency correction capability would have to be of the order of

$$\frac{\Delta f}{f} = 5.10^{-10}.365.10$$

$$= 1.8.10^{-6}$$

if the aging rate were constant at its worst assumed value, which is undoubtedly pessimistic. Three factors combine to ameliorate this situation. They are:

1) The aging rate tapers off with time.

2) The oscillators will tend to age together and only the difference needs to be controlled.

3) The time standard can be run at any rate to accommodate the mean or swarm of satellite oscillators.

APPENDIX D
NAVSAT COMMAND REQUIREMENTS

The NavSat Electrical Integration Assembly (EIA) provides a capability of 64 discrete commands. Three standard types of commands are supplied:

Type I	Low Level Pulses	
	True State	- 3.75V ± 1.25V
	False State	- 0.0V ± 0.5V
	Duration	- 40 MS ± 4 MS
Type II	Medium Power Pulses	
	True State	- 28.-V ± 2.0V
	False State	- 0.0V ± 1.0V
	Duration	- 40 MS ± 4 MS
Type III	Relay Closures	
	Momentary or Latching	- 40 MS ± 4 MS - Until Commanded Open
	2 Amp Maximum Capacity (Resistive Load)	

In addition, any of the above commands can be provided with a pulse duration selected by ground command. The only use of this capability in the present design is for the fire periods associated with thruster firing.

Table I presents a list of the commands selected for NavSat. A total of 21 unassigned commands exist in the present design.

Consideration of mission and orbital operations requirements was the primary influence in selection of the commands so that the capability was provided to:

- Initiate discrete events
- Command selected equipment ON or OFF
- Select redundant equipment
- Change to alternate modes of operation.

Selection of commands was also made in conjunction with selection of the telemetry measurements to ensure that if anomalous behavior of the spacecraft equipment were noted, a means to rectify it was available. For example, if Navigation Transmitter No. 1 was detected to be overheating, the capability to command it OFF and to command Navigation Transmitter No. 2 ON was provided.

TABLE I

NAVSAT COMMAND LIST

Command Number	Subsystem	Command	Function	Type
1	Attitude Control	Normal Mode	Sets control logic in dual earth sensor mode	II
2		Earth Sensor No. 1 Mode	Selects earth sensor No. 1 output for single earth sensor operation	II
3		Earth Sensor No. 2 Mode	Selects earth sensor No. 2 output for single earth sensor operation	II
4		Ground Despin Mode	Sets control logic for operation of MDA by Ground Control (AEP)	II
5		Valve Driver Set No. 1 ON	Selects No. 1 bank of thruster coils	II
6		Valve Driver Set No. 2 ON	Selects No. 2 bank of thruster coils	II
7		Valve Drivers OFF	Removes driver voltage to prevent inadvertent firing of thrusters	II
8		Axial Thrusters No. 1	Sets switch in EIA to route fire period command to axial thruster No. 1	I
9		Axial Thruster No. 2	Sets switch in EIA to route fire period command to axial thruster No. 2	I
10		Radial Thruster No. 1	Sets switch in EIA to route fire period command to radial thruster No. 1	I
11	Attitude Control	Radial Thruster No. 2	Sets switch in EIA to route fire period command to radial thruster No. 2	I

Command Number	Subsystem	Command	Function	Type
12	Navigation	T.D. Transponder OFF	Turns tracking data transponder OFF	II
13		T.D. Transponder Disable	Puts tracking data transponder in standby mode	I
14		Change Despin Electronics	Changes MDA electronics to alternate (redundant) mode	I
15		Frequency Adjust	Signal to time base unit to adjust oscillator frequency	I
16		Transponder Mode Override	Signal to time base unit to inhibit transponder modulation	I
17		Nav. Transmitter No. 1 ON	Turns navigation transmitter No. 1 ON, No. 2 OFF	II
18		Nav. Transmitter No. 2 ON	Turns navigation transmitter No. 2 ON, No. 1 OFF	II
19		Nav. Transmitters OFF	Turns navigation transmitters OFF for low power and test conditions	II
20		Time Base Unit No. 1 ON	Turns time base unit No. 1 ON, No. 2 OFF	III
21		Time Base Unit No. 2 ON	Turns time base unit No. 2 ON, No. 1 OFF	III
22		Time Base Units OFF	Turns time base units OFF for low power and test conditions	III
23		Data Encoder No. 1 ON	Turns data encoder No. 1 ON, No. 2 and No. 3 OFF	III
24	Navigation	Data Encoder No. 2 ON	Turns data encoder No. 2 ON, No. 1 and No. 3 OFF	III

Command Number	Subsystem	Command	Function	Type
25	Navigation	Data Encoder No. 3 ON	Turns data encoder No. 3 ON, No. 1 and No. 2 OFF	II
26	Navigation	Data Encoders OFF	Turns data encoders OFF for low power and test conditions	III
27	Telemetry and Command	T&C Transmitter No. 1 ON	Turns T&C Transmitter No. 1 ON, No. 2 OFF	III
28		T&C Transmitter No. 2 ON	Turns T&C Transmitter No. 2 ON, No. 1 OFF	III
29		T&C Transmitters OFF	Turns T&C Transmitters OFF	III
30		TLM Encoder No. 1 ON	Turns telemetry encoder No. 1 ON, No. 2 OFF	III
31		TLM Encoder No. 2 ON	Turns telemetry encoder No. 2 ON, No. 1 OFF	III
32	Telemetry and Command	TLM Encoders OFF	Turns telemetry encoders OFF	III
33	Propulsion	Apogee Motor Ignite	Fires apogee motor squibs	II
34	Power	Battery No. 1 Normal	Connects battery No. 1 to main bus	II
35		Battery No. 2 Normal	Connects battery No. 2 to main bus	II
36		Battery No. 1 OFF-Charge	Removes battery No. 1 from main bus and connects to charge circuit	II
37		Battery No. 2 OFF-Charge	Removes battery No. 2 from main bus and connects to charge circuit	II
38	Power	Battery No. 1 OFF - Recondition	Removes battery No. 1 from main bus and connects to reconditioning load	II

Command Number	Subsystem	Command	Function	Type
39	Power	Battery No. 2 OFF - Recondition	Removes battery No. 2 from main bus and connects to reconditioning load	II
40		Undervoltage Control - Normal	Allows undervoltage sensor to remove selected loads during low voltage conditions	I
41	Power	Undervoltage Control - Override	Inhibits above function	I
42	Electrical Integration	Current Monitors ON	Turns primary bus current monitor ON	I
43	Electrical Integration	Current Monitors OFF	Turns primary bus current monitor OFF to conserve power	I
44-64	Not Assigned			

APPENDIX E

TELEMETRY MEASUREMENTS

The telemetry encoder for the NavSat Program has been selected from the Intelsat III Program. This encoder provides three telemetry subcarriers which are amplitude and frequency modulated with the real time and housekeeping data as shown in Figure I. The three telemetry subcarriers are summed into a combined signal which phase modulates the telemetry transmitter carrier.

Real time data are provided for critical signals required for ground control of the spacecraft. These signals are the earth sensor and sun sensor pulse outputs, the mechanically despun antenna reference pulse, and the period for which the thruster solenoids are commanded to fire.

Housekeeping data are provided by 63 time-multiplexed channels of a ripple counter which operate at a rate of one frame per minute. The frame format has two synchronization channels which leaves a total of 61 channels for housekeeping information. The sample period for each channel is .85 seconds.

Table I presents a list of the housekeeping telemetry measurements selected for NavSat. The channel assignments for these measurements are shown in Figure II. Two types of housekeeping information are provided: analog outputs, which are varying parameters such as transmitter temperature, and discrete outputs, which are On/Off indications such as receiver signal presence. Most measurements are sampled at the rate of one per minute. Where better resolution is required, the measurement is supercommutated into additional channels such as primary bus current which is provided at four samples per minute. The telemetry list presented allows a spare capability of eight channels. The measurements selected provide sufficiently adequate information to determine the spacecraft operational, performance, malfunction, and diagnostic requirements.

The analog parameters are conditioned to a voltage range of 0 to 5 volts. The discrete parameters are summed three to a channel to provide more telemetry capability. Table II shows the summed channel voltage for three discretes (A, B, C) for the various true (1) and false (0) level combinations of the discretes.

TABLE II

Discrete A	B	C	Channel Voltage
0	0	0	0.00 V
1	0	0	0.71 V
0	1	0	1.43 V
1	1	0	2.14 V
0	0	1	2.86 V
1	0	1	3.57 V
0	1	1	4.28 V
1	1	1	5.00 V

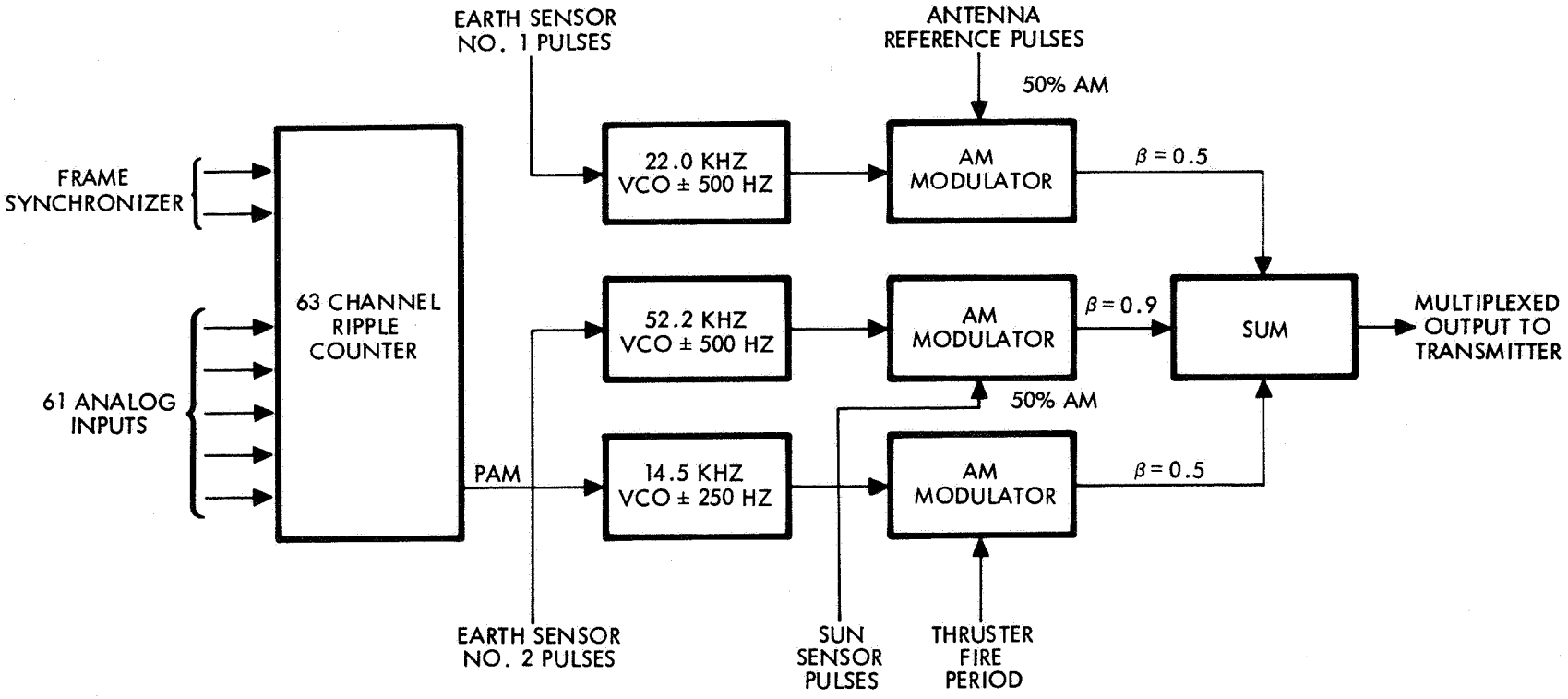

Figure E-1. NAVSTAR Telemetry Encoder

TABLE I

NAVSAT TELEMETRY LIST

Subsystem	Unit	Parameter	Samples per Minute	Data Type			Signal Conditioning Location
				Real Time	Analog	Discrete	
Attitude Control	Valve Driver Assembly	Valve Set No. 1 ON/OFF	1			x	EIA
		Valve Set No. 2 ON/OFF	1			x	EIA
		Radial Thruster No. 1 Switch ON/OFF	1			x	EIA
		Radial Thruster No. 2 Switch ON/OFF	1			x	EIA
		Axial Thruster No. 1 Switch ON/OFF	1			x	EIA
	Valve Driver Assembly	Axial Thruster No. 2 Switch ON/OFF	1			x	EIA
	Control Logic Assembly	Earth Sensor No. 1 Pulses	Cont.	x			CLA
		Earth Sensor No. 2 Pulses	Cont.	x			CLA
		Sun Sensor Pulses	Cont.	x			CLA
		Normal Mode Indication	1			x	EIA
		Ground Despin Mode	1			x	EIA
		Earth Sensor No. 1 Mode	1			x	EIA
	Control Logic Assembly	Earth Sensor No. 2 Mode	1			x	EIA
Attitude Control	Thruster	Thruster Fire Period	Cont.	x			EIA
Navigation	Mechanical Despun Antenna Electronics	Antenna Reference Pulse	Cont.	x			MDA
		Drive Waveform No. 1 Normal	1			x	EIA
		Drive Waveform No. 2 Normal	1			x	EIA

Table I
Page 2

Subsystem	Unit	Parameter	Samples per Minute	Data Type			Signal Conditioning Location
				Real Time	Analog	Discrete	
Navigation	Nav. Transmitter No. 1	Temperature	1		x		Transmitter
	Nav. Transmitter No. 2	Temperature	1		x		Transmitter
Navigation	Tracking Data Transponder	Temperature	1		x		Transponder
Telemetry & Command	T&C Transmitter No. 1	Temperature	1		x		Transmitter
	T&C Transmitter No. 2	Temperature	1		x		Transmitter
	Receiver No. 1	Signal Present	1			x	EIA
	Receiver No. 2	Signal Present	1			x	EIA
	Receiver No. 1	Loop Stress	1		x		Receiver
	Receiver No. 2	Loop Stress	1		x		Receiver
	Tlm. Encoder No. 1 or No. 2	Full Scale Calibration	1		x		Encoder
	Tlm. Encoder No. 1 or No. 2	Zero Scale Calibration	1		x		Encoder
	Cmd. Decoder No. 1	Audio Signal	1		x		Decoder
Telemetry & Command	Cmd. Decoder No. 2	Audio Signal	1		x		Decoder

Subsystem	Unit	Parameter	Samples per Minute	Data Type			Signal Conditioning Location
				Real Time	Analog	Discrete	
Propulsion	Apogee Motor	Case Temperature	1		x		Apogee Motor
Propulsion	Pressure Transducer	Tank Pressure	2		x		Pressure Trans.
Propulsion	Propellant Tank No. 1	Tank No. 1 Temperature	1		x		Tank
Propulsion	Propellant Tank No. 2	Tank No. 2 Temperature	1		x		Tank
Electrical Integration	Electrical Integration Assembly	Undervoltage Control Normal/Override	1			x	EIA
Electrical Integration	Electrical Integration Assembly	Primary Bus Voltage	4		x		EIA
Electrical Integration	Electrical Integration Assembly	Primary Bus Current	4		x		EIA
Power	Power Control Unit	Shunt Voltage	2		x		PCU
Power	Power Control Unit	Battery No. 1 Voltage	2		x		PCU
Power	Power Control Unit	Battery No. 2 Voltage	2		x		PCU
Power	Power Control Unit	Battery No. 1 Current	2		x		PCU
Power	Power Control Unit	Battery No. 2 Current	2		x		PCU
Power	Power Control Unit	Solar Array Voltage	2		x		PCU

Table I

Page 4

Subsystem	Unit	Parameter	Samples per Minute	Data Type: Real Time	Data Type: Analog	Data Type: Discrete	Signal Conditioning Location
Power	Battery No. 1	Battery No. 1 Temperature	1		x		Battery
	Battery No. 2	Battery No. 2 Temperature	1		x		Battery
	Solar Array	Solar Panel Temperature	1		x		Solar Panel
	Equipment Converter	Redundant Inverter Regulator A/B	1			x	Converter
		Temperature	1		x		
		-24 Volt Output	1		x		
		+15 Volt Output	1		x		
		-15 Volt Output	1		x		
		+10 Volt Output	1		x		
		+6 Volt Output	1		x		
		-6 Volt Output	1		x		
Power	Equipment Converter						Converter
Structure	Equipment Panel	Temperature	1		x		Equipment Panel

1 Frame Synchronization	2 Frame Synchronization	3 Full Scale Calibration	4 Zero Scale Calibration	5 Primary Bus Current	6 Primary Bus Voltage	7 Command Decoder No. 1 Audio Signal	8 Command Decoder No. 2 Audio Signal
9 Unassigned	10 Receiver No. 1 Loop Stress	11 Receiver No. 2 Loop Stress	12 Propellant Tank Pressure	13 Unassigned	14 Battery No. 1 Temp.	15 Battery No. 2 Temp.	16 Solar Panel Temp.
17 Battery No. 1 Voltage	18 Battery No. 1 Current	19 Battery No. 2 Voltage	20 Battery No. 2 Current	21 Primary Bus Current	22 Primary Bus Voltage	23 Shunt Voltage	24 Solar Array Voltage
25 Unassigned	26 Unassigned	27 Propellant Tank No. 1 Temp.	28 Propellant Tank No. 2 Temp.	29 Receiver No. 1 Signal Present Receiver No. 2 Signal Present Unassigned	30 Equipment Panel Temp.	31 Converter -24 Volt Output	32 Converter +15 Volt Output
33 Converter -15 Volt Output	34 Converter +10 Volt Output	35 Converter +6 Volt Output	36 Converter -6 Volt Output	37 Primary Bus Current	38 Primary Bus Voltage	39 Converter Temp.	40 Apogee Motor Case Temp.
41 Unassigned	42 Navigation Transmitter No. 1 Temp.	43 Navigation Transmitter No. 2 Temp.	44 Propellant Tank Pressure	45 Inverter Regulator A/B Undervoltage Normal/Override Unassigned	46 Tracking Data Transponder Temp.	47 T&C Transmitter No. 1 Temp.	48 T&C Transmitter No. 2 Temp.
49 Battery No. 1 Voltage	50 Battery No. 1 Current	51 Battery No. 2 Voltage	52 Battery No. 2 Current	53 Primary Bus Current	54 Primary Bus Voltage	55 Shunt Voltage	56 Solar Array Voltage
57 Unassigned	58 Unassigned	59 Valve Set No. 1 On/Off Valve Set No. 2 On/Off Axial Thruster No. 1 On/Off	60 Axial Thruster No. 2 On/Off Radial Thruster No. 1 On/Off Radial Thruster No. 2 On/Off	61 Unassigned	62 Antenna Despin Normal Mode Antenna Despin Earth Sensor No.1 Antenna Despin Earth Sensor No.2	63 Ground Despin Mode Drive Waveform No. 1 Drive Waveform No. 2	

Figure E-2. Telemetry Channel Assignments